Operation, Capabilities and Limitations of Existing Hypersonic Facilities

Herbert Olivier and Sangdi Gu
Shock Wave Laboratory
RWTH Aachen University
GERMANY

olivier@swl.rwth-aachen.de gu@swl.rwth-aachen.de

ABSTRACT

This paper presents an overview and analysis of the various aspects of hypersonic ground testing. For this, first the simulation requirements according to the different flow regimes of hypersonics flight are briefly described. Based hereon the methodologies of hypersonic ground testing are reviewed and the limitations of applicability are discussed. The characteristics and capabilities of the different hypersonic wind tunnels which facilitate hypersonic ground testing are discussed. The capabilities and limitations of these facilities are quantitatively assessed in regards to the simulation of relevant flight conditions. In addition, further limitations of the ground test facilities, such as test time and test model size, are assessed for reflected shock tunnels and expansion tunnels. Additionally, the often unavoidable problem of producing thermochemically excited test flows in high enthalpy facilities with stagnated flow in the nozzle reservoir are reviewed. The trend is that each type of hypersonic facility has its own unique advantages and disadvantages. So, success in experimental hypersonics would result from testing in a variety of different facilities in order to benefit from the advantages of each facility. Testing in shock tubes i.e. behind the incident shock wave is not considered in this paper since this type of experiments is mostly suitable for fundamental shock relaxation studies and not for detailed wind tunnel model testing.

1.0 INTRODUCTION

Research in the field of hypersonics is crucial for both national defence and space exploration purposes. Experimental hypersonics encompasses a significant portion of hypersonics research involving blunt bodies, slender bodies and propulsion systems. Experimental data is important for the validation of numerical codes, numerical simulation of the flowfield around flight vehicles and investigation of fundamental flow physics. Specific ground testing methodologies and facilities have been developed explicitly for hypersonic flows. The ground testing methodologies allow experimental data of subscale test models to be related to fight conditions. Due to driving power requirements and other constraints most of the hypersonic ground testing facilities are of intermittent or impulsive type, which therefore represents the biggest part of this paper.

The first period of hypersonic ground testing activity began in the late 1950s and continued through the 1960s, arising from the many hypersonic flight design projects and the feeling that theoretical knowledge of hypersonic flows was undeveloped [1]. During this period, numerous facilities were developed which generated hypersonic flows by reducing the temperature of the test gas through expansion to as low as possible while adding as little energy as possible to the test gas to increase its velocity. These are called ‘cold’ facilities and they allow for the simulation of high Mach numbers but not high velocities. At the same time, ‘hot’ facilities which produced hypersonic flows by expansion of high temperature gas in a reservoir were introduced and these facilities allow for the simulation of high velocities. A second period of intense activity began in the mid-1980s and continued into the 1990s during which the National Aerospace Plane project in the USA, the ‘HOPE’ re-entry glider project from Japan and the ‘Hermes’ re-entry glider project from Europe were active. It was during this period that the free-piston driver technique was successfully applied which, along with the detonation driver technique, unlocked previously unattainable performance envelops for ground test facilities.

In this paper, the characteristics, capabilities and limitations of different hypersonic test facilities and driver techniques are discussed. The capabilities and limitations of these facilities are quantitatively assessed in regards to the simulation of relevant flight vehicles. In addition, further limitations of the ground test facilities, such as test time and test model size, are assessed for reflected shock tunnels and expansion tunnels which are currently the two most important facility types for high enthalpy hypersonics research. Additionally, the often unavoidable problem of producing thermochemically excited test flows in high enthalpy facilities with stagnated nozzle reservoir flow is reviewed.

2.0 GROUND SIMULATION METHODOLOGY

While ground test facilities are often used to study the flow past generic models such as cylinders, spheres and wedges for fundamental investigation of specific phenomena, a significant portion of experimental work in hypersonics involves reproducing flows past actual aircrafts and spacecrafts for engineering purposes. However, ground test facilities generally cannot test a full scale flight vehicle over a complete range of flight conditions. Consequently, it is necessary to discuss the methodologies to simulate hypersonic flows over flight vehicles using ground test facilities.

2.1 Aerodynamic flow fields

2.1.1 Low enthalpy flows

Hornung in 1988 [2] reported a good strategy for subscale simulation of hypersonic aerodynamic flow fields. The lowest speeds at which chemical reactions become an important part of the flow field are about 2 km/s in blunt body air flows at sea level conditions. This corresponds to a stagnation temperature of about 2000 K. According to Figure 1, at speeds below 2 km/s, the perfect gas model applies for air as the isentropic exponent, γ, is either constant or varies only with temperature due to vibrational excitation. In this case any dimensionless quantity, Q, will depend on the dimensionless parameters of the flow. This means that duplication of all the dimensionless parameters of the flow ensures the duplication of the dimensionless quantity being investigated in some subscale model in a wind tunnel. In the case where the gas used is the same between flight and experiment, the model is scaled exactly with the flight vehicle and the model and flight vehicle are orientated in the same way relative to the flow [2],

$$Q = Q\left(M_\infty, Re, \frac{T_w}{T_0}, Fq\right) \tag{1}$$

where M_∞ is the Mach number, Re is the Reynolds number, T_w/T_0 is the wall temperature to total temperature ratio and Fq is a set of dimensionless parameters defining the flow quality in the wind tunnel. This is called the Mach-Reynolds-Simulation.

The importance of simulating M_∞, Re and T_w/T_0 is clear when observing, exemplarily, the rearranged flat plate laminar boundary layer thickness equation given by Ginoux [4]

$$\frac{\delta}{x} = \sqrt{\frac{C^*}{Re_{\infty,x}}}\left(3.07 + \frac{0.58(\gamma-1)}{2}M_\infty^2 + \frac{1.93T_w}{T_\infty}\right) \tag{2}$$

where δ is the boundary layer thickness, x is the distance downstream of the leading edge, $Re_{\infty,x}$ is the Reynolds number at the location x, C* is the Chapman-Rubesin factor evaluated at the reference temperature, M_∞ is the freestream Mach number and T_∞ is the freestream temperature. From equation 2, M_∞ and the T_w/T_∞ ratio, which is matched when M_∞ and T_w/T_0 in equation 1 are matched under perfect gas conditions, are particularly important parameters for simulating the boundary layer thickness, while the Reynolds number also needs to

be simulated. For typical hypersonic flight vehicles (altitude = 35 km, M_∞ = 6, T_∞ = 237 K, recovery temperature, Tr = 1670 K), T_w/T_∞ has a value of around 4 - 5. In cold hypersonic facilities where T_∞ can be around 60 – 80 K, using room temperature test models conveniently preserves the T_w/T_∞ ratio. However, in situations where wind tunnels are used to generate higher stagnation temperatures, e.g. in order to duplicate the total enthalpy and therewith the real flight velocity or real gas effects, which may influence viscous effects such as transition [5], heated test models must be used in order to preserve T_w/T_∞ [6]. Consider a flat plate in a typical short duration wind tunnel flow with $M_{\infty,wt}$ = 6, $T_{\infty,wt}$ = 237 K and $T_{w,wt}$ = 300 K i.e. $(T_w/T_\infty)_{wt}$ = 1.3, and a flat plate in flight with the same M_∞ and T_∞ i.e. same recovery temperature, but a wall temperature of $T_{w,fl}$ = 1185 K i.e. $(T_w/T_\infty)_{fl}$ = 5. Further it is assumed that the Reynolds number for flight and wind tunnel are the same which is a requirement of equation 1. Then for the considered case from equation 2, it follows,

$$\frac{\left(\frac{\delta}{x}\right)_{wt}}{\left(\frac{\delta}{x}\right)_{fl}} = 0.64 \tag{3}$$

where subscripts wt and fl denote wind tunnel and flight respectively, resulting in large differences in the boundary layer thickness at any given point behind the leading edge if the wall to freestream temperature ratio is not preserved. Hence, for these cases heated models must be used for simulating wall temperature effects in the laboratory. It has been shown that the wall temperature ratio strongly influences the size of separation bubbles [6]. It further influences the transition behaviour of boundary layers. Additionally, the heated model technique is also useful on blunt bodies in order to study ablation-radiation coupling as pioneered by Zander et al. [7].

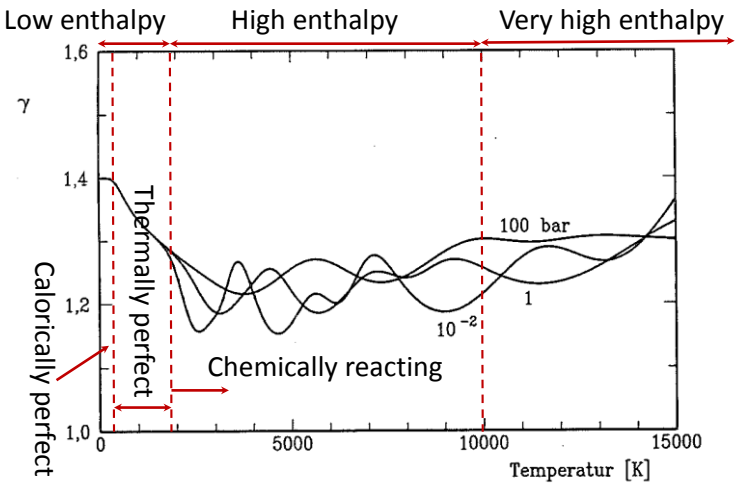

Figure 1: Variation of the isentropic exponent, γ, of air with temperature and pressure. [3]

On the other hand, the skin friction coefficient,

$$C_f = \frac{0.664}{\sqrt{Re_{\infty,x}}}\sqrt{C^*} \tag{4}$$

and the Stanton number,

$$St = \frac{0.41}{\sqrt{Re_{\infty,x}}}\sqrt{C^*} \tag{5}$$

have lower dependencies on M_∞ and T_w/T_∞ within a Mach number range that is not too large, as shown by equations 4 and 5 for a laminar boundary layer and illustrated in Figure 2. Hence more leniency on abiding by equation 1 may be given to the simulation of the skin friction coefficient and the Stanton number which depends strongly on the geometry instead. Furthermore, included in Fq in equation 1 are parameters related to the freestream noise level, freestream turbulence level and the surface roughness. These parameters are important for studies such as boundary layer transition. Current difficulties include defining the freestream noise and turbulence levels in high enthalpy facilities and, to a lesser extent, scaling the surface roughness in subscale test models so as to prevent artificial boundary layer transition or enhanced heating rates due to surface roughness. In practice, since the surface roughness needs to be scaled with the model geometry, a surface roughness of the order of 0.01 mm or even less is often required on the experimental test model, which is not always easy to obtain.

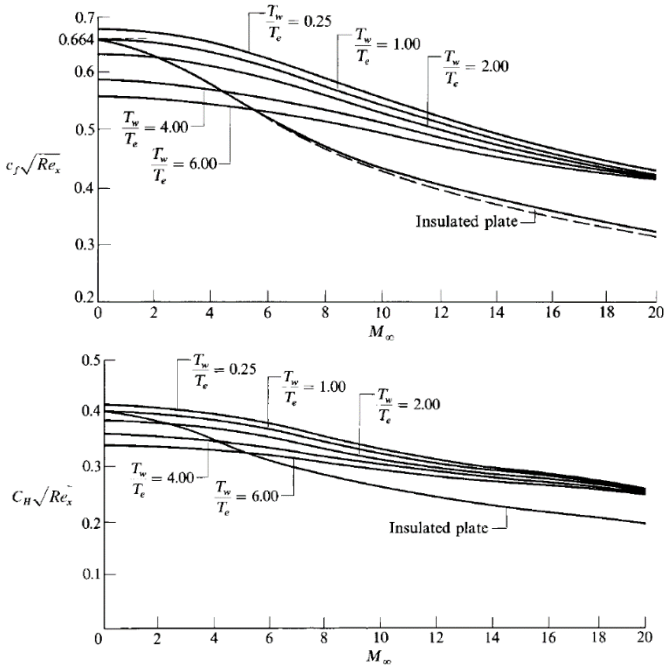

Figure 2: Flat plate skin friction coefficient, top, and Stanton numbers, bottom, for compressible laminar boundary layers. [8]

Another phenomenon of interest in hypersonic flows is the entropy layer. Correct simulation of the entropy layer is important as it can influence the heat flux distribution, skin friction, separation behaviour and boundary layer transition. For calorically perfect air at hypersonic conditions, the entropy change, Δs, across a normal shock can be written as,

$$\Delta s = \mathrm{R} * \ln(2.78 * 10^{-3} * M_\infty^5) \tag{6}$$

where R is the specific gas constant of air. The equation above shows that the entropy layer is strongly dependent on the Mach number. Hence, the duplication of the Mach number is important for the duplication of the entropy layer. The duplication of the Mach number is also important for the duplication of the laminar viscous interaction. The laminar viscous interaction parameter, $\bar{\chi}$, is given by,

$$\bar{\chi} = \frac{M_\infty^3}{\sqrt{Re_{\infty,x}}}\sqrt{C_\infty} \tag{7}$$

where C_∞ is the Chapman-Rubesin factor. The above equation shows that the Mach number has a strong influence on the viscous interaction while the Reynolds number and the wall temperature, which influences the value of C_∞, have weaker influence on the viscous interaction.

2.1.2 High enthalpy flows

For high enthalpy flows in principle the same requirements hold as those formulated in the previous subchapter for the low enthalpy flow regime. But at speeds greater than 2 km/s or about 2000 K total temperature in blunt body air flows, additional real-gas effects become important as shown in Figure 1 where γ varies with both temperature and pressure due to chemical reactions. A portion of hypersonic flows involves situations where dissociation reactions are dominant. In these situations, preserving the binary scaling product, $\rho_\infty L$ where ρ_∞ is the freestream density and L is the characteristic length, preserves the normalized distribution of the chemical composition behind a shock wave. This law was first mentioned by Birkhoff in 1955 [9]. From Anderson [8], the binary scaling law can be derived as follows: for simplicity consider a two-dimensional flow where the dominant chemical reaction is the oxygen dissociation reaction, $O_2 + M \rightarrow 2O + M$ where M is the collision partner, the species continuity equation for atomic oxygen can be written as,

$$u\left(\frac{dc_O}{dx}\right) + v\left(\frac{dc_O}{dy}\right) = \frac{M_O}{\rho} k_f \left(\frac{\rho c_{O_2}}{M_{O_2}}\right)\left(\frac{\rho c_M}{M_M}\right) \tag{8}$$

where c_O and c_{O2} is the mass fraction of O and O_2 respectively, u and v is the flow velocity in the x and y directions respectively, M_O, M_{O2} and M_M is the molar mass of O, O_2 and M respectively, ρ is the flow density and k_f is the forward reaction rate constant which is a function of temperature as described by the Arrhenius equation. Defining the nondimensional variables x' = x/L, y' = y/L, u' = u/U_∞, v' = v/U_∞ and ρ' = ρ/ρ_∞ where U_∞ and ρ_∞ is the velocity and density of the freestream respectively and L is a characteristic length, equation 8 can be written as,

$$u'\left(\frac{dc_O}{dx'}\right) + v'\left(\frac{dc_O}{dy'}\right) = \frac{K_1(\rho_\infty L)}{U_\infty} \rho' c_{O_2} c_M \tag{9}$$

where

$$\mathrm{K_1} = \frac{M_O}{M_{O_2} M_M} k_f \tag{10}$$

Equation 9 shows that for two flows with the same freestream velocity and temperature, resulting in the same K_1, the mass fraction distribution along the normalized directions x' and y' will be identical between the two flows if the product $\rho_\infty L$ is preserved. This is the statement of binary scaling and this is illustrated qualitatively in Figure 3. Also, from Hornung [2], for an ideal chemically reacting gas, the rate of dissociation R_D is,

$$\mathrm{R_D} = \rho \mathrm{T^n} e^{-\frac{D}{kT}} (1 - \alpha) \tag{11}$$

and the rate of recombination R_R is,

$$\mathrm{R_R} = \frac{\rho^2 \mathrm{T^n} \alpha^2}{\rho_d} \tag{12}$$

where ρ is the gas density, α is the mass fraction of the dissociated gas, T is the temperature, k is Boltzmann's constant, n is a dimensionless constant and ρ_d is the characteristic density of dissociation. From the above equations, the dissociation rate, which is a two body reaction, can be rewritten as,

$$R_D = \frac{d\alpha}{dt} = \frac{dc_O}{dt} = u\left(\frac{dc_O}{dx}\right) + v\left(\frac{dc_O}{dy}\right) \tag{13}$$

for steady flows. Then,

$$R_D = u'\left(\frac{dc_O}{dx'}\right) + v'\left(\frac{dc_O}{dy'}\right) = \frac{(\rho_\infty L)}{U_\infty}\rho' T^n e^{-\frac{D}{kT}}(1 - c_O) \tag{14}$$

where $1 - c_o = c_{o2}$. This is the same statement as given by equation 9. Accordingly, for the recombination reaction the scaling factor is $\rho_\infty^2 L$. It is interesting to note that de Crombrugghe et al. [10] made the discovery that the binary scaling law is not only applicable for preserving the nonequilibrium behaviour in shock layers but also maintain the same diffusion processes in binary scaled chemically reacting boundary layers, resulting in further applications in subsonic high enthalpy wind tunnels such as plasma tunnels.

The simulation strategy given by Hornung [2] for chemically reacting blunt body flows considering only dissociation reactions is therefore as follows,

$$Q = Q\left(U_\infty, \rho_\infty L, \alpha_\infty, \frac{T_w}{T_0}\right) \tag{15}$$

where α_∞ is the mass fraction of dissociated gas in the freestream. For strong bow shocks, the Mach number is omitted from the above equation due to the Mach number independence principle. Reynolds number is omitted because the post-shock Reynolds number is automatically satisfied when U_∞ and $\rho_\infty L$, is matched since the freestream static temperature has only a small influence on the post-shock temperature of a bow shock which is mainly influenced by U_∞ [11]. Consequently, duplication of the parameters in equation 15 gives a simulation of the temperature field, viscosity, Prandtl number and the specific heat ratio in the flowfield after a bow shock, between experiment and flight. However, for more slender bodies where Mach number and real-gas effects are important the Mach number has also to be matched, which for static temperatures less than 2000 K subsequently results in a duplication of the freestream static temperature T_∞ and freestream Reynolds number [12].

It is important to note that some important portions of hypersonic blunt body flows cannot be described by the binary scaling law which is derived based on the assumption of no radiation coupling and purely binary reactions. From de Crombrugghe et al. [13] [14], when binary scaling is applied, the impact of non-binary chemistry causes the shock layer in the subscale test model to be hotter and less dissociated than in flight, while the strength of radiation coupling increases with the length-scale of the flow resulting in the subscale flow having less radiation coupling than in flight which subsequently leads to the laboratory shock layer containing a greater enthalpy than the shock layer in flight. Furthermore, it should be noted that the duplication of the freestream dissociation level α_∞ in equation 15 is very difficult because the production of high enthalpy flows in the wind tunnels often requires heating the test gas to temperatures high enough to cause significant thermochemical excitation which normally does not relax to equilibrium at the test section. In flight, the freestream dissociation level is practically zero which is not the case for high enthalpy wind tunnels. A finite freestream dissociation level leads to a reduced density jump across a shock resulting in a larger shock stand-off distance [15]. Also, Fq from equation 1 is omitted in equation 15 because the flow quality that can be achieved in current real gas simulation facilities is only very low [2]. Consequently, these facilities are only used for investigations of effects that are less subtle than those that depend sensitively on Fq. Unfortunately, there are actually a number of important effects which do depend sensitively on Fq [2]. So, Lawson and Austin are currently investigating new ways to generate low-disturbance, high-enthalpy test flows [16]. It has to be mentioned that the flow quality in high enthalpy facilities strongly depends on the test condition. A good flow quality can be achieved, for example, in shock tunnels at low unit Reynolds numbers even at high enthalpies as it is proven by numerous heat flux measurements.

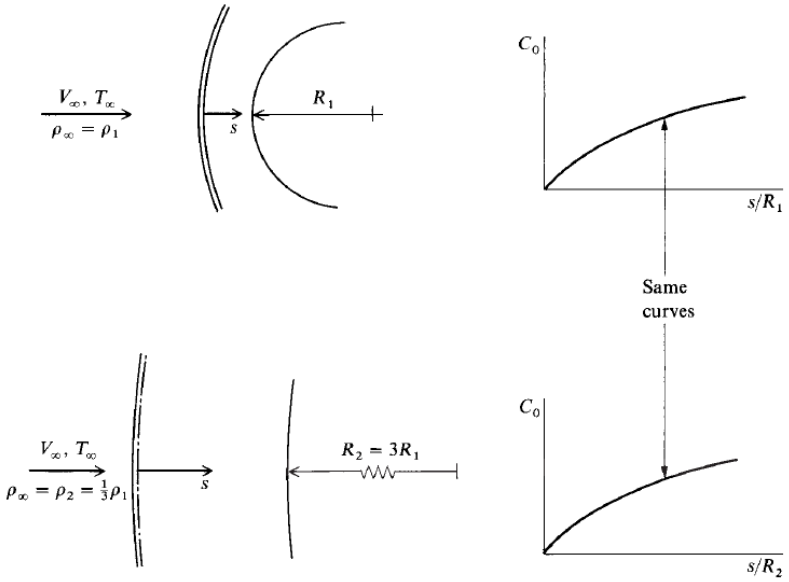

Figure 3: Description of binary scaling from Anderson. [8]

2.2 Airbreathing Propulsion testing

In hypersonics scramjets are of main interest as airbreathing propulsion systems. Therefore, the following considerations are focused on scramjet testing. Scramjet propulsion becomes of interest at speeds greater than 1.5 km/s. At these speeds and higher, there is a strong coupling between the external vehicle flowfield and the internal flow of the engine. Therefore, and due to other reasons, scramjet testing requires a sophisticated ground testing methodology.

From Stalker [1], ground simulation of scramjets involves producing the conditions which will allow the combustion process to reach the same degree of completion as in the equivalent flight configuration. One of the most popular scaling laws for scramjets is the pL-scaling, which was first stated by Stewart [17], where p is the static pressure and L is the characteristic length. The pL-scaling law states that, given that fuel distribution and heat transfer similarity is achieved in the scramjet, the scramjet combustor performance would scale with the factor pL [18]. So, if the inlet static temperature, inlet flow velocity and fuel-air mixture fractions (equivalence ratio), and hence the Mach number, ratio of specific heats and total enthalpy, are reproduced in the subscale test, duplicating the pL factor between experiment and flight, which also duplicates the Reynolds number, would result in a representative simulation of the flight scramjet [19].

An experimental investigation carried out by Pulsonetti and Stalker [18] into the validity of the pL-scaling law showed that the ignition time, generally defined as the time for the temperature rise to reach 5 % of the complete reaction temperature rise for a given temperature is proportional to one over pressure. The pL-scaling law is physically consistent because the ignition reaction which produces the free radicals responsible for initiating the reaction system is a two body reaction. They also mentioned that the wall boundary layer and viscous effects on the inside surface of the scramjet duct also scales with the pL law because for fixed Mach number and wall temperature ratio the boundary layer thickness, the displacement thickness and the momentum thickness are functions of the Reynolds number, for turbulent boundary layers. Pulsonetti and Stalker also showed that the pL-scaling law works for scaling the mixing efficiency, which measures the completeness of mixing, and other mixing effects for normal or tangential fuel injections. The scaling of the heat transfer, in terms of Stanton number, was shown to obey the pressure length scaling reasonably well as long as the boundary layer for the wind tunnel model or the flight vehicle does not become transitional [20]. Furthermore, as long as the scaled pressure distribution in the combustion duct and consequently in the

expansion nozzle is duplicated, which is achieved well in most cases by the pL scaling law [21], pL scaling preserves the thrust coefficient between scramjets of different scale. This can be shown as follows; given that the pressure distribution in the scramjet nozzle, which depends on the location x and y, is,

$$\mathrm{p_n} = f(\mathrm{x}, \mathrm{y}) \tag{16}$$

and the thrust coefficient is defined as,

$$\mathrm{C_\tau} = \frac{2\tau}{\mathrm{A_i}\rho_\infty \mathrm{U}_\infty^2} \approx \frac{2\tau}{\mathrm{A_i p_{0,\infty}}} f(M_\infty) \tag{17}$$

where τ is the thrust, $\mathrm{A_i}$ is a reference area and $\mathrm{p_{0,\infty}}$ is the total pressure. The thrust for scramjet 2, which is a scaled model of scramjet 1, can be expressed as,

$$\tau_2 = \int p_1 \frac{L_1}{L_2} dA_2 \tag{18}$$

where A is the internal local flow cross-sectional area and L is the characteristic length of the scramjets. Since,

$$dA_2 = \left(\frac{L_2}{L_1}\right)^2 dA_1 \tag{19}$$

equation 18 becomes,

$$\tau_2 \frac{L_1}{L_2} = \int p_1 dA_1 = \tau_1 \tag{20}$$

Using equation 17, for same Mach numbers this equation becomes,

$$C_{\tau,2}\mathrm{A_{i,2}p_{0,2}} \frac{L_1}{L_2} = C_{\tau,1}\mathrm{A_{i,1}p_{0,1}} \tag{21}$$

which can be simplified to,

$$C_{\tau,2}\mathrm{p_{0,2}} L_2 = C_{\tau,1}\mathrm{p_{0,1}} L_1 \tag{22}$$

Since,

$$\frac{p_0}{p} = \left(1 + \frac{\gamma - 1}{2} M^2\right)^{\frac{\gamma}{\gamma - 1}} \tag{23}$$

and in case both Mach number and γ are maintained between the two scramjet flows, equation 22 demonstrates that preserving the pL product preserves the thrust coefficient of the scramjets given that the scaled pressure distributions are duplicated.

Nevertheless, there are limitations to the pL-scaling law. The pL-scaling law is valid for scaling the combustion reaction time if the process is dominated by binary reactions. However, if three body reactions are significant and the combustion occurs under chemical nonequilibrium, which is not uncommon in subscale scramjets as shown by Karl et al. [19], the pL-scaling law would not hold. Karl et al. [19] showed that in small subscale scramjet testing at subsequently high static pressures, maintaining the pL factor, which consequently preserved the Reynolds number, often did not preserve the chemistry (Damköhler's first number) which scaled better

with $p^{1.7}L$. Consequently, in these cases it would be impossible to duplicate both the Reynolds number and the chemical time scales simultaneously As demonstrated by Pulsonetti and Stalker [18], a consequence of incorrectly simulating the nonequilibrium combustion chemistry could be that the final pressure achieved in the scramjet prior to the nozzle expansion is scaled incorrectly which would then influence the thrust produced. Furthermore, the pL-scaling law does not preserve the equilibrium composition. Therefore, under chemical equilibrium conditions, the static pressure changes would impact the amount of heat released due to combustion since more molecular species would form at high pressures which would result in larger energy releases [18]. Nevertheless, while the pL-scaling law may not work so well in certain cases, it is still regarded as a good first order approximation for scaling scramjet performances in most cases because the law provides a relation for predicting the fundamental phenomena occurring in a scramjet combustor [18] [22] [21]. Consequently, Karl et al. [19] mentioned the importance of the use of CFD tools to relate data from pL scaled scramjet experiments to flight scale scramjets.

3.0 TYPES OF HYPERSONIC GROUND TEST FACILITIES

To carry out hypersonic ground test experiments, a variety of different facilities exist. The facilities have different characteristics as shown in Figures 4 and 5 as well as in Table 1. Shock tunnels and expansion tunnels can generate conditions with very high velocities, but these facilities have very short test times. For example, the test time of expansion tubes in Table 1 are in the order of tens of microseconds. On the other hand, blowdown tunnels, Ludwieg tubes, hotshots and gun tunnels have long test times but are limited to producing low velocity conditions. The test times of gun tunnels and hotshots in Table 1 are in the order of tens of milliseconds, while the test times of blowdown tunnels are in the order of a few seconds, but within this group only hotshots can generate total temperatures of up to 6000 K. Reflected shock tunnels, generally with test times in the order of a few milliseconds, have medium duration test times and medium performance capabilities compared to the other facilities. The biggest hypersonic wind tunnel currently in operation is the JF12 reflected shock tunnel which has a test section diameter of 2.5 m [23]. The LENS XX expansion tunnel comes close with a test section diameter of 2.4 m [24]. Though, it should be noted that, in general, the test section size of expansion tunnels is much smaller than that of the LENS XX. It has also to be noted that, the test section size is not necessarily a measure of the reasonable model size. This topic is discussed in detail in section 4.2.1.

Nevertheless, it is not always desirable to test in facilities as big as possible. The advantage of having smaller facilities is the economy of operation and cost. It is also not always necessary to produce very high velocity conditions, for example in scramjet testing. Similarly, long test times may not be necessary for the study of thermochemical kinetics. Thus, different facilities are suited for different objectives. The characteristics of some of the popular facility types will be covered in this section.

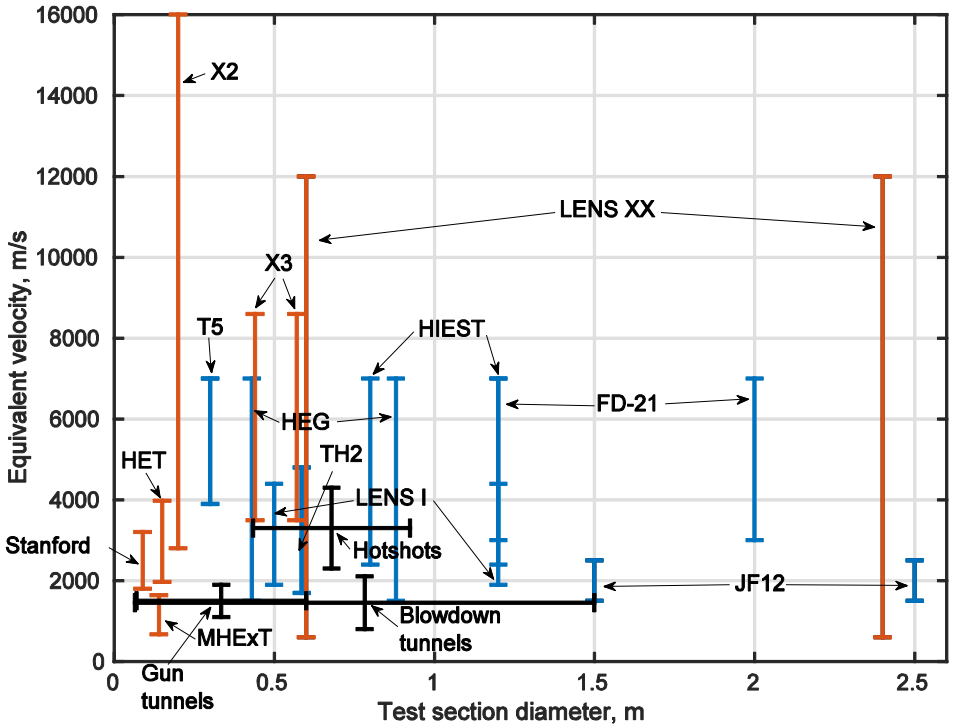

Figure 4: The ranges of velocity and test section size for different facility categories assuming air as the test gas. Expansion tubes are in blue, shock tunnels are in orange and other facilities are in black.

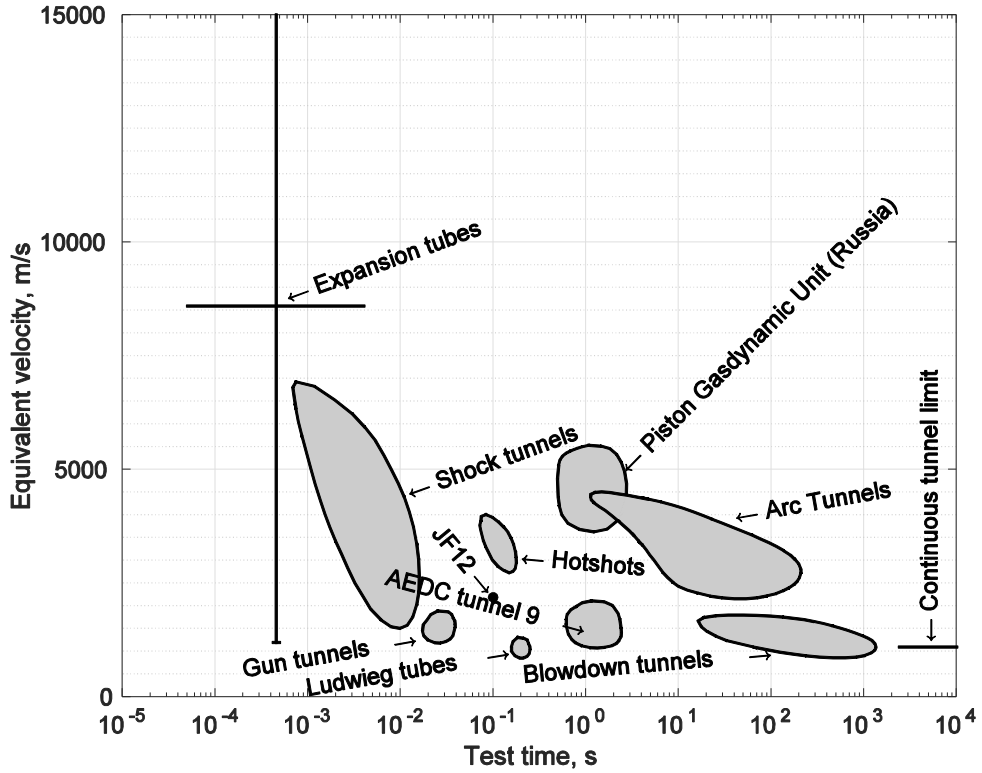

Figure 5: The ranges of velocity and test time for different facility categories assuming air as the test gas. Adapted from reference [51].

Table 1: Characteristics of existing hypersonic test facilities.

Facility type	Facilities	$P_{0,max}$, MPa	$T_{0,max}$, K	Typical test time, s	Test section diameter, m	Source
Continuous	AEDC Tunnel B	6.2	750	-	1.27	[25]
	AEDC Tunnel C	14	1200	-	1.27	[25]
Blowdown	AEDC Tunnel 9	145	1600	0.23 s – 15 s	1.5	[26]
	H2K	4.5	1100	Up to 30 s	0.6	[27]
	S4 Modane	15	1800	25 - 90 s	0.7 – 1.0	[28]
Gun tunnels	Longshot, VKI	400	2500	20 ms	0.36 – 0.60	[29]
	Cranfield University	10	1290	80 ms	0.2	[30]
	HS1	60	1150	20 ms	0.6	[30]
	Oxford University	9	1000	30 ms	0.21	[30] [31]
Hotshot	ONERA F4	76	6000	20 ms – 100 ms	0.43 – 0.92	[32] [33]
Reflected shock tunnel	TH2	63	7400	2 ms – 10 ms	0.586	[34]
	JF12	3.5	2500	100 ms – 150 ms	1.5 - 2.5	[23]
	T4	90	7540	0.5 ms – 5 ms	0.135 – 0.375	[35] [36] [37]
	T5	85	10000	1 ms – 2 ms	0.3	[35] [38]
	HEG	90	9900	1 ms – 6 ms	0.43 – 0.88	[35]
	HIEST	150	10000	More than 2 ms	0.8 – 1.2	[39]
	FD-21	-	10000	-	1.2 - 2	[40] [41]
	LENS I	200	7000	2 ms – 18 ms	0.5 - 1.2	[42] [43] [44]
Expansion tunnel	MHExT	1.4	2000	900 µs – 1000 µs	0.14	[45]
	Stanford University	3.3	4188	170 µs – 400 µs	0.089	[46]
	HET	53	5400	90 µs – 150 µs	0.15	[47]
	X2	19700	37000	50 µs – 200 µs	0.2	[22] [48]
	X3	27500	18200	300 µs – 1300 µs	0.44 - 0.57	[49] [50]
	LENS XX	-	0.6 – 12 km/s	200 µs – 8000 µs	0.6 – 2.4	[24]

3.1 Low Enthalpy Facilities

Under low enthalpy hypersonic conditions, approximately less than 2 MJ/kg, the gas behaves like a perfect gas and the Mach-Reynolds-Simulation is valid. For investigating low enthalpy conditions, blowdown tunnels and gun tunnels are suitable facilities.

A schematic of a conventional blowdown tunnel is shown in Figure 6. The flow condition at the test section depends on the pressure and temperature of the test gas in the plenum. Initially during the operation of a blowdown tunnel, the nozzle and test section are evacuated to low pressures and isolated from the plenum.

Gas from the high-pressure tank is used to pressurize the plenum. In the AEDC tunnel 9 blowdown facility, heaters are used to heat the fixed volume of pressurized test gas in the plenum to a particular pressure and temperature to create hypersonic conditions at the test section [26]. Once the gas in the plenum reaches the desired pressure and temperature, the diaphragm will rupture. The high pressure and temperature test gas will then expand through the nozzle resulting in a limited duration of hypersonic flow. As the high temperature and high pressure test gas leaves the plenum, high pressure gas from the high-pressure tank enters the plenum from the upstream end. This process is organized such that the cold gas from the high-pressure tank pushes the heated test gas downstream like a piston to maintain a constant nozzle inlet condition. Instead of a diaphragm, other facilities like H2K use a valve in front of the plenum chamber to connect the wind tunnel with the high-pressure reservoir and electric heaters placed upstream of the settling chamber and the valve [27].

A different form of a blowdown tunnel is the Ludwieg tube, shown in Figure 7, where upstream of the nozzle is a long tube containing high pressure test gas which is sometimes also heated. Once the diaphragm or valve separating the nozzle and high pressure tube opens and the test begins, an unsteady expansion forms. A large part of the expansion wave propagates upstream through the high pressure tube, reflecting off the end wall and back to the nozzle entrance. Once the first reflected expansion wave arrives back to the nozzle entrance, the test is terminated. During the upstream and downstream movement of the expansion wave, the conditions in the nozzle reservoir are at least theoretically constant which is an advantage of Ludwieg tubes. Generally, for blowdown facilities especially the reservoir pressure is not constant with time because of the constant volume of high-pressure reservoir. This leads to the fact that for constant volume reservoirs, the Reynolds number decreases during the measuring time.

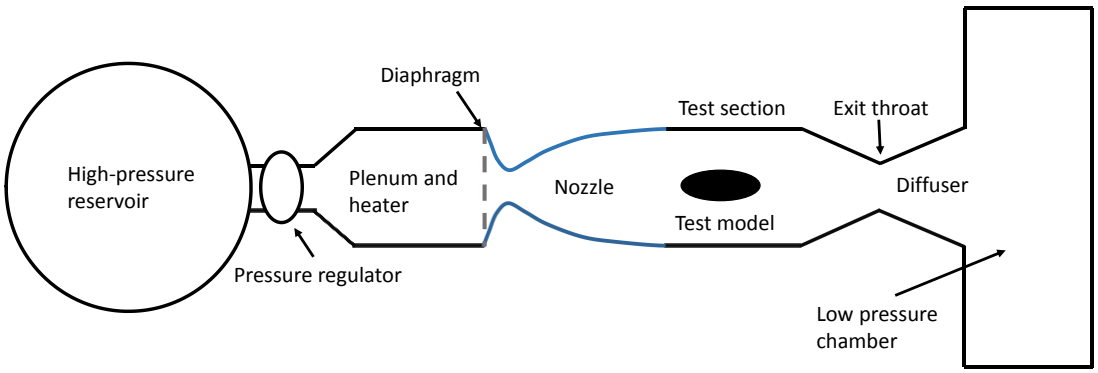

Figure 6: Schematic diagram of a blowdown wind tunnel like the AEDC Tunnel 9.

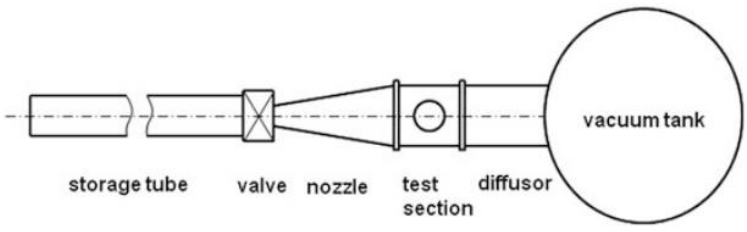

Figure 7: Schematic diagram of a Ludwieg tube. [52]

Another form of a blowdown tunnel are hotshots, where upstream of the nozzle is an arc chamber. The arc chamber is filled with the test gas. The test gas is then heated by an electric arc, creating a high pressure and high temperature reservoir for the nozzle inlet.

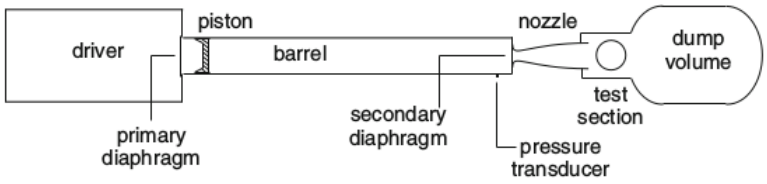

Figure 8: Schematic diagram of a gun tunnel. [30]

Another way to create high pressure and high temperature nozzle inlet reservoirs is to compress the test gas using a light free piston. Facilities operating in this way are known as gun tunnels, shown in Figure 8. To operate the gun tunnel, the driver section is pressurized and the barrel section is filled with the test gas. Once the primary diaphragm ruptures, the piston is pushed downstream through the barrel by the high pressure driver gas and compresses the test gas. A shock wave forms in front of the piston and propagates down the barrel at a higher velocity than the piston. The shock wave will reflect off of the end of the barrel and the secondary diaphragm will rupture. The shock wave will reflect between the upstream face of the piston and the end of the barrel multiple times as the piston travels downstream. As the piston travels downstream, it will decelerate as the test gas pressure increases. Eventually the piston will stop and a peak in test gas pressure in the barrel will be reached. In the case of the Longshot gun tunnel, as the peak pressure is reached, a system of valves at the downstream end of the barrel closes, trapping a high pressure and high temperature reservoir for the nozzle inlet [53]. In this case, the fixed volume reservoir will not be influenced by the motion of the piston as it rebounds upstream and this prolongs the test time.

3.2 High Enthalpy Facilities

Under high enthalpy conditions where the velocity is around 2 – 7 km/s, real-gas effects such as vibrational excitation and chemical reactions like dissociation and recombination occur behind strong shocks created by blunt bodies. For these kinds of blunt body flows, the Mach number becomes irrelevant while the freestream density and velocity become important simulation parameters. To create these high enthalpy conditions, higher pressure and temperature reservoirs are required at the inlet of a convergent-divergent nozzle compared to those found in low enthalpy facilities. This can be achieved by driving a strong shock wave through a tube filled with test gas while having a small enough nozzle throat, which at the beginning is closed by a secondary diaphragm, such that a reflected shock forms to create a stagnated nozzle inlet reservoir. These facilities are known as reflected shock tunnels, shown in Figure 9. In most cases, the test time terminates when the driver gas arrives at the test section and this topic is discussed in detail in section 4.2.1.

When the primary diaphragm ruptures, for given filling conditions in the driven tube the speed of the shock wave formed in the shock tube depends on the initial driver gas pressure and driver gas speed of sound, which consequently depends on the temperature and chemical composition. This relationship is shown in Figure 10 for a pure helium driver assuming calorically perfect and thermochemical equilibrium gas, where the equilibrium results were computed using the PITOT code [54]. From Figure 10, one of the results is that real gas effects decrease the shock speed. It is also important to note that the driver section often has a larger diameter than the shock (driven) tube. In this case, after diaphragm rupture for a free piston driver, the driver gas undergoes a steady expansion to a choked throat condition, M = 1, before an unsteady expansion into the driven section [54], provided the driver gas behind the contact surface reaches supersonic speed. This is done for improved performance, as can be observed in Figure 10 with shock speed improvements of around 20 %, because a steady expansion provides a higher velocity increase in subsonic flow than an unsteady expansion for a given pressure difference [55] [56]. Furthermore, one of the most important result in Figure 10 is that for a given driver gas at high pressure ratios, an increase of its temperature is much more effective than an increase of its pressure, concerning a gain in shock speed. As a matter of fact, at infinitely large pressure ratios, p_4/p_1, the shock speed U_s approaches the finite value,

$$U_s = \frac{\gamma_1 + 1}{\gamma_4 - 1} a_4 \tag{24}$$

where a_4 and γ_4 is the speed of sound and ratio of specific heats of the driver gas respectively, assuming calorically perfect gas. In this aspect, it is desirable to select a driver gas with a low molecular weight, resulting in a naturally high speed of sound at a given temperature, for use as the driver gas. Consequently, helium and hydrogen are popular driver gases. Using electrical resistance heaters, helium and hydrogen can be heated up to 800 K [57]. Assuming air as the test gas, $a_4/a_1 \approx 4.8$ and $a_4/a_1 \approx 6.2$ can be obtained using heated helium and hydrogen respectively. From heated helium, the TH2 reflected shock tunnel could produce a nozzle exit velocity of up to 3.6 km/s while, from heated hydrogen, the LENS I reflected shock tunnel could produce a nozzle exit velocity of up to 5.0 km/s [43]. However, to produce velocities greater than 4 - 5 km/s, it is necessary to use other methods which allow the driver gas to be heated beyond 800 K as it is unsafe, expensive and inefficient to use very high driver pressures for performance gains. In fact, for a given a_4/a_1, it is impossible to attain certain shock speeds regardless of how high the driver pressure is because the shock speeds effectively asymptotes as shown in Figure 10 and by equation 24.

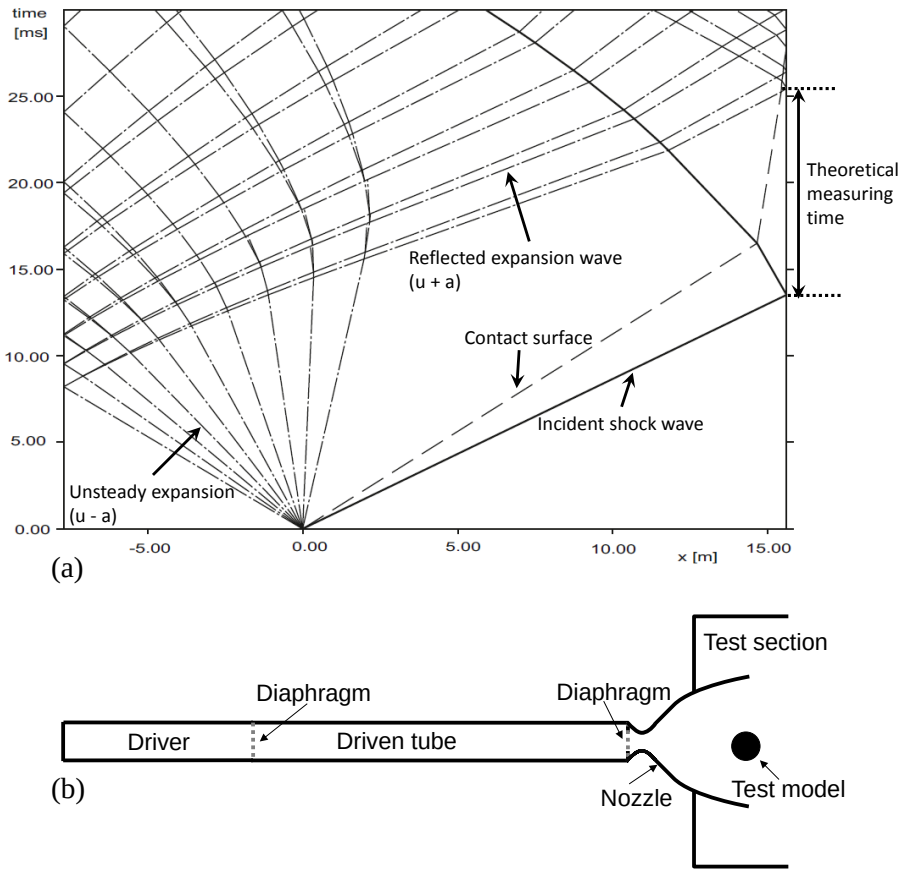

Figure 9: Wave diagram (a) and schematic (b) of a reflected tunnel.

One way to achieve very high driver gas temperatures is heating the driver gas with an electric discharge. Such drivers are known as electric arc drivers and can heat helium to 20000 K resulting in $a_4/a_1 \approx 24$ [58]. This driver method is used for the 10 cm inner diameter shock tube facility EAST (Electric Arc Shock Tube) at the NASA Ames Research Centre, which can also run as a shock tunnel [59]. When operated as a reflected shock tunnel, total specific enthalpies of more than 30 MJ/kg could be achieved. However, the total pressures corresponding to these high enthalpy conditions were less than 20 MPa [57]. Consequently, while there is no doubt that

electric arc heating can generate very high temperature driver gas, it remains to be seen whether high temperature gas can be produced at high pressures necessary for high total pressure operation.

Another way to achieve high heating of the driver gas is to compress the gas almost adiabatically, and virtually isentropically [60] [61], with a heavy free piston. This method was first reported by Stalker and Besant in 1959 [62] and is currently used in various reflected shock tunnels around the world, including HEG in Germany, HIEST in Japan, T5 in the USA and T4 in Australia [35]. These free piston driven shock tunnels are known as Stalker tunnels, named after the pioneer of the free piston driver. Helium is normally used as the driver gas for free piston drivers. A certain amount of argon is sometimes mixed with helium to control the performance of the free piston drivers. The driver gas typically gets compressed to pressures in the range of tens to the low hundreds of MPa when the diaphragm ruptures [63] [61]. Values of $a_4/a_1 \approx 12$ can be achieved in free piston drivers [64] [65], as is demonstrated by the free piston driver of HEG, T4 and T5 which heats helium driver gas to over 4000 K [63]. The largest Stalker tunnel currently in regular operation is HIEST with a test section diameter of up to 1.2 m [39]. A new Stalker tunnel, FD21, is currently being put into operation in China and would become the biggest Stalker tunnel in the world, having a test section diameter of 2.0 m and a total length of more than 110 m [40].

A third way to heat helium driver gas is to add a certain amount of hydrogen-oxygen, for example, with the helium driver and this allows the use of deflagrative combustion to heat the driver gas mixture. The optimum helium content for performance, is about 50 - 80 % by volume [66]. While the combustion process allows the gas mixture to be heated to about 2500 K, the amount of water vapour formed from combustion increases the average molecular weight of the driver mixture. As a result, this driver method can produce $a_4/a_1 \approx 7$ - 8. Currently, no hypersonic facility in operation utilizes this deflagrative combustion driver method. The issue with this method is that the post-combustion pressure is limited to about 40 MPa due to the need to suppress detonation. Consequently, detonative combustion methods have been developed to overcome the pressure limitation of the deflagrative combustion method. For the detonation driver, the optimum helium content for performance, is about 30 - 60 % by volume and this can result in $a_4/a_1 \approx 7 – 8$ [66]. So the performance characteristics of the detonation driver is similar to that of the deflagrative driver except detonation drivers allow for higher driver pressures to be attained. Currently operating detonation driven shock tunnels include TH2 in Germany and JF12 in China [67].

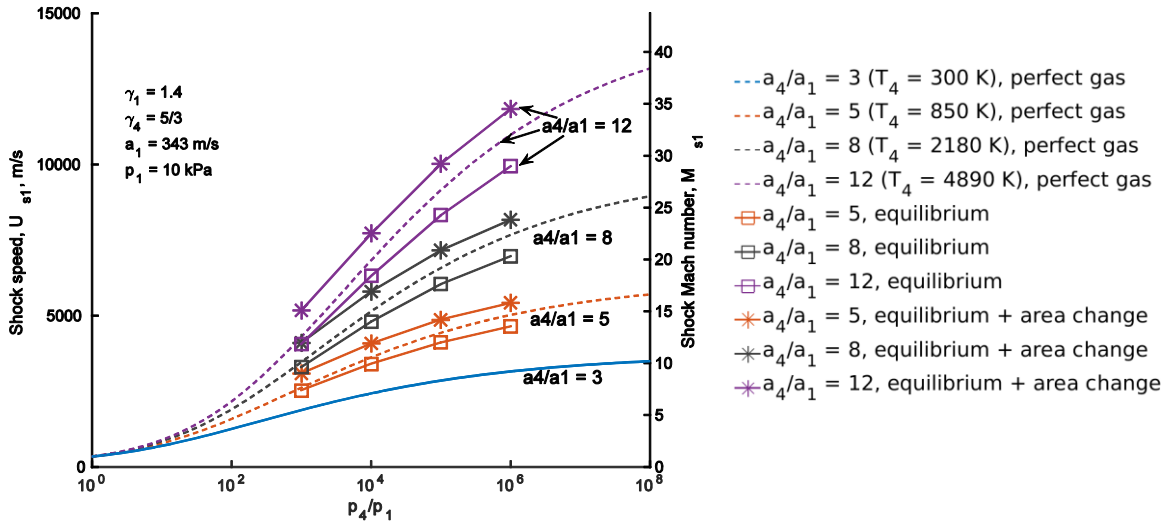

Figure 10: Relationship of shock speed and pressure ratio between the driver pressure, P_4, and test gas fill pressure, P_1, with different speed of sound ratios between the driver, a_4, and test gas, a_1, for a pure helium driver.

Compared to the free piston driver, the clear disadvantage of the detonation driver is the inferior performance. Furtheron, the storage and handling of hydrogen requires safety precautions. After each experiment the water as product of the detonation combustion has to be removed off the facility by evacuation or other means. This limits the number of shots within a certain period of time. Nevertheless, detonation drivers are sometimes selected over free piston drivers due to its low cost. Free piston drivers are much more expensive. Also, free piston drivers are much more complex in their mechanical setup and therefore require much more experience in operation. Detonation drivers do not need any complex mechanical systems and therefore are much easier to operate than free piston drivers. Hence, detonation drivers allow for a convenient performance upgrade from a conventional helium/hydrogen driven shock tunnel without significant hardware modification. An example of a facility doing such an upgrade is the TH2 [68] reflected shock tunnel.

In a reflected shock tunnel, three different processes can occur in the shock tube when the reflected shock wave meets the constant surface. This is illustrated in Figure 11. In the undertailored operation, the shock wave interaction with the contact surface causes a transmitted shock and a reflected expansion wave that propagates towards the end of the shock tube. In the overtailored operation, a transmitted shock as well as a shock wave which reflects off the contact surface is generated. In this case, behind the first interaction the contact surface continues to travel downstream while reflected shock waves travel back and forth between the contact surface and the end of the tube. In the tailored operation, the reflected shock wave travels through the contact surface and, in case of a closed shock tube, reduces the velocity of the contact surface to zero. In this case, no further expansion waves or reflected shock waves are formed. Generally, the tailored operation is the most desirable form as it allows for a steady nozzle reservoir state and a long test time. Furtheron, it results in a reduced driver gas contamination of the test gas (see section 4.2.1) because in this case there is only one interaction of the reflected shock with the contact surface. In case of an overtailored operation the multiple reflections of the shock at the contact surface cause the generation of a new driver gas wall jet with each reflection. Therefore, driver gas contamination is a serious concern for overtailored operation. For the undertailored mode, during the first shock-contact surface interaction, the reflected expansion wave accelerates the hot test gas away from the nozzle entrance and therefore the velocity of the driver gas wall jet is at least decelerated which leads to a reduced driver gas contamination. Therefore, in respect to driver gas contamination a slight undertailored operation is desirable.

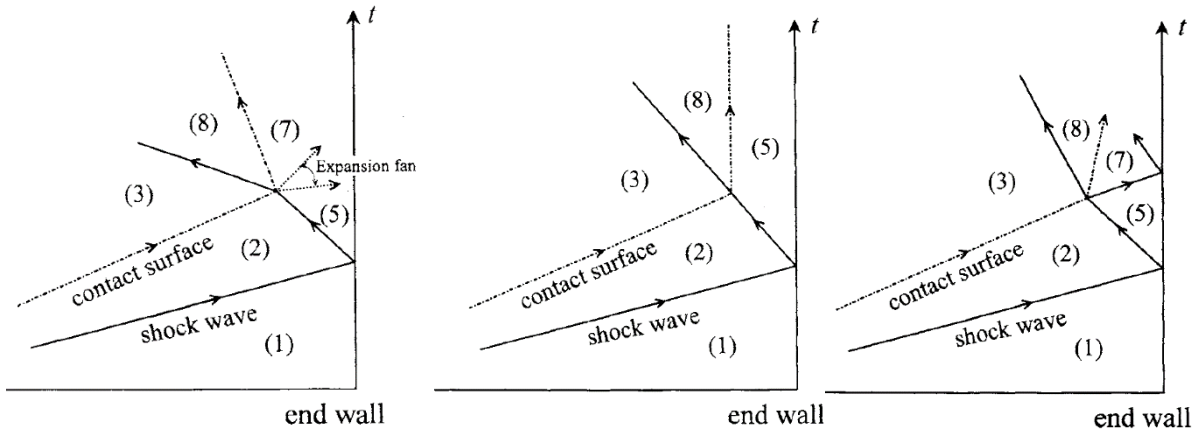

Figure 11: x-t wave diagrams of shock wave/contact surface interactions for undertailored (left), tailored (middle) and overtailored (right) configurations. Dashed lines represent contact surfaces while solid lines represent shock waves. [69]

For a given driver condition, a tailored operating condition can only be obtained for a unique driven section filling condition and vice versa. Using the methodology outlined by Nishida [69] and assuming inviscid, calorically perfect gas, the driver conditions necessary for tailored operation and the resulting shock speeds were calculated for different driver gases given that the test gas initially filled in the shock tube is air at room

temperature. The results are presented in Figure 12. This figure should only give qualitatively an estimation of the magnitude of the shown parameters since the assumption of a calorically perfect gas is not valid for the shown high driver gas temperatures and shock speeds. Because of the requirement of tailored operation, it is not so convenient to vary the shock speed which could otherwise be done by varying the driver gas temperature and the ratio of driver pressure, p_4, to driven section fill pressure, p_1, to any arbitrary combination. As an example from the results in Figure 12, to generate a 6 km/s shock in room temperature air using a helium driver, the driver needs to have a temperature of around 6300 K and a pressure of around $3000p_1$ for tailored operation. If the facility cannot heat helium to 6300 K, compensating by increasing the value of p_4/p_1 is not an option as it would result in untailored interface conditions. Instead, a solution could be to use hydrogen as the driver gas as it would produce a 6 km/s shock when heated to only around 2200 K. Hence, as mentioned by Lukasiewicz [56], operation of reflected shock tunnels often involves using different types of driver gas conditions and driver gas mixtures to maintain tailored interface configurations at different total enthalpy test conditions. Nevertheless, from Olivier [34], Marineau et al. [70] and Sudani et al. [71], operating reflected shock tunnels at slightly off-tailored conditions may still be acceptable. In particular, operating at a slightly undertailored condition is even recommended by Sudani et al. [71] for improved test time at the cost of a slightly less steady nozzle exit condition. However, operating overtailored should always be avoided due to pronounced driver gas contamination on top of a less steady nozzle exit condition [71] [72] [37].

Assuming a tailored interface, the ratio of nozzle reservoir pressure, p_5, to driver pressure, p_4, for different shock speed conditions are calculated assuming as above inviscid, calorically perfect gas and in the same way as Nishida [69]. The ratio p_5/p_4 is often called the pressure recovery factor or the recovered pressure. The results are presented in Figure 13 and they show that the driver pressure, p_4, needs to be of a comparable value to the desired total pressure of the test condition as the pressure recovery factor is about 0.9 for most conditions. Similarly, for a free piston helium driver, Stalker and Hornung [73] calculated the pressure recovery factor for air as test gas to be about 1.8 under tailored interface operation in the case of an area change at the driver-shock tube junction. With the influence of real gas effects, p_4 should still be in the same order of magnitude as the desired total pressure of the test flow under tailored conditions. This means that the value of p_4, and consequently p_1 due to Figure 13, cannot be arbitrary if a test condition with a particular total pressure is desired. For example, if heated helium is used as the driver gas and a test condition with a total pressure in the hundreds of MPa is required, then p_4 also needs to have a value in the hundreds of MPa while p_1 needs to have a value around the hundreds of kPa. Also, from Figures 12 and 13, it can be observed that the total pressure of the test conditions can be varied without influencing the shock speed while operating under tailored interface conditions.

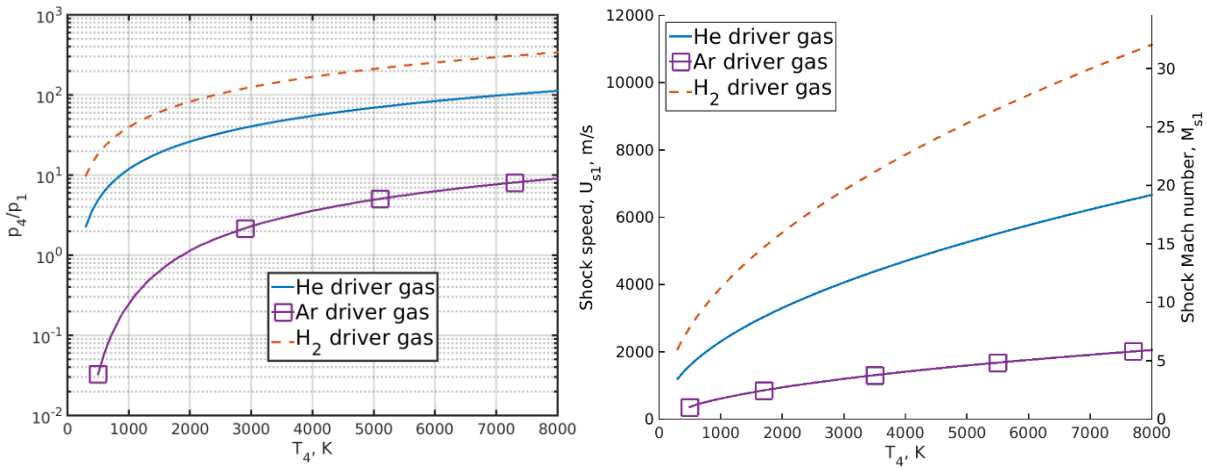

Figure 12: The ratio of driver pressure, p_4, to driven section fill pressure, p_1, (left) and the shock speed, U_{s1}, (right) for tailored operation at various driven gas temperatures, T_4, for a test gas of air initially at room temperature and three different driver gases.

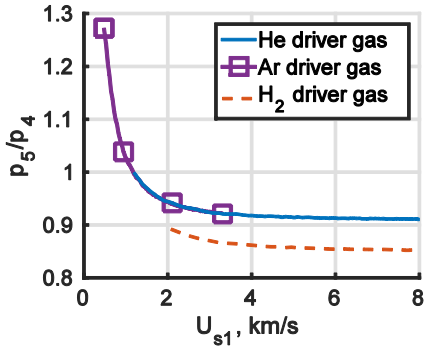

Figure 13: The ratio of nozzle reservoir pressure, p_5, to driver pressure, p_4, versus shock speed, U_{s1}, for tailored operation given a test gas of air initially at room temperature and three different driver gases.

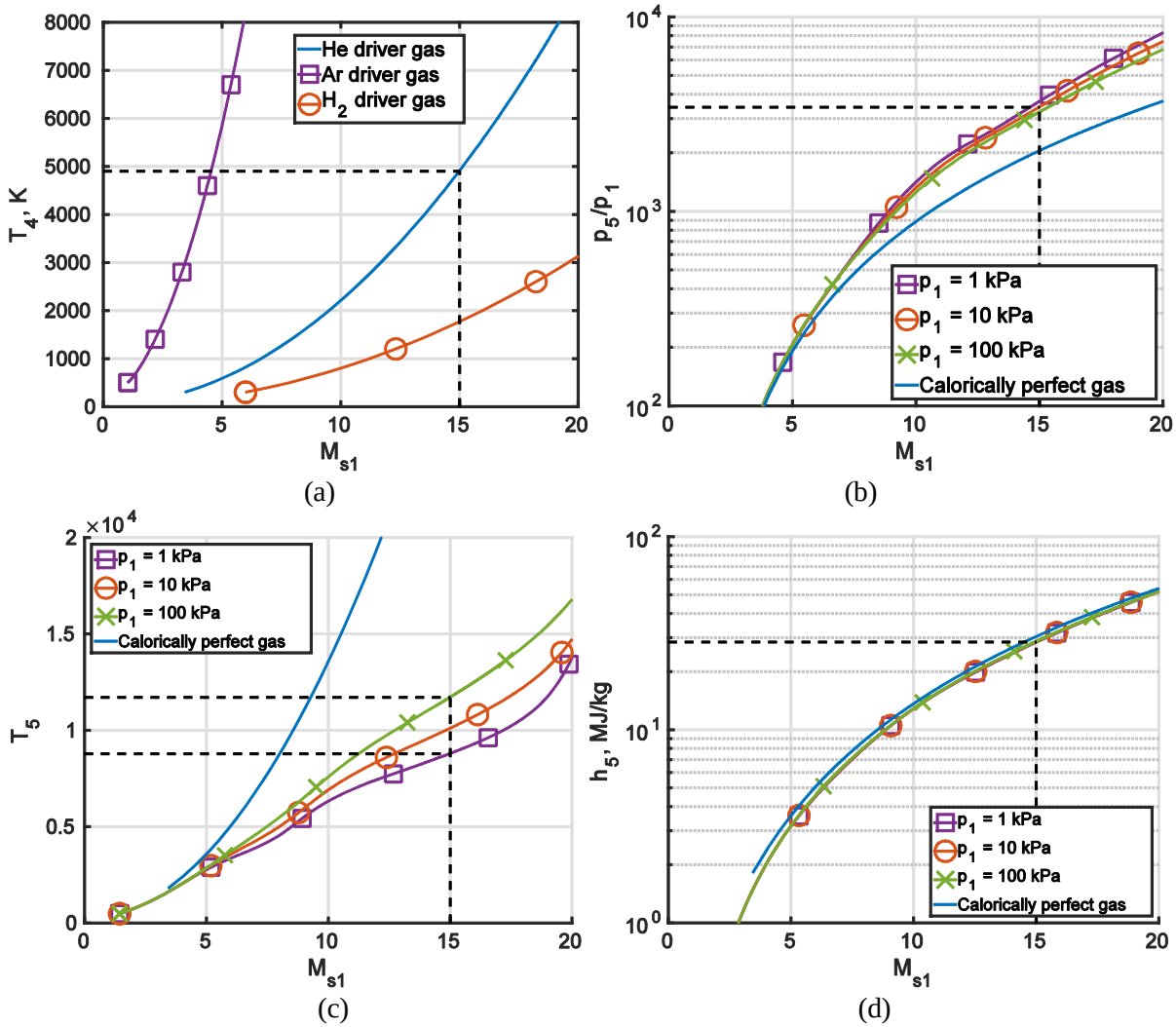

Figure 14: The driver temperature and shock Mach number, M_{s1}, relationship for tailored operation is shown in (a) for calorically perfect gas. Figure (b), (c) and (d) shows the relationship of the nozzle reservoir pressure, P_5, temperature, T_5, and enthalpy, h_5, respectively with M_{s1} for both thermochemical equilibrium and calorically perfect gas.

Consider a representative high performance free piston driver heating helium to around 5000 K, a shock Mach number, M_{s1}, of 15 is produced for tailored operation in a reflected shock tunnel as shown in Figure 14 (a). It has to be noted that the graph shown in Figure 14 (a) has been determined for calorically perfect gas since the underlying theory is only valid for calorically perfect gas. Figure 14 (b) to (c) show the nozzle reservoir conditions for a range of M_{s1} at typical shock tunnel fill pressures of air assuming thermochemical equilibrium. All thermochemical equilibrium calculations reported in this paper were performed using the CEA code of NASA [74]. Given $M_{s1} = 15$, the resulting nozzle reservoir condition is, $p_5 \approx 3.4 – 340$ MPa for the given initial pressure, $T_5 \approx 8800 – 11700$ K and $h_5 \approx 28$ MJ/kg. The currently operational reflected shock tunnels generally do not operate above these conditions. The performance of reflected shock tunnels is generally limited to about 7 km/s for nozzle exit velocity, 25 MJ/kg for total enthalpy, 10000 K for total temperature and 200 MPa for total pressure [66]. However, the main contributor to this performance limitation is generally not from driver capabilities as modern impulse facility drivers, particularly free piston drivers, have the potential of supporting higher velocity and total pressure conditions. The performance limitation of reflected shock tunnels mainly arises from the current material limitations. The high stagnation pressure causes a structural problem while the high stagnation temperatures causes a material heating problem. Furthermore, the influence of premature arrival of driver gas at the test section increases with increasing shock velocity resulting in almost no test time beyond 7 km/s (25 MJ/kg) for the case of the T3 [60] and T5 [65] reflected shock tunnels. Also, significant radiation losses by the nozzle reservoir above total enthalpies as low as 10 MJ/kg [75] make reflected shock tunnels inefficient facilities for producing very high enthalpy flows.

3.3 Very High Enthalpy Facilities

So far, all the facilities discussed involves expansion of a stagnated reservoir through a converging-diverging nozzle. However, in order to generate conditions with higher total pressures and total temperatures, it is necessary to not stagnate the test gas. In this way, one such facility which allows high enthalpy conditions is the non-reflected shock tunnel. This facility is almost identical to a reflected shock tunnel except the nozzle is a purely diverging nozzle because the test gas does not stagnate at the end of the shock tube but, instead, travels "straight-through". While non-reflected shock tunnels allow for higher performance, the test time of a shock tunnel in non-reflected mode is always significantly less than its test time in reflected mode [57]. There are currently no non-reflected shock tunnels in operation.

Alternatively, a shock tunnel can be operated without a nozzle, as just a shock tube. Shock tubes have been in use for studying shock waves since 1899 [76] and still remains an important research instrument today for the study of thermochemical kinetics and radiation [77]. Shock tubes are often used to study low and medium enthalpy conditions as well as high enthalpy conditions. In general, unlike the other facilities, shock tubes are not used to generate flows around test models. Instead, the moving shock wave (in the lab frame of reference) in the shock tube is studied. While the obvious disadvantage is that the variety of experiments in shock tubes are limited, there are numerous advantages of shock tube experiments. Firstly, the core flow in a shock tube is limited to one-dimension which allows the thermochemical kinetics and radiation to be studied under a simple gasdynamic environment. In fact, for low and medium enthalpy conditions, a fully stagnated condition can be created at the end of the shock tube to force a zero-dimensional gasdynamic environment to completely isolate the thermochemical kinetics and radiation phenomena. In addition, showing that the shock tube has versatility, the Electric Arc Shock Tube (EAST) at NASA Ames will soon be used to study the nonequilibrium and radiation of expanding flows [78].

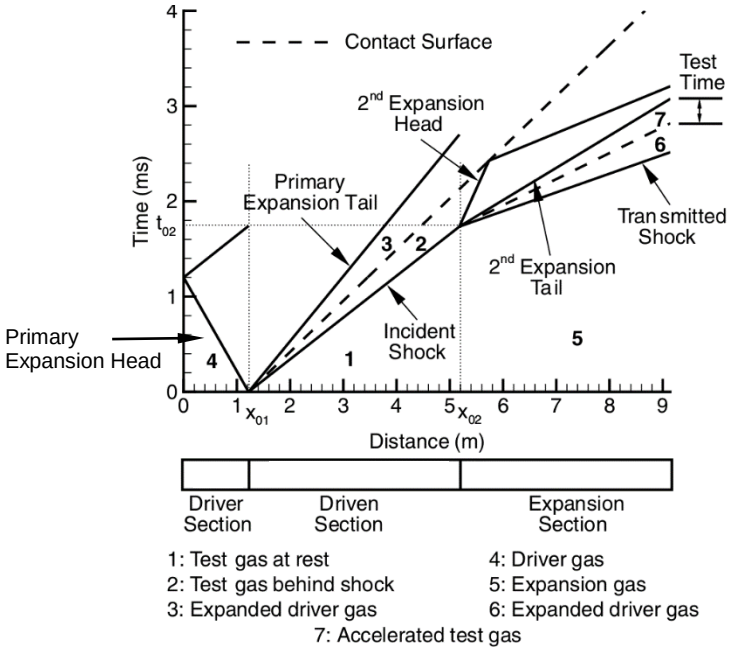

Figure 15: Schematic and x-t diagram of an expansion tube showing the typical wave processes which occur during operation. [47]

Another advantage of shock tubes is that it has an accurately defined freestream condition. Studying shock waves which are moving in the lab frame of reference, the freestream condition is just the stationary shock tube fill condition, of which the pressure, temperature and chemical composition are known. This is in contrast to the other test facilities where the experimental freestream is the hypersonic nozzle exit condition. In these cases, the experimental freestream could be very difficult to define accurately and this is discussed in detail in section 4.2.3.

Another facility which can be used to produce high enthalpy conditions is the expansion tube, shown in Figure 15, which was first proposed by Resler and Bloxsom in 1952 [79]. In the expansion tube, the shock tube is connected to an additional tube of the same inner diameter, called the acceleration tube, which is initially separated from the shock tube by a weak diaphragm and is evacuated to very low pressures. When an expansion tube experiment is initiated, a shock wave passes through the shock tube, shock heating the test gas and then breaking the secondary diaphragm when it reaches the end of the shock tube. An unsteady expansion forms after the rupture of the secondary diaphragm. The shock heated test gas travels through the unsteady expansion as it flows through the acceleration tube and this increases the total pressure and total enthalpy of the test gas. The unsteady expansion performs work by the time-dependent pressure force which according to the equation [56],

$$\frac{dh_0}{dt} = \frac{1}{\rho}\frac{\partial p}{\partial t} \tag{25}$$

leads to a total enthalpy increase for part of the gas. As explained by Morgan [80], the unsteady expansion causes a total pressure and total enthalpy multiplication, the magnitude of which depends purely on the Mach number of the expanded test gas, M_7, according to perfect gas analysis. This general trend is also observed in thermochemical equilibrium analysis, shown in Figure 16 and calculated using the PITOT code [54], where the relationship between M_7 and the magnitude of multiplication was calculated for an air test gas with a fill pressure of P_1 = 10000 Pa subjected to different shock speeds, $U_{s,1}$. For the range of M_7 shown, which is realistic for a typical expansion tube, the test gas total enthalpy and total pressure could increase by a factor of around 2 – 4 and 40 – 1000 respectively from its value after shock heating in the shock tube. Thus, for a given

driver, the expansion tube can generate the highest total pressure and total enthalpy conditions of all the facilities.

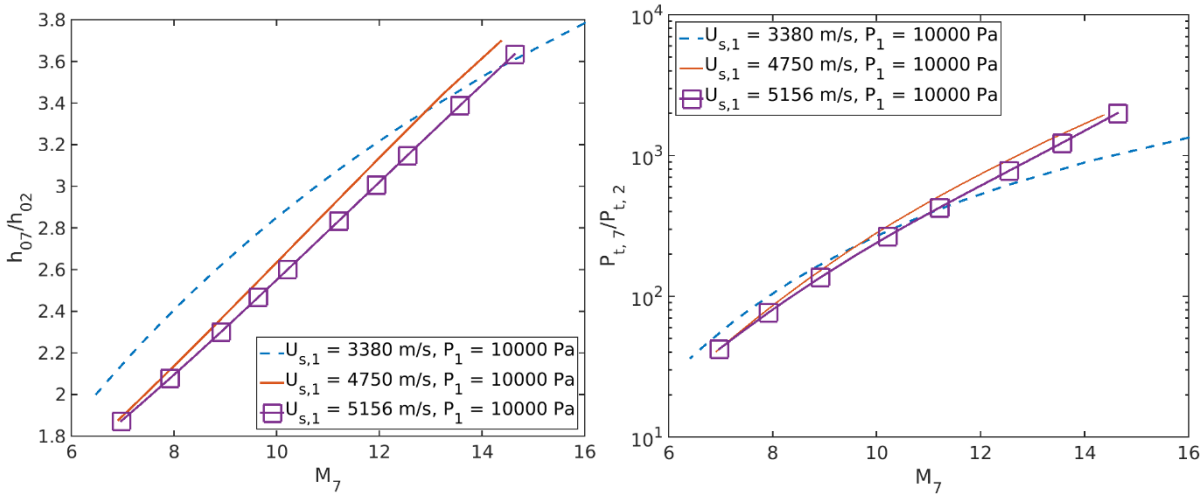

Figure 16: Total enthalpy (left) and total pressure (right) gains across an unsteady expansion under thermochemical equilibrium conditions. h_{07} and $P_{t,7}$ refers to the total enthalpy and total pressure respectively of the test gas after unsteady expansion to a Mach number M_7. h_{02} and $P_{t,2}$ refers to the total enthalpy and total pressure respectively of the test gas after shock heating by a shock with speed $U_{s,1}$ for a fill pressure of P_1.

One of the earliest operational expansion tube was run by Miller [81] at NASA Langley in the 1970s. While the facility demonstrated its performance potential, it was decommissioned in 1983 because very few usable operating conditions could be produced due to severe noise in the test flow. Consequently, the expansion tube facility was not established as a reliable research tool until the early 1990s when Paull and Stalker [82] found a solution to inhabit the severe perturbation present in the test flow. The noise in the test flow was found to be acoustic disturbances transferred from the expanded driver gas, and the source of the noise in the driver gas was the primary diaphragm rupturing process. All frequency components of the acoustic disturbance in the test gas are focused into a narrow frequency bandwidth during the unsteady expansion causing significant noise during the test time. The noise in the test flow can be reduced by reducing the transmission of acoustic disturbances from the expanded driver gas to the test gas prior to the unsteady expansion of the test gas. This can be done by designing the test conditions such that the speed of sound in the shock processed test gas is at least 1.3 times larger than the speed of sound in the expanded driver gas, as proposed by Morgan [80]. Meeting this requirement permits the contact surface to act like an acoustic buffer which attenuates the transmission of acoustic disturbances from the expanded driver gas to the test gas. Nowadays, Lawson and Austin [16] reports that it may even be possible to generate conditions in the expansion tube with freestream disturbances low enough for accurate boundary layer transition studies with real gas effects.

Expansion tubes can be fitted with nozzles to operate as expansion tunnels. The expansion tunnel has a distinctly longer test time than the non-reflected shock tunnel and a significant reason for this is because the accelerator gas, instead of the test gas, is used for nozzle start-up, unlike in a shock tunnel where test gas is wasted on nozzle start-up. Nevertheless, the expansion tunnel still has a much shorter test time compared to a reflected shock tunnel of a similar size. Additionally, although expansion tubes can be operated with nozzles to provide an increase in the test section size (and a small increase in the test time), the area increase by expansion tunnel nozzles are much small than that by reflected shock tunnels. For example, the nozzle exit area to shock tube area of HEG nozzles range from 8:1 to 34:1 while the nozzle area ratio of the X2 expansion tunnel is only 5.64. Therefore, for a shock tube of the same diameter, a reflected shock tunnel would always have a much larger test section than an expansion tunnel.

The expansion tube and tunnel, however, are not exclusively used for generating high total pressure and/or total enthalpy conditions, as shown in Figure 20. Expansion tubes such as the one at Stanford University [46] and the one at The University of Michigan (MHExT) [45] operates low enthalpy test conditions for the study of combustion, while the X2 expansion tunnel operating with a conventional helium driver provides medium enthalpy conditions for the study of CO_2 thermochemical nonequilibrium and radiation [83]. Hence, while the reflected shock tunnel has significantly longer test times and allows for the use of larger test models than the expansion tube, the thermochemical state of the test flow generated by expansion tubes is more realistic of flight. This is because in a reflected shock tunnel, complete thermochemical equilibration is unlikely to occur through the nozzle expansion. So, as the test gas never stagnates in the expansion tube and the occurrence of the unsteady expansion provides a total enthalpy multiplication, the test gas does not reach as high of a temperature as would be required in a reflected shock tunnel to generate the same condition.

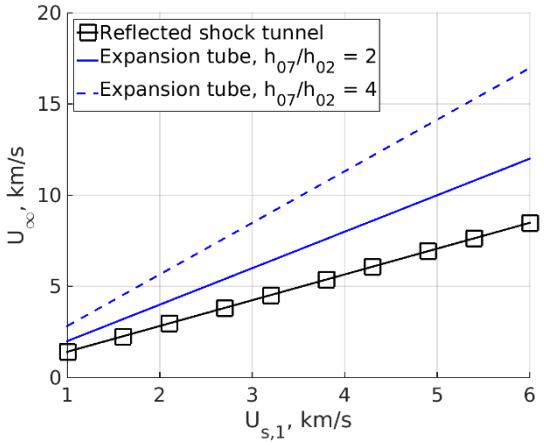

Figure 17: An approximate relationship between the test section velocity and the shock speed required for reflected shock tunnels and expansion tubes.

Assuming that the total enthalpy of the shock heated test gas is $h_{02} \approx U_{s,1}^2$ [57] which holds for high shock Mach numbers and assuming the total enthalpy of the test flow is $h_{0\infty} = 0.5U_{\infty}^2$, Figure 17 is produced which illustrates the benefits of the total enthalpy multiplication occurring in expansion tubes. The figure shows that, given a required test section velocity, U_{∞}, the shock speed, $U_{s,1}$, required to generate this test flow is significantly less in expansion tubes compared to reflected shock tunnels. For example, to generate a 4.0 km/s flow at the nozzle exit of a reflected shock tunnel, a shock tube shock speed of about 3.0 km/s is necessary and this would heat the test gas to a temperature of almost 6000 K after shock reflection, resulting in significant dissociation of the test gas. On the other hand, to generate the same condition in an expansion tube, a shock tube shock speed of only about 2.0 km/s is required, resulting in very little dissociation of the test gas. Therefore, for a given test condition, the one generated by an expansion tube will always be closer to thermochemical equilibrium compared to the one generated by a reflected shock tunnel. Furthermore, even for superorbital expansion tube conditions where significant dissociation occurs in the test gas by shock heating, some experimental results seem to indicate thermochemical equilibrium across the unsteady expansion [84] and this will be discussed in detail in section 4.2.3.

4.0 REQUIREMENTS AND LIMITATIONS OF GROUND TEST FACILITIES

The previous section introduced the characteristics of various different hypersonic ground test facilities. Now it is necessary to identify what is required of the facilities so that the capabilities and limitations of the current facilities can be recognized.

4.1 Performance Requirements and Limitations to Simulate Flight

As discussed in section 2, a significant portion of experimental work in hypersonics involves reproducing flows past actual aircrafts and spacecrafts for engineering purposes. Therefore, it is important to identify portions of flight trajectories which can and cannot be simulated by current ground test facilities. Some representative trajectories of typical flight vehicles are shown in Figure 18 and these values are used for the analysis in this section.

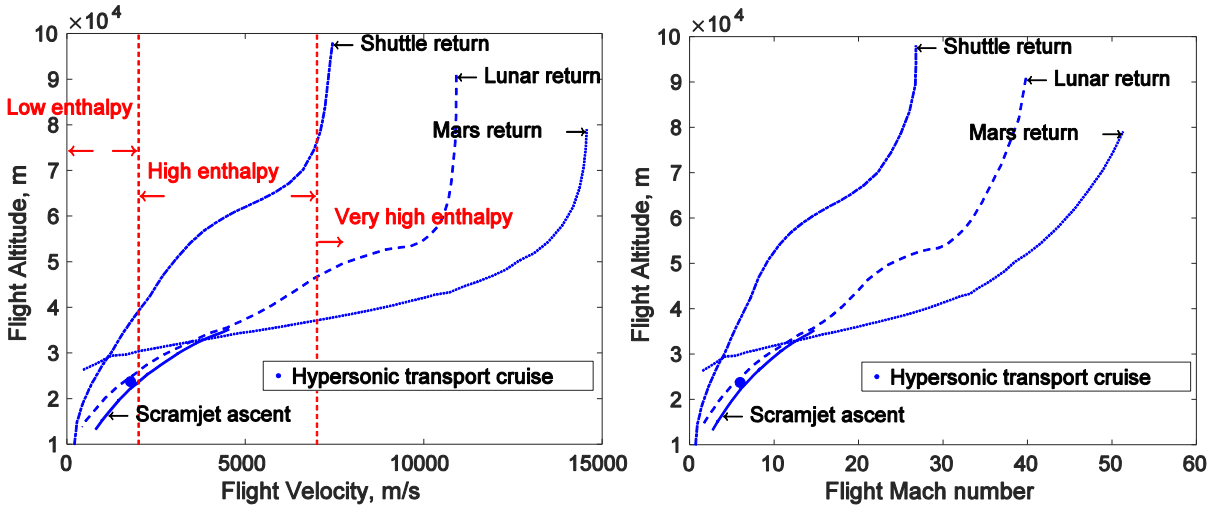

Figure 18: Representative trajectories of typical flight vehicles direct entry given in terms of the Mach number, left, and velocity, right, obtained from [22] [85] [86] [87].

An ideal ground testing would require the duplication of the real atmospheric and flight data. In order to recreate the Mach number, Reynolds number, ρ-L scaling, velocity and total enthalpy of a flight vehicle, it would be necessary to recreate the chemical composition, freestream velocity, freestream static temperature and, in the case of using a full scale test model, the freestream static pressure/density of the flight condition.

4.1.1 Low enthalpy flow regime

It is easy to show that full scale testing for hypersonic flow conditions is not feasible even for relatively low enthalpy conditions. Exemplarily, a wind tunnel of 5 m x 5 m cross-section simulating the flow conditions at 35 km altitude at Mach number 6 would require a theoretical driving power of 700 MW. Therefore, scaled model testing is the normal case. As shown in section 2.1.1, in low enthalpy flows no chemical reactions take place and therefore the gas can be considered as thermally perfect. In this flow regime the most important simulation requirements are given by the Mach number, the Reynolds number and for certain flow cases the wall temperature ratio. Depending on the considered flow phenomena, the freestream velocity may or may not be duplicated. The duplication of the flight velocity is of importance, for example, for full scale scramjet testing in order to simulate the correct travelling time of the flow through the engine. In case there is no need to duplicate the freestream velocity, this leads to some weaker requirements on the wind tunnel testing parameter as it is shown in the following. In this case only Mach and Reynolds number should be duplicated leading to the statement given in equation 1. The Reynolds number is given by,

$$Re = \frac{\rho_\infty U_\infty L}{\mu_\infty} \tag{26}$$

with

$$\rho_\infty = \rho_0 * f_1(\gamma, M_\infty) \tag{27}$$

$$U_\infty = a_\infty M_\infty = \sqrt{\gamma R \frac{T_\infty}{T_0}} * \sqrt{T_0} * M_\infty \tag{28}$$

$$U_\infty = \sqrt{T_0} * f_2(\gamma, M_\infty) \tag{29}$$

and the usual approximation for the viscosity,

$$\mu_\infty = C * T_\infty^n \tag{30}$$

where the subscript 0 refers to the total conditions and C is a constant. With this and the equation of state for the reservoir condition, the Reynolds number can be reformulated as a function of the total pressure, temperature and Mach number,

$$Re = \frac{p_0 L}{T_0^{n+0.5}} f(\gamma, M_\infty) C_1 \tag{31}$$

where C_1 is a new constant. From the simulation requirement, $Re_{wt} = Re_{fl}$, then for identical Mach numbers it directly follows,

$$\frac{p_{0,wt}}{p_{0,fl}} = \left(\frac{T_{0,wt}}{T_{0,fl}}\right)^{n+0.5} \frac{L_{fl}}{L_{wt}} \tag{32}$$

where L_{wt}/L_{fl} is the model scale. It is desirable to keep the wind tunnel total pressure and temperature as low as possible. The lower limit of the wind tunnel total temperature follows from the desired freestream Mach number and the condensation onset of air which is pressure dependent. However, typically the freestream temperature should not be lower than 50 K to avoid condensation. In this case the total temperature amounts to 410 K for $M_\infty = 6$ and to 1050 K for $M_\infty = 10$. It is obvious that the wind tunnel total temperature can be less than the flight total temperature, for example the factor with the total temperature ratio in equation 32 is less than one resulting in a reduction of the wind tunnel total pressure. However, the wind tunnel total pressure is proportional to one over the model scale. This impressively shows the smaller the model scale the larger the necessary wind tunnel total pressure. In other words, large wind tunnel models allow lower reservoir pressures.

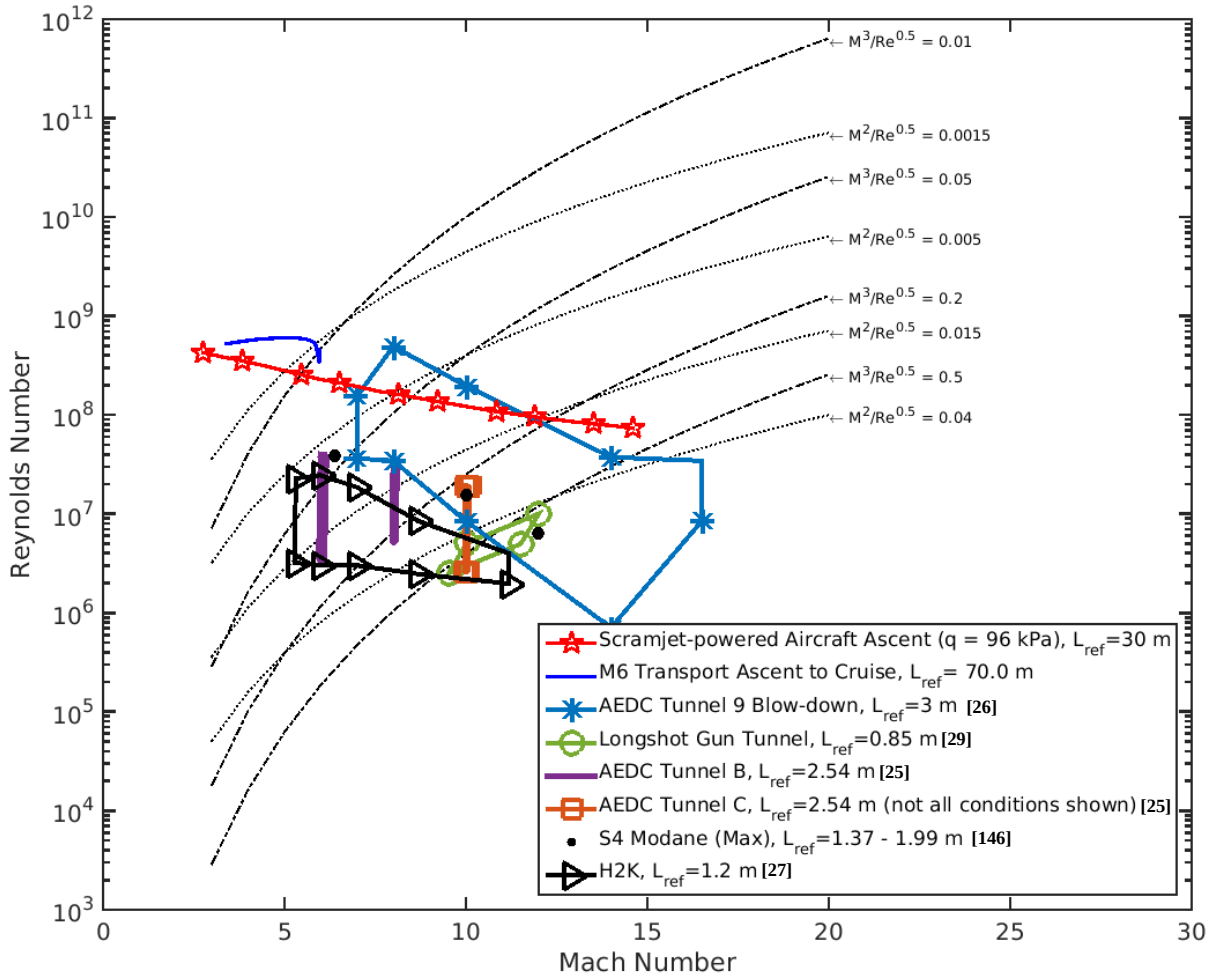

Figure 19: Reynolds number versus Mach number capabilities of low enthalpy facilities compared to flight trajectories.

In case the freestream velocity should be replicated beside of the Mach and Reynolds number, it follows from the Mach number that the freestream static temperature and therewith also the viscosity are identical for both flight and wind tunnel. In this case the requirement of identical Reynolds number yields,

$$(\rho_\infty L)_{wt} = (\rho_\infty L)_{fl} \tag{33}$$

or for identical Mach numbers,

$$\left(\frac{p_0}{T_0} L\right)_{wt} = \left(\frac{p_0}{T_0} L\right)_{fl} \tag{34}$$

Since Mach number and freestream static temperature are identical, the same holds for the total temperatures. Therefore, it follows,

$$\frac{p_{0,wt}}{p_{0,fl}} = \frac{L_{fl}}{L_{wt}} \tag{35}$$

which also results from equation 32 for $T_{0,wt} = T_{0,fl}$.

The dependence of the wind tunnel total pressure on the model scale leads to enormous total wind tunnel pressure for high Mach numbers. For example, Table 2 gives the necessary total pressure and temperature for a wind tunnel duplicating the flight Reynolds number for 35 km altitude as well as the flight Mach number and velocity for a typical model scale of 1:50 of a hypersonic transport vehicle. The data in Table 2 has been determined for equilibrium air chemistry. This simple example notably shows that for continuous running facilities there is not only a limitation due to power requirements but also due to the necessary high total pressures and temperatures. For the continuous running facilities there is a clear Reynolds number limitation as shown for the AEDC tunnel B and C facility in Figure 19. For impulsive facilities like blowdown facilities and gun tunnels, AEDC tunnel 9 yields the highest performance. But the limitation of the wind tunnel stagnation temperature (Tunnel 9, $T_{0,max}$ = 930 K at M_∞ = 8) does not allow a simulation of the freestream velocity. Only tunnel C at M_∞ = 4 allows a simulation of the freestream velocity, but in this case the Reynolds number is limited to 23 million.

Table 2: Necessary wind tunnel total pressure and temperature for duplicating flight Mach number, Reynolds number and flight velocity at 35 km altitude with a model scale of 1:50.

M_∞	4	5	6	7	8	9
$P_{0,wt}$, MPa	4.4	16.5	54.5	162	444.4	1140
T_0, K	960	1325	1750	2220	2730	3280

The low enthalpy facilities mentioned in section 3.1, such as continuous, blowdown and gun tunnels, produce test conditions with low static temperatures of typically around 50 – 100 K. Consequently, as shown in Figure 19, the Mach-Reynolds simulation capabilities of these facilities are not bad considering that the total pressures and total temperatures of these facilities are generally less than 100 MPa and 2000 K respectively, though the AEDC tunnel 9 could achieve total pressures of up to 150 MPa [26]. The reference length was chosen as twice the nozzle exit diameter, which is approximately the maximum allowable size of slender wind tunnel test models [29]. However, it is important to note that, because of their relatively low total temperatures they are restricted to so-called cold hypersonic flow phenomena. The limited total temperatures are due to technological limits of the continuously working heaters. Of course, the big advantage of these facilities is given by their long running time which allows detailed and accurate measurements of various flow and model parameters. Nevertheless, for hypersonic transport vehicles flying between 25 and about 30 km altitude and having typically 30 to 70 m length the Reynolds number is in the order of 100 to 300 million. This is well beyond the scope of most of the hypersonic facilities as shown in Figure 19. Only tunnel 9 of AEDC might be able to generate these high Reynolds numbers with sufficiently large wind tunnel models. For these high Reynolds number tests, the boundary layer is turbulent. For low Reynolds number tests, tripping of the boundary layer is a usual technique. But at hypersonic Mach numbers, tripping is only efficient for Reynolds numbers which are not too low. The state of the boundary layer has strong influence on its separation behaviour, friction drag, shock boundary layer interactions etc. and is therefore of overall importance. A lack of Reynolds number capabilities therefore represents a severe limitation of aerodynamic wind tunnel testing. Nevertheless, in cases where the simultaneous duplication of the Reynolds number and Mach number is not quite possible, recreating the laminar boundary layer thickness or viscous interaction in the flight vehicle is still possible if the characteristic parameter for laminar boundary layer thickness, $M_e^2/\sqrt{Re}$, or the characteristic parameter for viscous interaction, $M_e^3/\sqrt{Re}$, is simulated respectively. Hence, contour lines for constant values of $M_e^2/\sqrt{Re}$ and $M_e^3/\sqrt{Re}$ are included in Figure 19.

4.1.2 High enthalpy regime

For the high enthalpy flow regime (see Figure 1) the temperature behind strong shocks is sufficiently high to initiate chemical reactions. It was shown in chapter 0 for dissociation reactions the ρL-scaling law holds. So, in addition to Mach and Reynolds number, the ρL-scaling should also be satisfied which also requires the duplication of the flight velocity. In this case, for matching the Reynolds number, the duplication of the

freestream static temperature is necessary. The ρL-scaling directly shows that for downsized wind tunnel models the freestream density has to be higher than in flight. Since for the considered case the freestream static temperature is the same as in flight, for the wind tunnel the freestream pressure and therewith the total pressure increases proportional to one over model scale. For perfect gas, this is particularly obvious from the corresponding equations for isentropic flow. However, for the high enthalpy flow regime the total temperature reaches high values and accordingly the required total pressure and temperatures for ground testing, shown in Figure 20 calculated for equilibrium air, also reach high values. Total temperatures up to 10000 K can be achieved by reflected shock tunnels which are the most common type of facility in the temperature range from about 1500 K to 10000 K. This figure already shows that for reasonable small models, a simultaneous duplication of ρL, U_∞, and Mach and Reynolds number is only possible for a very small part of the trajectory. For the Shuttle return, with a feasible model scale of 1:100 only the LENS I facility and HEG are able to fulfil the requirement for the simultaneous duplications, but only for a low temperature range up to 2000 K. For the temperature range of interest, 3000 K to 8000 K, there is no facility which fulfils this simulation requirement.

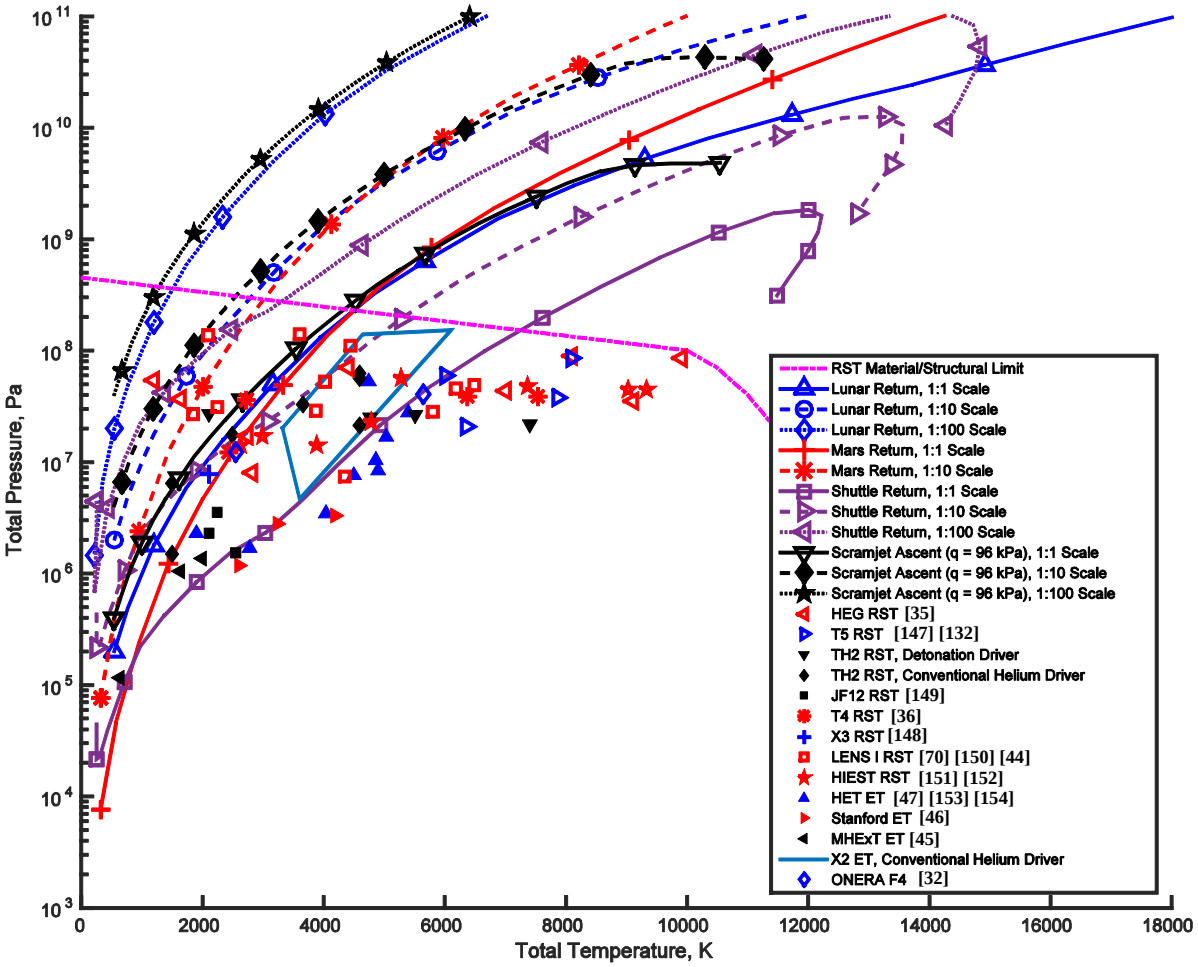

Figure 20: Total pressure and temperature requirements under thermochemical equilibrium compared with high enthalpy facilities. RST and ET refer to reflected shock tunnels and expansion tunnels respectively.

From Figure 20, it is obvious that material technology limitations restrict reflected shock tunnels to total pressures of about 100 MPa at 10000 K total temperature. Consequently, only the lower end of the flight trajectories can be simulated with respect to simultaneous Mach number, Reynolds number and ρL duplications, even if a full scaled test model is used. Even smaller portions of flight trajectories can be tested

if scaled test models have to be used, which is the case in most facilities. Nevertheless, in cases where flight conditions can be simulated by a reflected shock tunnel, good quality experimental measurements can be taken due to the typically longer test times and larger test models in reflected shock tunnel experiments compared to expansion tube experiments. However, in other cases where a better defined thermochemical state of the experimental test condition is particularly important, the expansion tube would be the preferred facilities as discussed in section 3.3. Hence, it can be observed in Figure 20 that expansion tubes are designed for lower performance conditions in addition to the high performance conditions in Figure 24, for certain applications. For example, Gu et al. [83] developed a conventional helium driver for the X2 expansion tube in order to study the thermochemical nonequilibrium and radiation of CO_2 at a freestream static pressure of around 300 Pa and a velocity of around 2.8 – 4 km/s, which were too low to achieve using the free piston driver. Interestingly, this is probably the first case of a facility downgrading its driver to generate lower performance conditions because traditionally the vice versa is true. At laboratories fortunate enough to have both an expansion tube and a reflected shock tunnel, such as the Centre for Hypersonics at The University of Queensland with X2&3 [88] and T4 [61], the Graduate Aerospace Laboratories at California Institute of Technology with HET [47] and T5 [89], Calspan at the Buffalo Research Center with LENS XX [24] and LENS I & II [42], State Key Laboratory of High-Temperature Gas Dynamics at the Chinese Academy of Sciences with JF10&12 and JF16 [90], and JAXA with HIEST [39] and HVET (a new expansion tube) [91], it is encouraged to repeat experiments in both types of facilities. This allows experimentalists to benefit from the advantages of both facilities and permits a comparison between the results to insure that findings are facility independent.

In general, duplication of the most important similitudes in high enthalpy flow - Mach number, Reynolds number, ρ-L and total enthalpy - is not easy to achieve. Still, although some phenomena require the recreation of all the similitudes, the study of some other types of hypersonic flows might suffice from the duplication of just some of the scaling parameters. In the case of a blunt body flow, real-gas effects would be the dominate phenomenon of interest and that means the simulation of ρ-L and the freestream velocity, U_∞, is most important. Therefore, a ρ-L versus velocity graph shown in Figure 24 is created to study the capabilities of the facilities in this aspect. For each facility, the reference length, L_{ref}, is defined as half of the core flow diameter, or 1/3 of the nozzle exit diameter for cases where the core flow size is unavailable. For the Mars and Lunar return capsule, the diameter of the FIRE II and Apollo 11 capsules respectively were used as $L_{ref.}$. For the shuttle, its fuselage length of 33 m was used as L_{ref}. It has to be mentioned that due to the high total pressure requirements, shock tunnels usually are operated at lower Mach numbers than the flight Mach number. In this case the freestream density is higher and consequently the ρL-scaling law can be satisfied for higher flow velocities. The lower Mach numbers are argued by the Mach number independence principle which holds for higher Mach numbers but strictly only for blunt bodies or strong shocks. Therefore, this strategy has to be carefully considered, for example, for slender bodies or for flows for which high-temperature gas effects as well as Mach and Reynolds number effects are important.

It can be observed that the facilities shown in Figure 21 can simulate the real-gas effects on the Mars return and shuttle flight vehicles at velocities around 2 – 6 km/s but fails to simulate the high velocity part of the Lunar return trajectory. This is because, while the Mars return and Lunar return trajectories are similar, the Lunar return capsule, Apollo 11, is an order of magnitude larger than the Mars return capsule, FIRE II. This meant that a larger ρ-L requirement is necessary for Lunar return flight simulations. Nonetheless, manned missions to Mars has been proposed using spacecrafts with diameters of around 10 - 20 m [92], which are even larger than the spacecrafts used in manned missions to the Moon. Due to their size, the flow past these human-scaled configurations are difficult to simulate in wind tunnels. It is also important to note that many of the facilities shown in Figure 21 were probably never designed to provide real gas simulation of Earth re-entry vehicles in the first place. For example, the conventionally driven X2 expansion tube was designed to study thermochemical nonequilibrium and radiation of CO_2 past a wedge model for Mars entry applications [83], while the JF12 reflected shock tunnel was designed to simulate slender hypersonic vehicles flying at a speed of around Mach 7 and at an altitude of around 35 km [23].

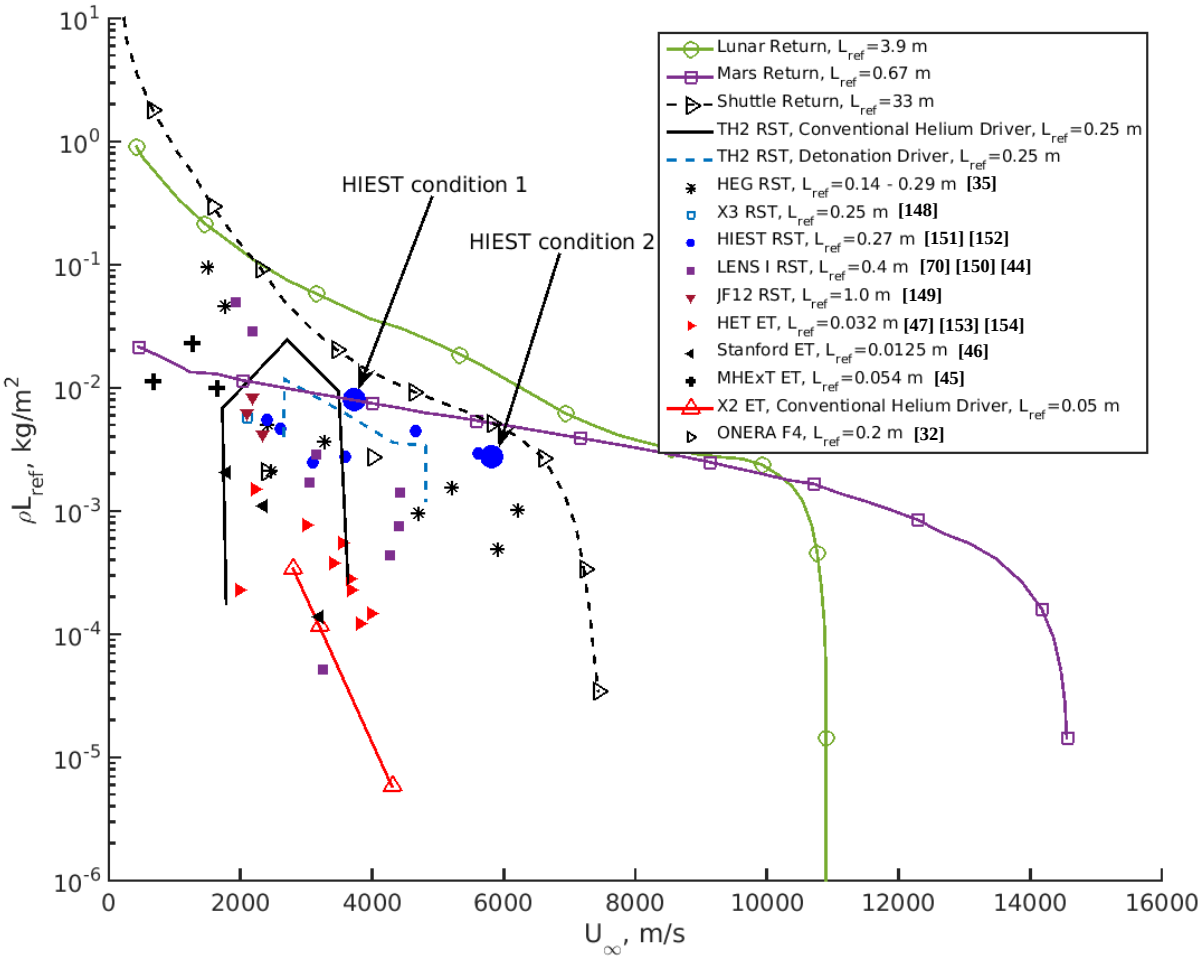

Figure 21: ρ-L versus velocity capabilities of high enthalpy facilities compared to the flight trajectories.

Beside high-temperature real gas phenomena, Mach and Reynolds number effects are also of importance which should be simulated in the high enthalpy flow regime as well. Boundary layer growth, local heating rates, flow separation behaviour, shock boundary layer interactions are only a few of the phenomena which are strongly dependent on Mach and Reynolds number. Therefore, also for the high enthalpy flow regime the Mach – Reynolds performance of ground testing facilities is of interest. Figure 22 shows the Reynolds number versus Mach number capabilities of various high enthalpy facilities mainly reflected shock tunnels and expansion tunnels compared to the different flight trajectories. The considered vehicles are of blunt body shape, therefore as reference length for the lunar and Mars return the typical vehicle diameter has been chosen and for the shuttle its body length because of its large angle of attack in this flight regime. For the wind tunnels as reference length the maximum feasible blunt body model diameter has been chosen which was estimated as half of the core flow diameter. From Figure 22 it is obvious that only the LENS facilities, HEG, T6 and the HXT expansion tunnel are able to simulate a part of the lunar and Mars return trajectories up to Mach numbers of about 8 to 10. For this Mach number range, the Reynolds numbers for the Mars return trajectory are an order of magnitude lower caused by the shorter reference length which corresponds to the diameter of a typical Mars return sample probe. It is also obvious that the simulation range of the high enthalpy facilities is limited to a maximum Mach number of about 10. As mentioned above, this ensures high freestream densities and therewith positively influences the ρL and Reynolds number simulation capabilities. However, there is a big discrepancy between the ρL – U simulation capabilities and the Mach – Reynolds number performance for high stagnation enthalpies. Comparing the ρL simulation capabilities in Figure 21 with the Mach – Reynolds

number performance in Figure 22, the flow conditions yielding high ρL values at high velocities are achieved for a low Mach number, low Reynolds number flow condition. Since the Mach number is kept as low as possible to achieve a high density, this results in high freestream static temperatures reducing the Reynolds number. This is demonstrated exemplarily in Figure 21 and Figure 22 by the marked data points indicating the same flow conditions for two HIEST conditions. The two conditions are close to the ρL trajectory for the Shuttle return, but they are far off from the trajectory concerning Mach and Reynolds number. This is the usual behaviour for high enthalpy testing.

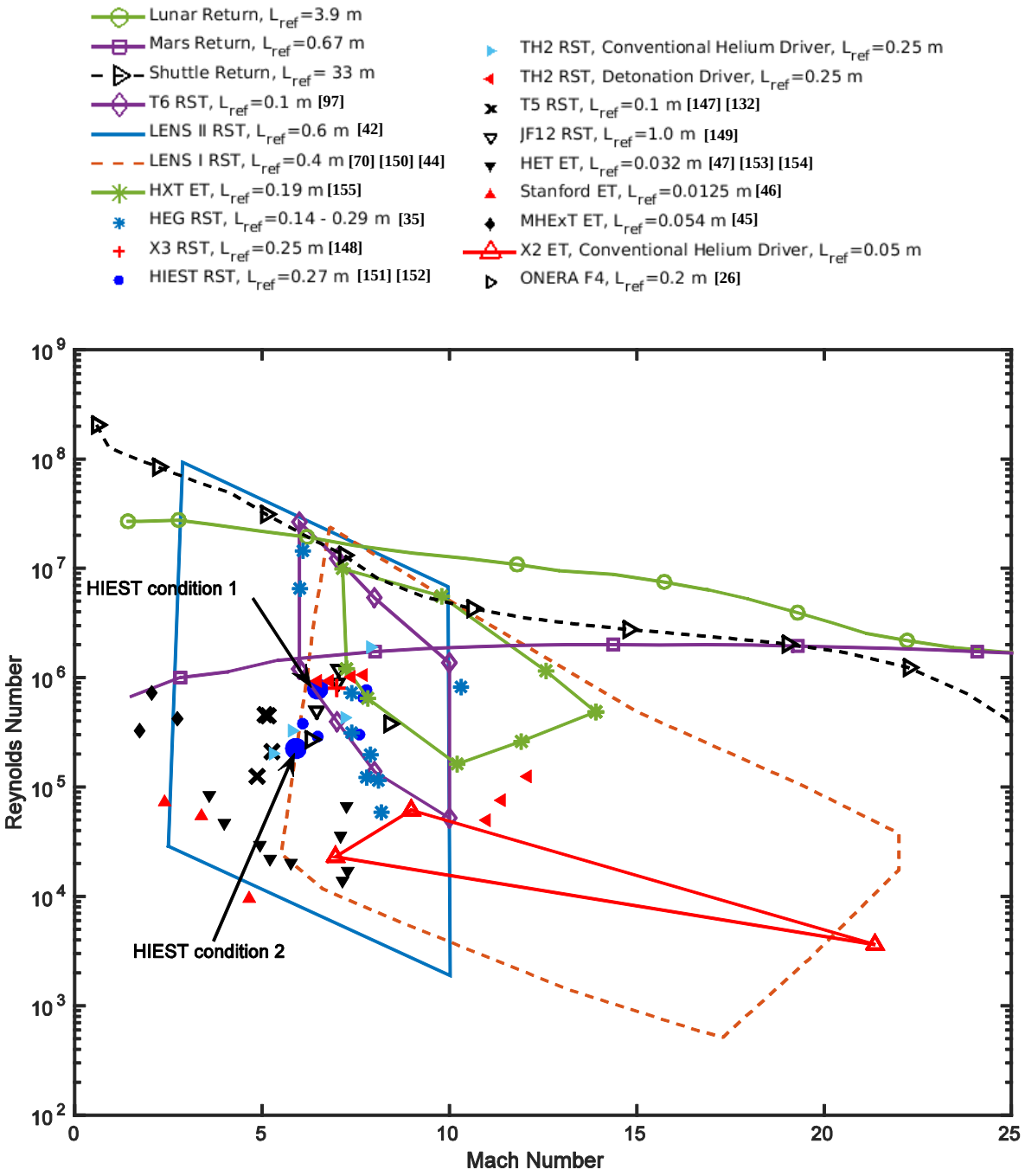

Figure 22: Reynolds number versus Mach number capabilities of high enthalpy facilities compared to the blunt body re-entry trajectories.

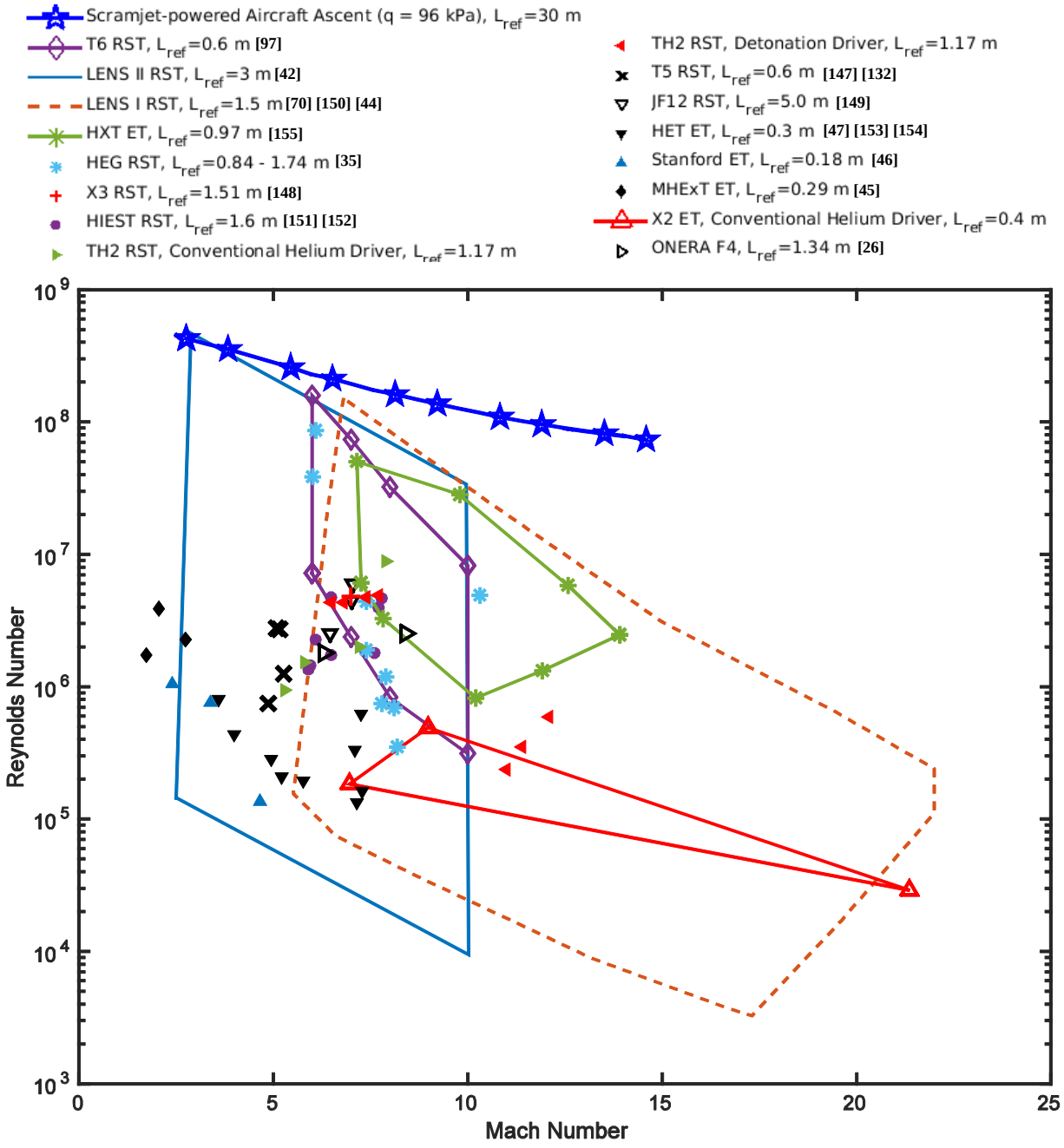

Figure 23: Reynolds number versus Mach number capabilities of high enthalpy facilities compared to the scramjet flight trajectory.

For more slender configurations a reference length based on the body length is meaningful. For example, scramjet powered vehicles may fly as slender body configurations at low to medium total enthalpy conditions. As stated in section 2.2 the simulation of the flight velocity or the corresponding total enthalpy in ground testing in addition to the pL-scaling is important for a correct simulation of the combustion processes. Because of the additional importance of Mach - Reynolds number effects for this type of vehicles, Figure 23 shows the Mach - Reynolds simulation capabilities of the corresponding wind tunnel facilities compared to a scramjet-powered ascent flight trajectory of a vehicle of 30 m length. For the ground test facilities, the reference length was chosen as twice the nozzle exit diameter, which approximately represents the maximum length of a slender

body wind tunnel model [29]. Only T6, the LENS facilities and HEG come close to the flight trajectory for a narrow Mach number regime at about five to seven.

4.1.3 Very high enthalpy regime

Figure 24 shows the total pressure and temperature requirements to simulate the ρL-scaling, Mach number and Reynolds number for blunt body return trajectories compared to the simulation range of some expansion tunnels. Unfortunately, no total pressure and temperature data was available for the LENS XX facility in literature. Therefore, in this chart the performances of this facility are missing. It is clear from the figure that using scaled test models significantly increases the total pressure requirements of the ground test facilities. Thus, obtaining sufficiently high total pressure conditions may be the most difficult challenge for ground test facilities. While reflected shock tunnels struggle to achieve total pressures of more than 10^8 Pa, expansion tunnels can achieve total pressures of more than 10^{10} Pa which is not particularly surprising given the huge total pressure gains across an unsteady expansion as shown in Figure 16. For example, Gildfind et al. [22] operated the free piston driven X2 expansion tube with a secondary driver to produce medium enthalpy conditions with total pressures around 10^9 – 10^{10} Pa for the purposes of scramjet testing. These conditions allow for the testing of scramjets as small as 1/10 of flight. Figure 24, shows that these same conditions can also be used to simulate the medium enthalpy portions of the shuttle, lunar return and Mars return flight trajectories for certain model scales. Similar conditions could have been generated by the free piston driven RHYFL expansion tube [93] and the free piston driven HYPULSE expansion tube [94], but these facilities were just designed and never completed.

Note that for Lunar return and Mars return, a large portion of the trajectory is in the high enthalpy region where the total temperature is greater than 15000 K. In such cases, as shown in Figure 24, neither the existing expansion tubes nor the conceptual expansion tubes could provide high enough total pressures, even if full sized test models are used. This is because the particular drivers of the expansion tubes were not designed to facilitate these conditions. For example, the free piston driver of the X2 expansion tube, which can heat helium up to 3000 K [95] to achieve a speed of sound ratio, a_4/a_1, of 9.4 for air as the test gas, is not particularly powerful for a free piston driver and it was never designed to provide total pressures of more than 10^{11} Pa at total temperatures of more than 15000 K [63]. Consequently, this issue may be resolved by providing expansion tubes with higher performance free piston drivers to specifically support flight simulation of these high enthalpy conditions [96]. For estimation of the maximum performance of an expansion tunnel operating with a helium piston driver, a maximum driver pressure of 100 MPa and a driver gas temperature of 5000 K has been assumed. From the currently available technology this seems to well represent the maximum achievable conditions. Even higher pressures and/or temperatures would cause burning of piston seals, strong erosion and other problems. Helium is assumed as driver gas because of its high performance and its ease of handling without any safety precautions. Hydrogen as driver gas would significantly increase the tunnel performance but at the expense of having highly demanding operations and extensive safety precautions. From the PITOT code [54], the approximate theoretical upper limit of performance for this fictitious expansion tunnel operating without a secondary driver is shown in Figure 24 for realistic fill conditions in the shock and acceleration tube, and assuming thermochemical equilibrium throughout. Compared to X2 operating with a single stage driver, the maximum total temperature increased by about 5000 K, while the maximum total pressure increased by approximately an order of magnitude. Although this fictitious expansion tunnel comes close to duplicating the total temperature and pressure required for simulation of a full scale lunar return vehicle at the very high total temperature region, there is more to be desired in terms of simulating the Mars return and scaled lunar return conditions. Stalker mentioned that there are no theoretical performance limitations of a free piston driver [1]. Though, practical limitations may include heating the driver to temperatures so high that the facility wall begins to melt, significant heat loss due to radiation and containment of the high pressure driver gas. Furthermore, there is the known Page-Stalker loss mechanism for free piston drivers which is discussed in section 4.2.4.

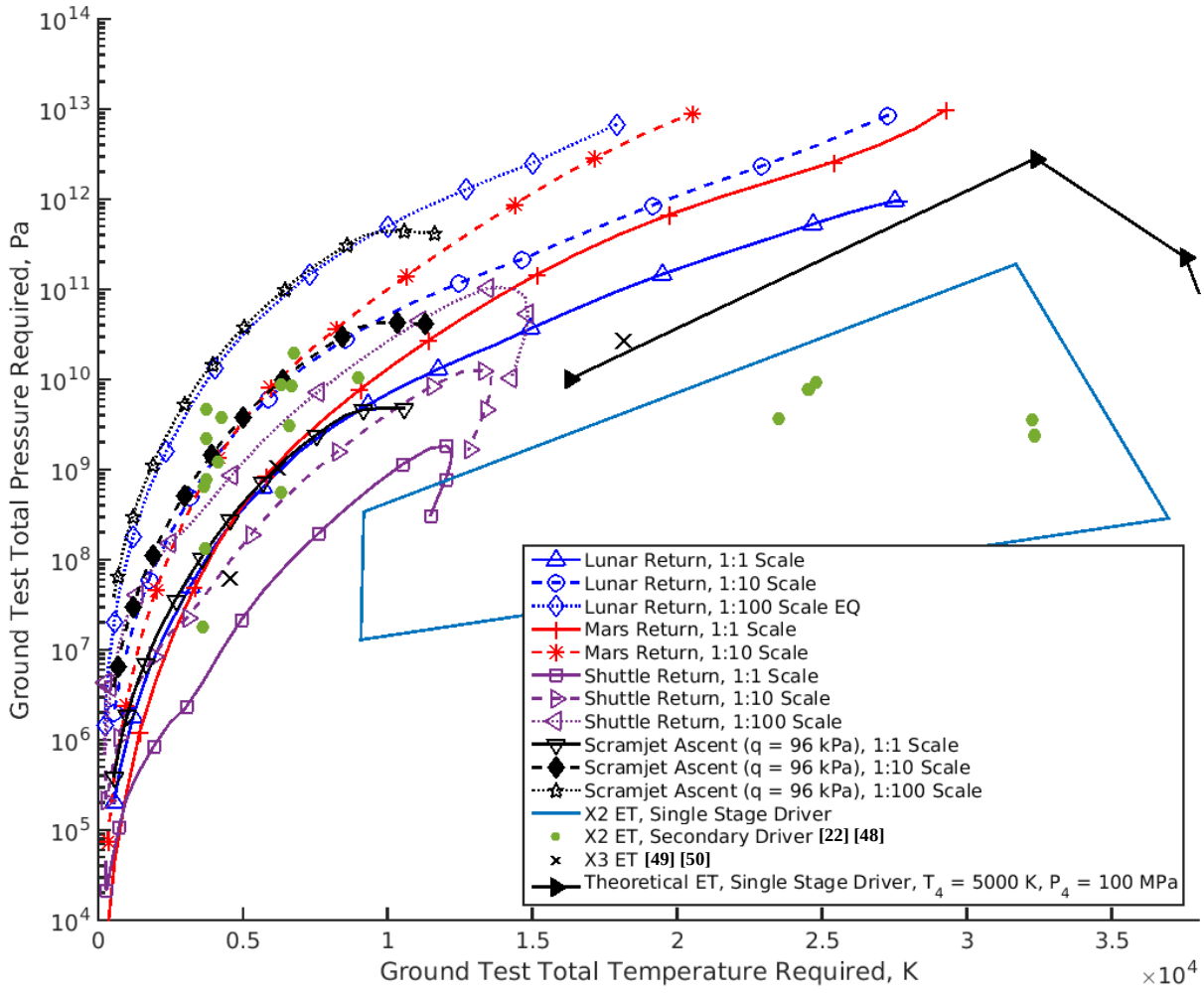

Figure 24. Total pressure and temperature requirements under thermochemical equilibrium compared with the performance of expansion tunnels.

The ρL-scaling capability of the expansion tunnels is shown in Figure 25. From this figure, the LENS XX expansion tunnel [24] seems to be capable of almost complete ρ-L simulation of all the trajectories of flight vehicles considered. The X2 expansion tunnel is capable of ρ-L simulations at velocities of around 3 - 4 km/s but falls slightly short at higher velocity conditions. The T6 expansion tunnel [97], which is currently being developed, looks to have similar ρ-L capabilities as the X2 expansion tunnel. The reason why the LENS XX has distinctly better ρ-L capabilities compared to the other expansion tunnels is due to its size. The LENS XX allows for the use of a 0.8 m diameter test model which is significantly larger than that allowed in the second biggest expansion tunnel, the X3 expansion tunnel, of 0.24 m [49]. The LENS XX actually has similar ρ versus velocity capabilities as the X2 expansion tunnel, but because LENS XX is much bigger than X2, the ρ-L capabilities of LENS XX is superior to that of X2. Concerning this data, it is very important to note the following. As reference length in Figure 25, half of the core flow diameter has been taken which is the usual procedure described in literature. At the highest enthalpy conditions, all shown expansion tunnels have a useful running time of about 100 - 200 µs. In this case the flow establishment time should not exceed about 70 µs to ensure a sufficiently long steady state flow time. Hence, the flow establishment time put a severe limitation on the maximum allowable model size, which is discussed in detail in section 4.2.1. From this follows (see Table 3) that a typical flow establishment time of 70 µs at a flow velocity of 10 km/s allows a maximum model size of only 23 mm for blunt bodies and 70 mm for more slender configurations. These correspond to typical model sizes of X2. The ρL values for the LENS XX facility would reduce by a factor of about 30 for blunt

bodies. For X3, the ρL data would be reduced by a factor of about nine for the highest enthalpy condition for blunt bodies and it would be significantly off the trajectories. For T6, no reference length has been given, only the product ρL. This impressively shows that the available testing time poses a severe limitation on the allowable model size and therewith on the ρL simulation capability of expansion tunnels. Additionally, it should be mentioned that a model size of about 23 mm does not allow much instrumentation on the model.

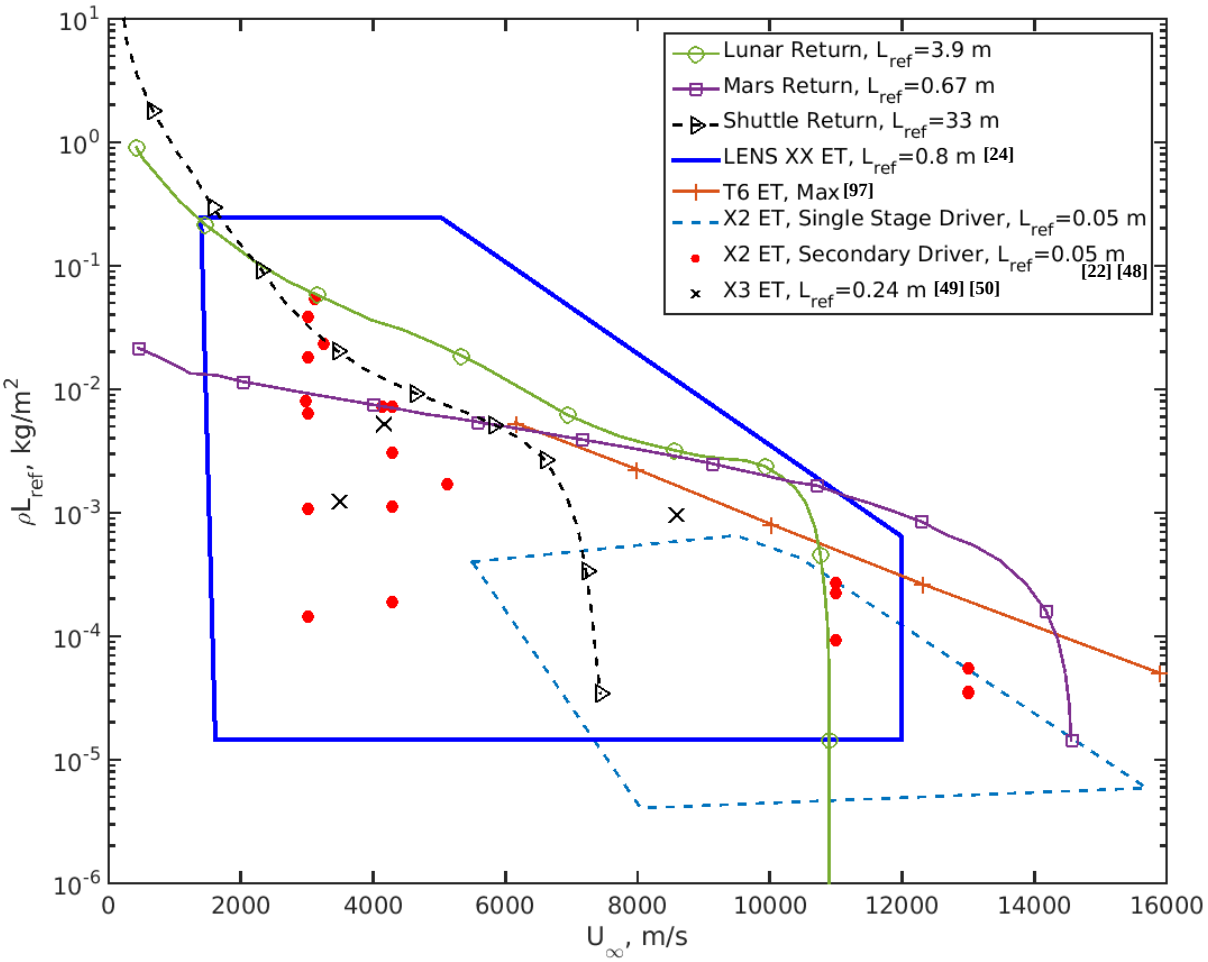

Figure 25. ρ-L versus velocity capabilities of expansion tunnels compared to the flight trajectories.

It is important to note that a category of flight trajectory not shown in Figure 25 is that of meteoroid entries. Meteoroid entries occur at velocities of around 25 – 30 km/s on average [98]. Hence, none of the expansion tunnels shown in Figure 25 comes close to duplicating these velocities. Research in meteoroid entry is now gaining prominence [98] [99]. Consequently, in the future, there would likely be motivation to install more powerful drivers in expansion tunnels to facilitate the study of meteoroid entry, which would also simultaneously allow for even greater ρ-L capabilities. Nevertheless, it is important to note that, while theoretically the velocity obtainable in the expansion tube can increase indefinitely with increase in driver performance, the static temperature of the test flow may eventually be so high that the thermochemical state of the test flow resembles nothing like flight. This may be an effective velocity limitation of expansion tubes in terms of simulating flight.

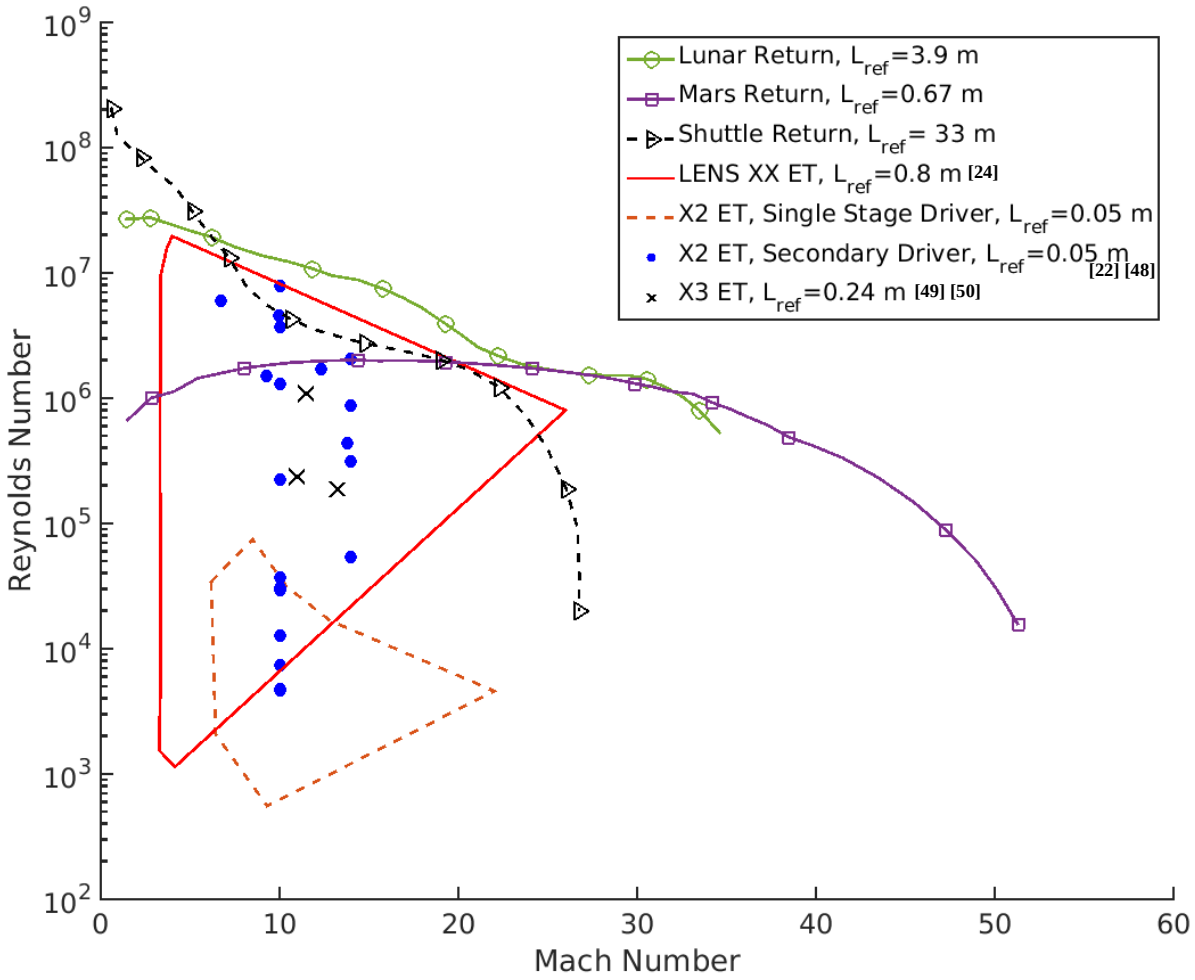

Figure 26: Reynolds number versus Mach number capabilities of expansion tunnels compared to the blunt body flight trajectories.

The Mach - Reynolds number performance of expansion tunnels is shown in Figure 26 and compared with blunt body re-entry trajectories. The LENS XX and X2 with secondary driver allow a simulation of the blunt body trajectories over a wide range of Mach numbers. However, as for the high enthalpy facilities, it has to be kept in mind that the points in the ρL and the Mach - Reynolds number chart do not correspond to each other. Probably even more important is the fact that as mentioned above, the chosen reference length is that typically used in literature. But as before, the resulting model size does not allow a full flow establishment during the running time. For sufficiently small models of about 23 mm for blunt bodies according to Table 3, the Reynolds number drops significantly and there is no longer a match with the flight trajectories.

The Mach - Reynolds number performance of expansion tunnels compared with a scramjet ascent trajectory is shown in Figure 27. Apart from the X3 expansion tunnel and the X2 expansion tunnel operated in single stage driver mode, the expansion tunnels in Figure 27 comes close to providing Mach - Reynolds simulations of the full-size scramjet-powered hypersonic aircraft. However, the reference length used is defined as twice the nozzle exit diameter. Hence, as mentioned in the preceding paragraph, due to the model size requirement for flow establishment, this probably results in an over estimate of the Mach - Reynolds number capabilities.

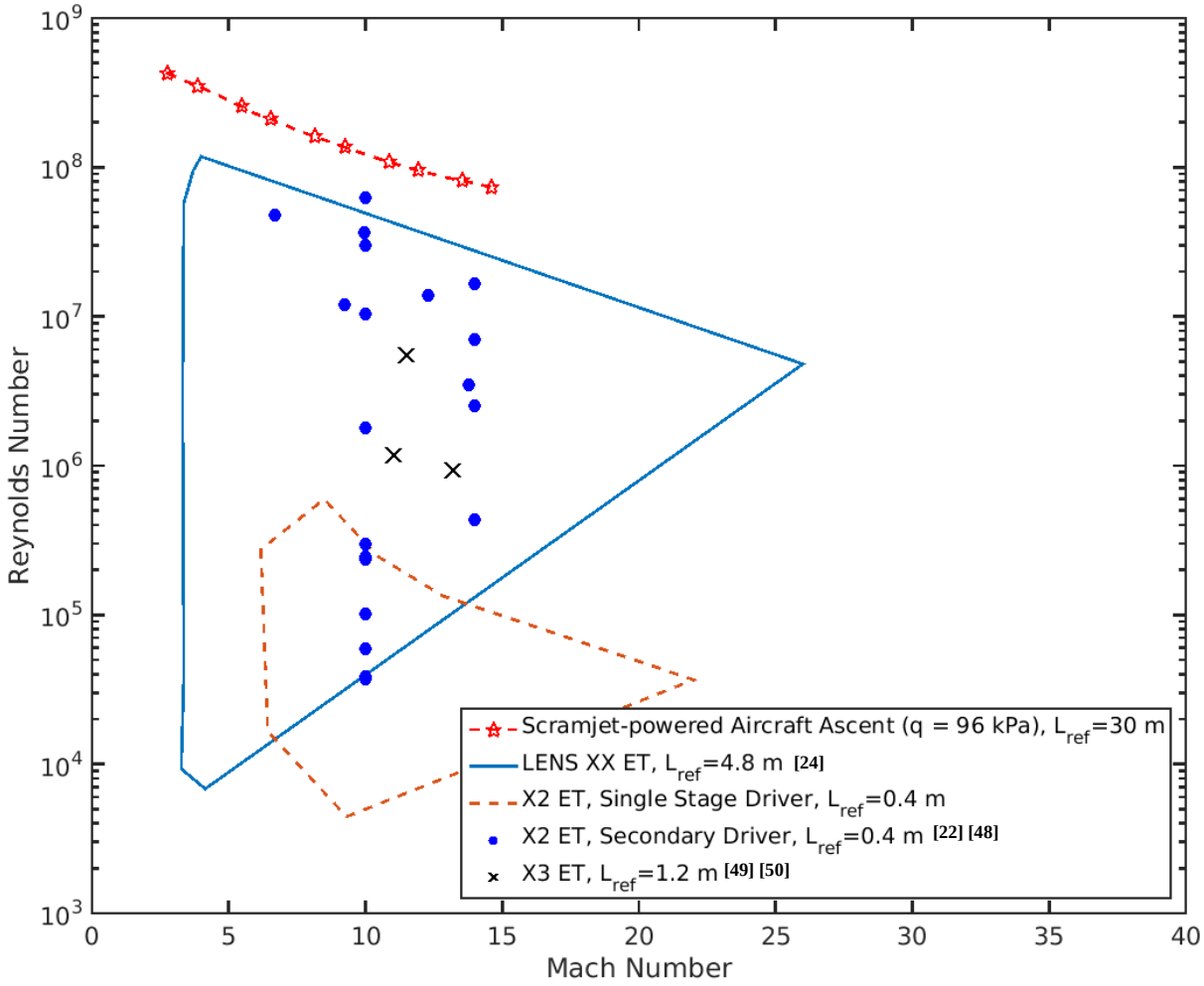

Figure 27: Reynolds number versus Mach number capabilities of expansion tunnels compared to the scramjet flight trajectory.

4.2 Other Limitations

Aside from the performance aspects, especially reflected shock tunnels and expansion tubes suffer from other limitations. These other limitations are related to the test time, test model size and the flow quality. This section will focus on these topics.

4.2.1 Test time and model size

Although the test time of reflected shock tunnels are considered long relative to the high enthalpy facilities discussed in section 3.3, it could be even longer under ideal conditions. Under inviscid conditions, the test time in reflected shock tunnels could end when the driver gas contact surface arrives at the test section. However, in reality, interactions between the reflected shock, contact surface and the boundary layer creates a wall jet of driver gas and vortices behind the reflected shock. The vortices interact with the jet of driver gas, carrying it towards the centre of the shock tube and into the nozzle resulting in premature driver gas contamination [72]. This process is illustrated in Figure 28 without the vortices. Other transport mechanism as vortical structures behind the reflected shock also lead to a premature driver gas contamination. Consequently, significant work has been done to understand the general characteristics of this phenomenon and provide methods to experimentally detect the premature arrival of the driver gas at the test section.

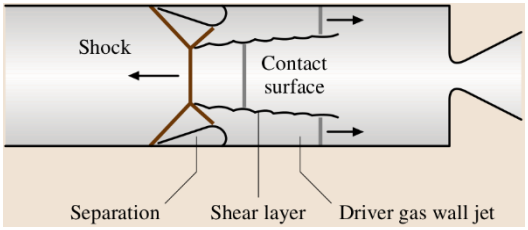

Figure 28: Schematic of the reflected shock/boundary layer interaction which results in driver gas wall jets. [57]

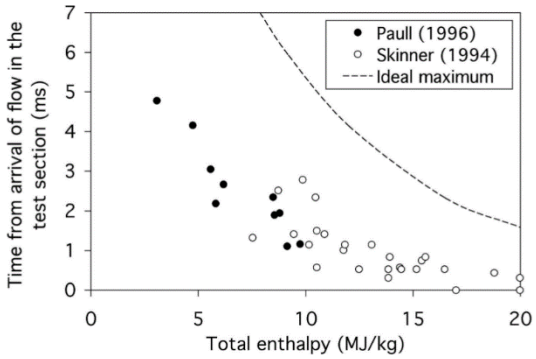

Figure 29: The time of arrival of 7.5 %, Paull (1996) [100], and 10 %, Skinner (1994) [101], mole fraction of driver gas compared to the latest arrival of driver gas in an ideal case. [37]

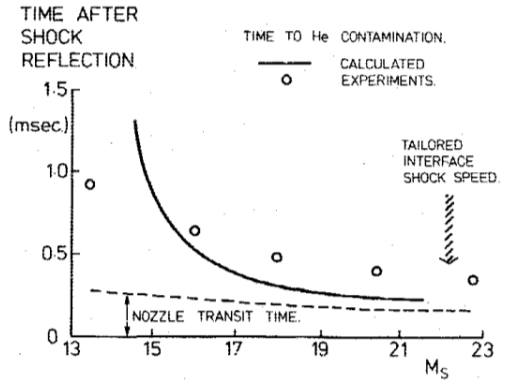

Figure 30: Theoretical and experimental premature driver gas arrival time for 10 % molar concentration compared with the estimated nozzle start up time for the T3 reflected shock tunnel. [102]

An important characteristic of the shock/boundary layer interaction in Figure 28 is that the severity of the interactions is essentially independent of total pressure but increases with increase in total enthalpy resulting in more significant driver gas wall jets, for a given facility [37] [65]. This is illustrated in Figure 29 by Boyce et al. [37] for the T4 reflected shock tunnel. Part of the uncontaminated test flow will be wasted to start up the nozzle flow resulting in very little useful test flow at higher enthalpies as illustrated in Figure 30 for the T3 facility. Eventually, the facility will produce test conditions with inadequate test times as total enthalpy increases. Consequently, the performance of reflected shock tunnels may often be limited by premature driver gas contamination rather than the more obvious material limitations. For the T3, T4 and T5 reflected shock tunnels, the total enthalpy is limited to about 25 [60], 15 [21] and 22 [65] MJ/kg respectively due to premature

driver gas contamination. Stalker et al. [21] notes that the reason why T4 is particularly susceptible to premature driver gas contamination might be because its shock tube has a length to internal diameter ratio of 133 instead of the usual value of 80 - 100 and this extra length may have allowed extra turbulent mixing at the driver-test gas interface. From analysis of numerous contamination-free test time data from various facilities, Stalker postulated that the contamination free flow length increases with increasing shock tube diameter [1]. This makes sense because, as stated by Hornung [65], the relative importance of wall effects decreases with increase in diameter. A consequence of this is that a direct scale-up of a particular reflected shock tunnel would result in a relative increase in the total enthalpy limit from premature driver gas contamination. Alternatively, direct scaling of the shock tube and driver, while the nozzle size is kept the same, would result in larger increases in the test time and subsequent larger increases in the total enthalpy limit. Though, eventually, the performance of the facility will be limited by the nozzle melt limit, which is discussed in detail in section 4.2.2, due to too much test time.

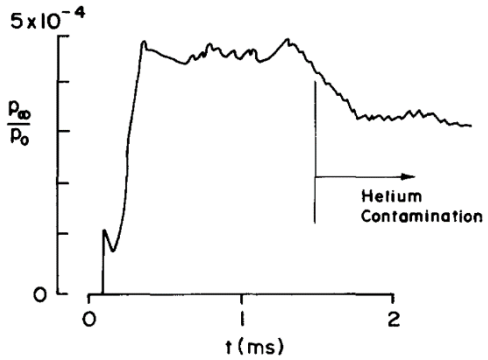

Figure 31: Static pressure measurements in T4 at the test section using a flat plate. [104]

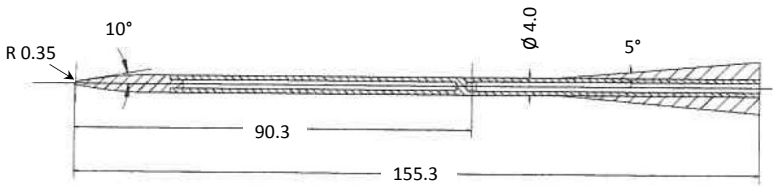

Figure 32: Static pressure probe with dimensions in mm. [105]

Due to the occurrence of premature driver gas contamination, various methods and devices have been made to experimentally measure the arrival of the driver gas in a reflected shock tunnel. One of the earliest methods to measure driver gas contamination was using a mass spectrometer to directly detect helium as demonstrated by Crane and Stalker in 1977 in T3 [103]. Another early method of detecting driver gas contamination was taking static pressure measurements at the nozzle exit as reported by Stalker and Morgan in 1988 for T4 [104]. An example of their measurement is shown in Figure 31. It was taken using a flat plat with a pressure orifice located 200 mm from the leading edge which was aligned with the nozzle exit plane. Stalker and Morgan noted that, while the static pressure dropped distinctly after about 1.1 ms as shown in Figure 31, the pitot pressure measurements remained roughly the same which likely indicates helium contamination due to the increase in heat capacity ratio caused by helium addition. Alternatively, Hornung in 1991 took high speed photography of the shock from a wedge, which was used to provide an indication of freestream helium content as the shock location was also shown to be sensitive to helium presence in the freestream [89]. Subsequently, in 1996, Paull developed a device which works by choking of a small duct as the contamination rises above a preset level [100]. Also in 1996, like Stalker and Morgan in 1988, Kindl et al. measured the nozzle exit static pressure to determine helium contamination [105], except Kindl et al. used a small static pressure probe, shown in

Figure 32, instead of a flat plat as used by Stalker and Morgan. Kindl et al. also explained two methods to determine the time-resolved helium contamination percentage at the nozzle exit from the static pressure measurements. In the first method, perfect gas relations were used to derive a relationship for the ratio p_∞/p_0 with the nozzle area ratio and the heat capacity ratio of the gas. Using the measured nozzle exit pressure, p_∞, and the measured nozzle reservoir pressure, p_0, the estimate of the heat capacity ratio of the gas can be determined which is subsequently used to give an estimate of the helium percentage by applying the mixing rule for the specific heats. This is called the mixing rule method. Strictly, this method is only valid for relatively low enthalpies where the specific heats are not yet influenced by high temperature effects. In the second method, called the calibration method, nozzle exit static pressures were taken numerous times for different amounts of helium initially mixed in with the test gas before each experiment. For this method, in all cases the shock tunnel experiments were performed for tailored interface conditions, thus minimizing the effect of a premature driver gas contamination due to shock-boundary layer interaction. This gave an experimentally derived relation between the helium percentage in the gas and the nozzle exit static pressure as shown in Figure 33. Using this, the freestream helium percentage in the actual test condition can be determined from its static pressure measurements. The freestream helium percentage deduced from both methods are shown in Figure 33. The two methods show differences of up to 20 %, which is comparable to the uncertainties of the other helium detection methods. Various ideas like suction slots and a sleeve as insert at the end wall have been proposed to delay the helium contamination [71] [106] [107]. The sleeve in particular shows a positive effect for overtailored conditions. But the longest test times are still achieved without any device for slightly undertailored conditions [71].

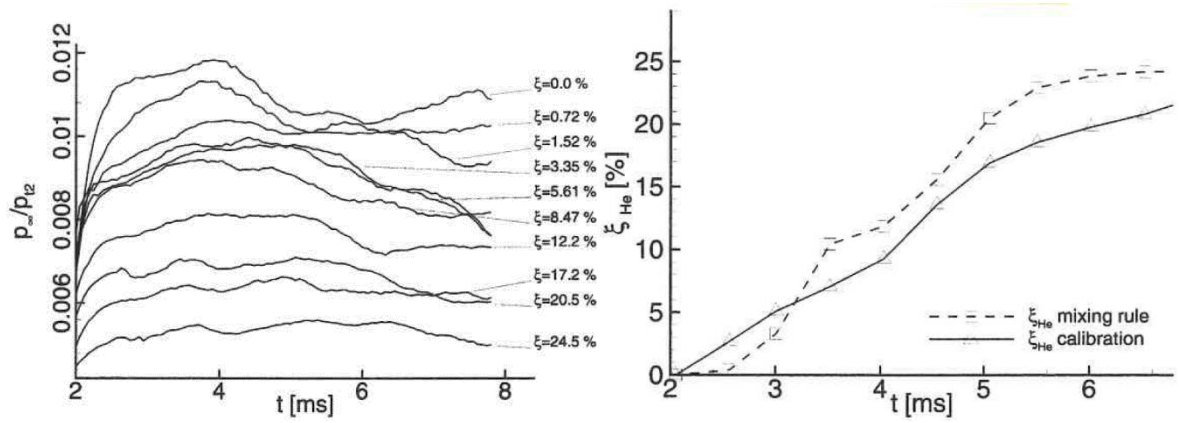

Figure 33: Static pressure measurements at the nozzle exit. The left figure shows the calibration values while the figure on the right shows the final deduced helium mass fractions. [105]

In detonation driven facilities, whether the mechanism of driver gas contamination is the same as that of helium driver gas is uncertain. The experimental results of Olivier [34] indicated that the detonation driver gas contamination mechanism is qualitatively the same as that of helium drivers. However, the CFD investigation by Chue et al. [108] showed the opposite result where the detonation driver contamination mechanism was observed to be qualitatively the same but quantitatively more prominent compared to those for helium drivers, resulting in more severe driver gas contamination in detonation driven facilities. Most of the above methods for determining driver gas contamination are useless in situations where detonation drivers are used. At the test section, the detonation driver gas consists mainly of gaseous water which has a similar heat capacity ratio as the most commonly used test gas - air. Therefore, it is necessary to employ optical diagnostics for detecting driver gas contamination in detonation driven facilities [109], which are more complicated techniques compared to those used to detect helium driver gas.

While driver gas contamination determines the upper end of the test time, the necessary flow establishment time represents the lower end of the useful test time interval. In literature there are a lot of empirical and semi-

empirical relations to estimate the flow establishment time, but there is no conclusive and reliable theory for this. This is not surprising because the flow establishment time depends on the model geometry, the type of establishment time determining flow phenomenon etc., in addition to the freestream conditions. In case of facilities utilizing the expansion of the flow in a nozzle, the nozzle starting process and the model flow establishment may happen in parallel, which complicates the estimation of the pure flow establishment time.

While the problem of helium wall jetting should not occur in expansion tubes [109] [80], expansion tubes have inherently less test time than reflected shock tunnels, by an order of magnitude in general. Expansion tube test times are generally ended by the arrival of wave processes at the test section. There are generally three ways for the test time in an expansion tube to end. From Figure 15, test time can be terminated by either 1) the tail of the secondary unsteady expansion fan, 2) the reflected head of the secondary unsteady expansion fan, or 3) the reflected head of the primary unsteady expansion fan, whichever occurs first. Which one of the three wave processes terminates the test time depends on the test condition and the facility dimensions, though most of the time it is either case 1 or case 2 because the driver section should be sized correctly so as to not interfere with the test flow. Paull et al. also postulated the possibility of a fourth way for test time termination where "bubbles" of driver gas, created due to mixing at the contact surface, get accelerated through the unsteady expansion and arrive at the test section prior to the wave processes [110].

In expansion tubes, while the accelerator gas which precedes the test gas helps with flow establishment, consumption of valuable test gas is often still required for flow establishment. Figure 34 presents the trace from a radiation sensor and a 10 mm diameter pitot probe, obtained in the X2 expansion tunnel. The radiation sensor measured infrared radiation from a point in the flow past a small two-dimensional wedge test model, with dimensions shown in Figure 37, at a location of about 5 mm above the convex corner. The pitot probe was placed 20 mm below the wedge. Because the pitot probe was small, its establishment time was negligible and its trace is approximately a reflection of the state of the freestream, while the establishment of the test model flowfield can be accurately monitored from the infrared sensor trace [111]. In this case, which was for a 4.0 km/s CO_2 freestream, the establishment time of the wedge model took about 80 µs in which 35 µs out of the 135 µs of test flow was consumed.

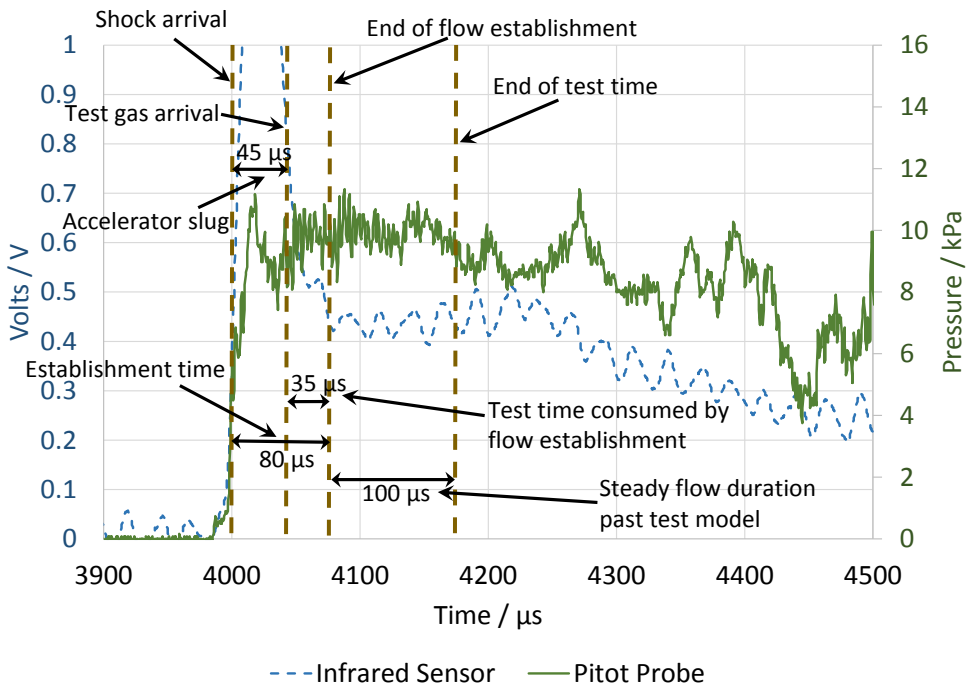

Figure 34: Radiation sensor and pitot probe traces for a 4.0 km/s CO_2 freestream in the X2 expansion tunnel.

Different flow phenomena take different amounts of time to establish. In general, inviscid flow phenomena need a much shorter establishment time than viscous ones. Steady flows establish much faster than pseudo-steady flows like some shock oscillation modes, etc. The flow establishment time, t_e, can be estimated by,

$$t_e \approx K\frac{L_e}{U_\infty} \tag{36}$$

where K is a constant with a value depending on the flow phenomenon, L_e is the characteristic length and U_∞ is the freestream velocity. The values of K and L_e are shown in Table 4 for the different flow phenomena. The various flow establishment times are subsequently calculated and shown in Figure 35 for two different flow velocities. From Abul-Huda and Gamba [45], a conservative estimate of the total flow establishment time over the relevant test model is the sum of the relevant individual processes. Furthermore, as the accelerator gas proceeds the test gas in the expansion tube, the effective flow field establishment time can reduce to as much as 2/3 of the total establishment time [45]. Thus, the effective total establishment time, t_{total}, for an expansion tube can be approximated as,

$$t_{total} \approx \frac{2}{3}\sum_i t_{e,i} \tag{37}$$

which is used to produce the results in Figure 35. Also shown in the figures is a representative test time for the X2 expansion tunnel and the approximate maximum model sizes for the X2 test section. From the results, in the high velocity case, the test time is just enough to establish a steady flow around the maximum size test model, while a steady flow never develops around a maximum size test model for the low velocity condition.

Table 3: Maximum model size for attached (K=10) and separated (K=30) flows which ensure a flow establishment time, t_e, of 30 % of the running time after flow initiation.

U_∞, m/s	2000	4000	6000	8000	10000
t_m, ms	6	3	1.5	0.3	0.2
t_e, ms	2	1	0.5	0.1	0.07
Le, m (K=10)	0.4	0.4	0.3	0.08	0.07
Le, m (K=30)	0.13	0.13	0.1	0.027	0.023

Table 4: Flow establishment time parameter values from Abul-Huda and Gamba [45]. L_{model} is the model length and D_{model} is the model diameter while ρ_7 and ρ_{7s} are the pre-shock and post-shock densities respectively.

Flow process	L_e	K
Laminar boundary layer	L_{model}	3.33
Turbulent boundary layer	L_{model}	2
Bluff body separated flow	D_{model}	30
Bow shock	$1.1D_{model}(\rho_7/\rho_{7s})$	$(\rho_{7s}/\rho_7-1)\ln(0.05^{-1})$

From equation 36, K is the ratio of required test gas slug length to establish the flow over the model size. As explained above, no exact data or theory exist which can accurately determine the flow establishment time or the value K in equation 36. As a rule of thumb for attached flows the value K should be about 3 to 10 and for separated flows at least 30. From this, in Table 4, the maximum possible model size has been determined as function of the flow velocity and typical flow establishment times, t_e, which have been assumed as one third of the typical measuring time. The typical measuring time, t_m, depends on the flow velocity and represents the average value of corresponding facilities, i.e. conventional shock tunnels to 4000 m/s, piston driven shock tunnels up to 6000 m/s and expansion tunnels from 8000 to 10000 m/s. The results show that especially for

the high velocity range from 8000 m/s and higher, the short measuring times at these conditions require very small models which would not allow an extensive instrumentation.

This result is fairly common for expansion tubes as mentioned by Hornung [65]. In the case of scramjet duct flows, since the flow studied is internal, and the expansion fan originating at the tube/nozzle exit does not enter the scramjet intake, the maximum model length is probably always limited by the test time. It should also be mentioned that bluff body separated flows are rarely studied in expansion tubes due to the long establishment times, though it has been done before by Hollis and Perkins [112] and by Park et al. [113]. Instead, the bow shock is most often the sole phenomenon of interest during bluff body flow research using expansion tubes. This consequently would allow for larger test models to be used since the flow establishment time of the bow shock is less than that of the separated flow. Since both the facility test time and the model flow establishment time scales approximately linearly, the only way to increase the amount of test time left over after flow establishment is to increase the facility size while keeping the model size roughly constant or decrease the model size while facility size is constant. Hence, test time is one of the fundamental limitations of expansion tubes.

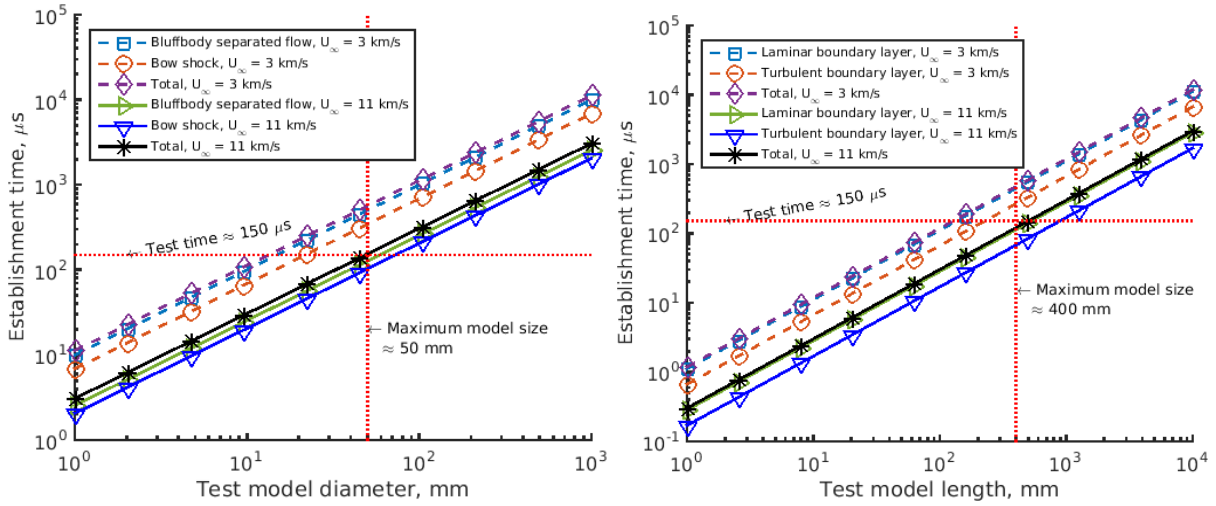

Figure 35: Flow establishment times for bluff bodies, left, and slender bodies, right, for two different flow velocities. Also shown is a representative test time for the X2 expansion tunnel and the approximate maximum model sizes for X2.

4.2.2 Limitation due to throat melting

Flow establishment time and remaining testing time are a severe concern for expansion tunnels while reflected shock tunnels must pay a performance penalty due to the throat-melt limit. As the test time is increased in the reflected shock tunnels, the throat of the nozzle will eventually experience surface melting. Significant throat melting during the experiment is highly undesirable because the throat diameter would increase causing changes to the test flow properties. Additionally, the melted products of the nozzle throat will form as contaminates at the test section and the melted throat surface may cause flow disturbances in the test section which is unwanted. Therefore, it is necessary to avoid throat melting. This means that as a reflected shock tunnel is scaled up, eventually, the total pressure and total temperature attainable in the facility will be limited by the throat melting while the strength of the facility structure becomes irrelevant.

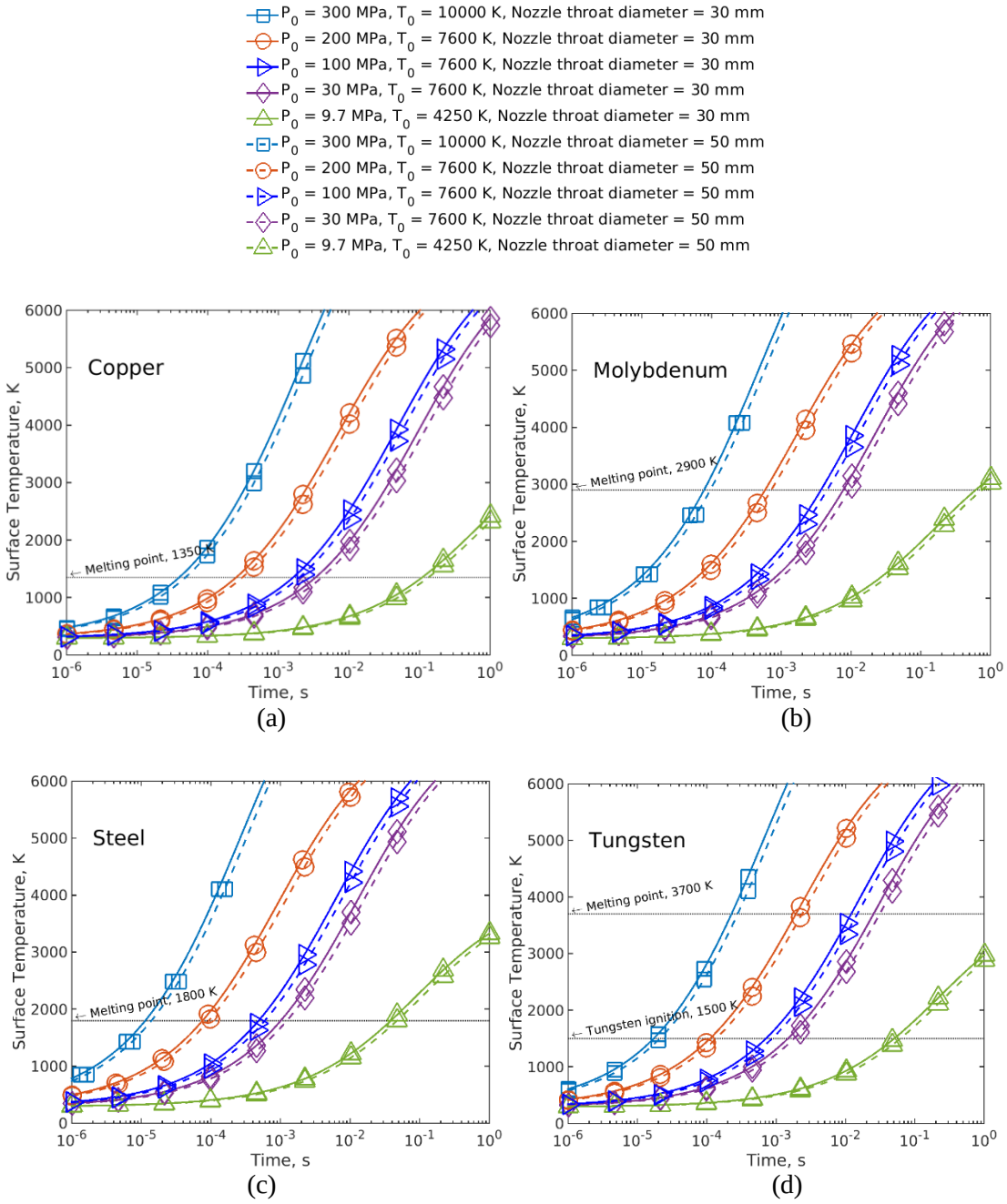

Figure 36: The nozzle throat surface temperature versus time of different materials for different total pressures and total temperatures at different throat diameters and at a constant nozzle throat diameter to nozzle throat radius of curvature ratio of 2.

Using Bartz's nozzle heating equation [114], the nozzle throat surface temperature was calculated for different total pressures and total temperatures at different throat diameters and at a constant nozzle throat diameter to nozzle throat radius of curvature ratio of 2. The results are shown in Figure 36 for different nozzle throat materials. From the results, tungsten seems to be a good material based on the melting point, being able to withstand a total pressure and total temperature of 100 MPa and 7600 K respectively for about 10 ms. However, tungsten oxidizes strongly and this is responsible for direct removal of the throat material [89]. Hence, tungsten is not a good material for the nozzle throat. Steel, while it is good structurally, is particularly bad at withstanding transient heating as it melts after around 1 ms from a total pressure and total temperature

of 30 MPa and 7600 K respectively, while copper is too soft for the high pressures of the nozzle reservoir region. Therefore, molybdenum seems to be one of the best materials, being able to withstand a total pressure and total temperature of 100 MPa and 7600 K respectively for more than 3 ms. For a reservoir state of 300 MPa and 10000 K, no material can allow for any reasonable amount of test time, while for a reservoir state of 9.7 MPa and 4250 K, the throat melt limit is irrelevant as even steel can allow for test times of more than 10 ms. Promising throat materials are tungsten-molybdenum alloys which combine the advantages of both materials. In industry these alloys are used for high thermally and mechanically loaded parts.

The nozzle throat heating mainly depends on total pressure and total temperature. There is a small dependence on the throat diameter, and an even smaller dependence on the throat diameter to throat radius of curvature ratio, hence this was kept constant at a value of two in Figure 36. It can be seen in Figure 36 that, given a certain test time, there is a limit for the nozzle reservoir condition in order to avoid throat melting. For example, if the facility has a test time of 10 ms and a nozzle throat made out of molybdenum, the nozzle reservoir condition must be less than about 30 MPa and 7600 K in order to avoid throat melting. Hence, large reflected shock tunnels with long test times generally do not produce high performance conditions. Therefore, the only way to produce high performance conditions in large facilities is by shortening the shock tube so that the test time is repressed. Nevertheless, there still needs to be enough test gas to establish a steady flow in the nozzle and around the test model. A significant portion of the available test time in Figure 36 could be wasted on nozzle start-up. So there could be situations where the throat melts before a steady flow can be established.

4.2.3 Thermochemical nonequilibrium expanding flows

Except for the case of shock tubes, the generation of hypersonic flows always involve rapid expansion processes. In most cases, the test gas will be heated to a state with at least significant vibrational excitation, if not significant dissociation and ionization. The test gas should not be able to maintain thermochemical equilibrium during the rapid expansion process in most cases. Hence, the test flow generated is often expected to be at an excited thermochemical state. For example, even a cold hypersonic facility like the AEDC tunnel 9 could generate test flows with significant vibrational excitation [115].

Thermochemical excitation in the freestream could have significant influences on a number of different hypersonic flow phenomena. Having a thermochemically excited test flow is undesirable but, unfortunately, it is often unavoidable. Hence, various review papers have stated that correctly characterizing both the vibrational excitation state and the chemical composition of the test flow for the study of blunt body, slender body and scramjet flows must be regarded as being of first-order importance [1] [77] [94] [116] [117]. Unfortunately, this is difficult because our current understanding of nonequilibrium expanding flows is lacking as most studies of thermochemical nonequilibrium were performed under post-shock conditions. Nonetheless, some notable results for nonequilibrium expanding flows have been obtained and these will be discussed in this section.

Table 5: Computed nozzle exit properties for the AEDC Tunnel 9 Mach 14 nozzle for varying amounts of water vapour contamination. [115]

H_2O Mole Fraction	T (K)	T_{vN2} (K)	T_{vH2O} (K)	u (m/s)	M
0	41.9	1542	--	1784	13.52
0.0001	41.1	1213	598	1785	13.52
0.0005	42.1	917	542	1787	13.51
0.001	42.3	782	522	1790	13.50
0.005	43.3	534	501	1804	13.43

Most of the existing experimental results, which were performed in the 1960s to 1970s, indicated that vibrational relaxation time constants observed in expanding flow conditions were significantly faster than those observed in post-shock conditions. The experiments showed that the vibration relaxation time constants

under expanding flow conditions for N_2, CO and CO_2 were around 5 – 70 [118] [119], 1 – 1000 [120] and 1.06 – 1.14 [121] times shorter respectively than the corresponding vibrational relaxation time constants under post-shock conditions. However, due to the inability to theoretically explain the reason for the accelerated vibrational relaxation in expanding flows [122] [123] [124] and the existence of the minority which reported that the expanding flow vibrational relaxation rates were similar to those in post-shock conditions [125], the accelerated vibrational relaxation were often considered an experimental artefact. In particular, water vapour contamination (often from outgassing by the tube walls) was hypothesised as the cause of the accelerated vibrational relaxation in expanding flows because water molecules are very efficient quenchers of vibrational excitation [126] [127]. Candler and McConaughey numerically showed the influence of water vapour on the AEDC Tunnel 9 Mach 14 nozzle flow for a pure nitrogen test gas with a total pressure of 14 MPa and a total temperature of 1543 K [115]. The results are shown in Table 5 and it can be seen that even a mole fraction of 0.005 of water can reduce the vibrational temperature of nitrogen at the nozzle exit from 1542 K to 534 K. While this proves that water vapour contamination can cause accelerated vibrational relaxation, it does not prove without a doubt that the earlier experimentally observed accelerated vibrational excitation in expanding flows were caused by this contamination. In fact, one of the most recent investigations of nonequilibrium expanding flows, reported by Gu in 2018 for CO_2 [128], seemed to indicate that the accelerated vibrational relaxation is not an experimental artefact such as that caused by water vapour contamination.

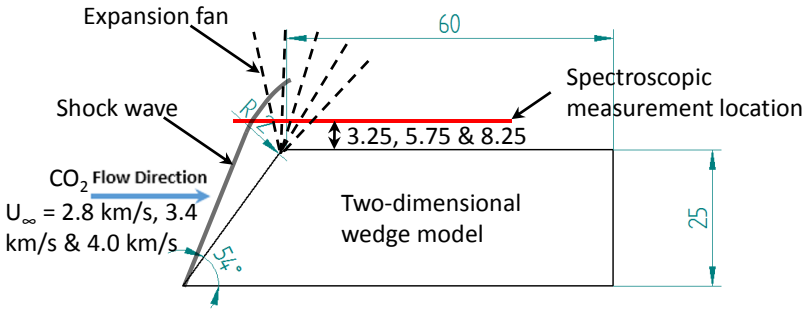

Figure 37: Two-dimensional test model geometry and measurement location. The model has a width of 100 mm. Dimensions shown are in mm and degrees. Not to scale.

Gu took horizontal spectroscopic measurements at three locations along a single spatial dimension above a two-dimensional wedge model as shown in Figure 37. Unlike previous measurements of expanding flows, this measurement contained a simultaneous measurement of the post-shock nonequilibrium and the expanding flow nonequilibrium. Through a spectral fitting method, the spectroscopic measurements were used to deduce the rotational-translational temperature, T_r, and the vibrational temperature, T_v, along the single spatial dimension. To study the nonequilibrium, the ratio T_v/T_r were obtained and compared to numerical computations. The results are shown in Figure 38 for a 4.0 km/s CO_2 test condition. Ignoring the negative spike at the vicinity of the shock front which is impossible to capture experimentally, the result shows good agreement between experiment and CFD in the shock layer region, but poor agreement in the expanding flow region. In the expanding flow region, CFD over-predicted the degree of nonequilibrium by as much as 40 %, suggesting an accelerated vibrational relaxation in the experiment. Because no obvious accelerated vibrational relaxation was observed in the shock layer region, water vapour contamination being the cause of this behaviour may be ruled out since water vapour contamination would influence vibrational relaxation in both the post-shock and expanding flow regions [127]. Instead, this result of Gu seems to indicate that the accelerated vibrational relaxation in expanding flows is a naturally occurring phenomenon and not an experimental artefact. The same finding was observed in a 2.8 km/s condition and a 3.4 km/s condition.

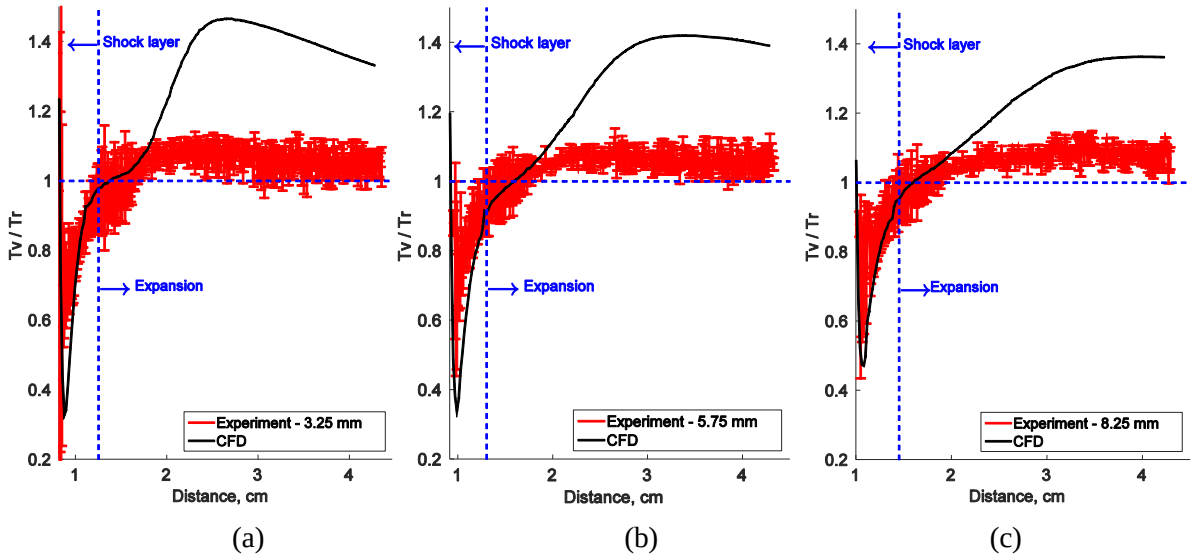

Figure 38: The ratio of the vibrational temperature to the rotational temperature for the 4.0 km/s condition at locations of 3.25 mm (a), 5.75 mm (b) and 8.25 mm (c) respectively above the wedge.

Other relatively recent experimental results of nonequilibrium expanding flows were produced by the nozzle flow in reflected shock tunnels, but the results were independently conflicting. Maclean and Holden in 2006 [129] reported that the shock standoff on the test model measured at the nozzle exit of their LENS shock tunnel was significantly greater than what they predicted in their CFD. This is shown in Figure 39 (a) where the CFD result (blue contour) is overlaid on top of the experimental measurement. This mismatch was consistently observed in their lower density test conditions [130]. They believe this mismatch was caused by the carbon dioxide freestream being frozen at a complex non-equilibrium state since excess energy frozen in the thermal and chemical modes in the freestream increases shock standoff. Research was conducted at simulating the non-equilibrium condition at the nozzle exit of the reflected shock tube using advanced thermochemical models but it failed to predict the necessary magnitude of frozen thermochemical energy needed to replicate the experimentally observed shock stand-off [131]. However, these results from Maclean and Holden could not be reproduced in the T5 shock tunnel by Leibowitz and Austin in 2018 [38]. As shown in Figure 39 (b), Leibowitz and Austin obtained a good match in shock stand-off between experiment and CFD using a freestream predicted from conventional non-equilibrium nozzle simulations. This result is in contrast to the result of Maclean and Holden [129] who argued that the nonequilibrium in the nozzle flow was more significant than what was predicted in their CFD simulation. On the other hand, an assessment of the nozzle exit static pressure measurements of various air test conditions by Marineau and Hornung in 2009 gave an indication that there were distinctly more nonequilibrium present in the T5 nozzle than what CFD predicted [132]. This is because the measured static pressures, which are very sensitive to nonequilibrium, unlike the pitot pressures, were 10 – 17 % lower than those computed from conventional non-equilibrium nozzle simulations. Olivier et al. [133] showed that the finite freestream dissociation level in a high enthalpy nozzle flow leads to a decrease of the density change across the bow shock at a blunt body and therewith to an increase of the shock stand-off distance as it is typically observed in reflected shock tunnels. Interestingly, Hannemann et al. in 2010 reported static pressure measurements more than 15 % higher than those computed from non-equilibrium nozzle simulations for the HEG nozzle [134], which indicated an equilibrium nozzle flow.

Less work has been reported on the nonequilibrium behaviour in expansion tubes. For conditions produced in the expansion tube, the flow velocity is also very sensitive to the nonequilibrium, as is the static pressure, due to the unsteady expansion. Even in works as early as the work by Trimpi in 1962 [135], the total enthalpy multiplication feature discussed in section 3.3 was shown to be distinctly influenced by nonequilibrium. The magnitude of the multiplication increased with increasing thermochemical activity because, as described by

Morgan et al. [136], "the total enthalpy multiplication feature of unsteady expansions works only on the static component of enthalpy, through its influence on sound speed, so that if recombination does not occur the high potential final enthalpy will not be reached". Neely and Morgan in 1993 [84] took shock speed measurements as well as static pressure measurements at the end of the acceleration tube for superorbital air conditions. Subsequent analysis showed that the measured static pressure and shock speed could only have been obtained if the unsteady expansion occurred under near thermochemical equilibrium conditions. The same result was obtained by Morgan et al. for superorbital CO_2 conditions [136] and by James et al. [54] for other hypervelocity air conditions. However, recent spectroscopic investigation by Gu indicated moderate vibrational excitation in the test flow from the expansion tunnel mode of X2 [128]. Spectroscopic measurements were taken at the nozzle exit for the three different velocity CO_2 freestreams shown in Figure 37. Even though the shock speed and static pressure measurements in the acceleration tube indicated equilibrium unsteady expansion, Tv/Tr ratios of 1.1 – 1.5, 1.1 – 1.5 and 1.0 – 1.1 were found in the 2.8, 3.4 and 4.0 km/s conditions respectively at the nozzle exit. While complete freezing through the nozzle flow may explain the moderate nonequilibrium observed in the 2.8 and 3.4 km/s freestreams, it fails to explain why the 4.0 km/s condition, which has the highest velocity and lowest density, exhibited the least nonequilibrium while the 2.8 and 3.4 km/s conditions, which has lower velocities and higher densities, exhibited more nonequilibrium. For this reason, the nonequilibrium observed in the freestream of the 2.8 and 3.4 km/s conditions is not believed to be caused by the nozzle, due to operation as an expansion tunnel, which has an area ratio of only 5.6 anyways.

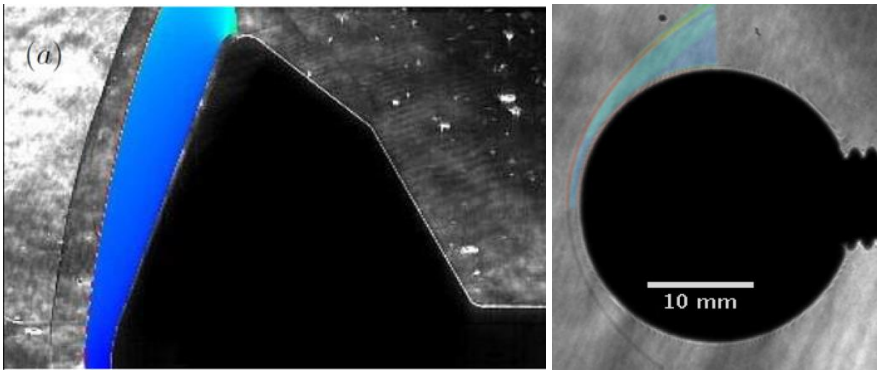

(a) (b)

Figure 39: Shock wave comparison between experimental measurements from (a) LENS I (h_0 = 5.6 MJ/kg) [129] and (b) T5 (h_0 = 5.6 MJ/kg) [38] and CFD predictions for a pure CO_2 test gas.

So, nonequilibrium in expanding flows is very much an open problem. Fortunately, research in this area is beginning to gain prominence due to its application not only in wind tunnels but also in the design of atmospheric entry capsules, for which expanding flows are produced around the shoulder and afterbody area [78]. For now, the inability to accurately characterize the degree of nonequilibrium in the experimental freestreams is also a big concern for high enthalpy ground testing. In terms of simulating flight, having a thermochemically excited experimental freestream significantly complicates things because a strict simulation of flight requires duplication of the thermochemical state. At present, there is no clear quantitative understanding of how non-equilibrium freestreams effect the various hypersonic flow parameters. Stalker in 1989 [12] gave a rough rule for blunt bodies which states that, if the freestream enthalpy is less than a third of the total enthalpy, then effects of freestream non-equilibrium on the real-gas effects in the flow over the body are small. In the same paper, Stalker also derived similitude rules which accounted for freestream non-equilibrium in the ground simulation of shock layers with moderate to large shock angles. However, studies on the effects of non-equilibrium freestream on hypersonic flow parameters of other configurations could not be found. Therefore, this needs to be considered in the future and similitudes that include freestream non-equilibrium need to be developed for improved ground simulation of flight.

In addition to the thermochemical state of the test flow, the primal flow variables density, velocity and total enthalpy cannot be determined to a satisfactory accuracy at present. Olivier in 1993 reported a good method to provide time-resolved estimates of the freestream density, velocity and total enthalpy without the need to make particular assumptions about the thermochemical state of the freestream [137]. The method involved taking static pressure, pitot pressure and stagnation point heat flux measurements at the nozzle exit, along with the use of the normal shock governing equations and the Fay and Riddell relation for spherical stagnation point heat flux [138], to deduce the primal freestream variables. Due to the uncertainties of the stagnation point heat flux measurements at higher enthalpies, the authors are currently developing an improved variation of Olivier's 1993 method by avoiding stagnation point heat flux measurements.

4.2.4 Other limitations of importance

It is important to mention that the popular free-piston drivers suffer from a loss phenomenon which Hornung et al. [89] called the Page-Stalker effect. Page and Stalker [139] in 1983 reported that the pressure recovery factors, p_5/p_4, observed in free-piston driven shock tunnels were much lower than predicted. In light of this, Hornung and Belanger [140] as well as Eitelberg et al. [141], showed that the shock speeds, in addition to the pressure recovery factors, were lower than predicted in the T4 and HEG facilities respectively as shown in Figure 40. Using data from many different free-piston driven facilities, Page and Stalker reported an important correlation in regards to this effect, as shown in Figure 41, where the theoretical value of $\log(p_5/p_4)$ should be 0.26 [73]. It is obvious that the Page-Stalker effect diminishes as the ratio L_1/d increases, where L_1 is the distance of the piston from the end of the compression tube at the time of diaphragm rupture, and d is the shock tube diameter. The cause of this behaviour is not fully understood. Hornung et al. [89] postulated that the Page - Stalker effect was due to the formation of a very strong ring vortex in front of the piston which will significantly influence the flow into the shock tube, causing losses, the closer it gets to the end of the compression tube. Due to the Page-Stalker effect, Morgan [61] recommends the use of longer compression tubes.

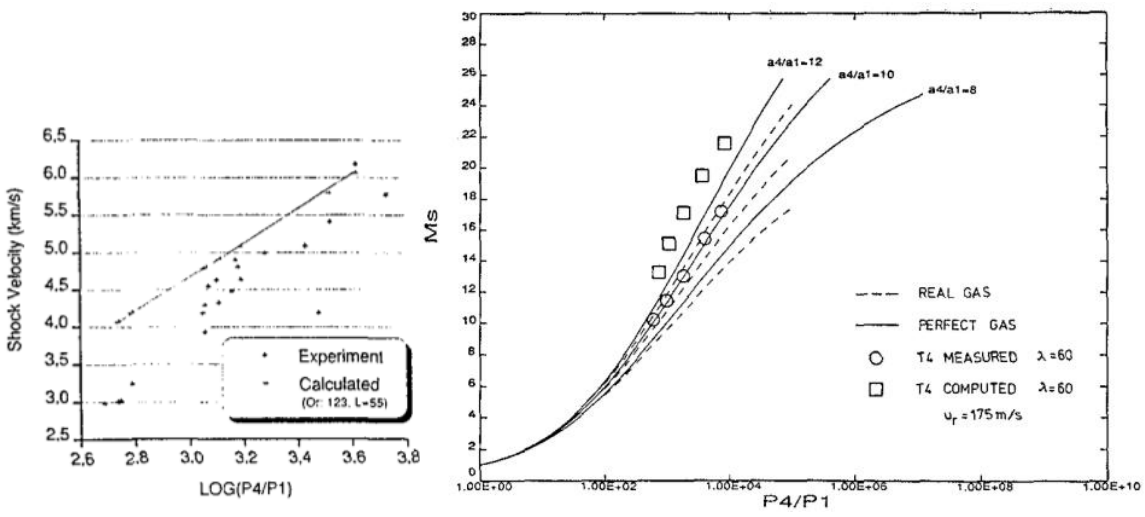

Figure 40: Calculated and measured shock speeds in the HEG (left) [141] and T4 (right) [140] shock tunnels.

In addition to the Page-Stalker effect, a more minor loss in free-piston drivers is the heat loss due to the small but finite flow in the driver gas induced by the piston motion, and it can be estimated using the turbulent heat transfer model for a flat plate [142]. As a measure of the heat loss, Itoh et al. [143] defined a heat loss factor,

$$\xi = \frac{T_r}{T_{r,adiabatic}} \tag{38}$$

where T_r is the driver gas temperature at diaphragm rupture. Itoh et al. [143] reported an empirical value of $\xi = 0.9$. For the free-piston driver of the X2 expansion tunnel, Gildfind [144] estimated $\xi = 0.86 - 0.90$. Gildfind mentioned that the main variables influencing the driver heat loss is the period of the piston stroke and the driver gas volume compared to its surface area. For shorter tubes with larger diameters and rapid piston strokes, the heat loss would be small and vice versa.

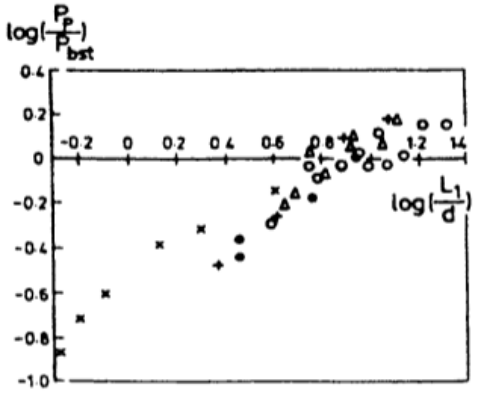

Figure 41: Pressure recovery factor, p_5/p_4 or p_p/p_{bst}, variation with L_1/d. [139]

Other minor losses in the free-piston driver include the pressure loss of the secondary reservoir gas, leakage of the driver gas through the clearance between the piston and the wall surface, and friction between the piston wear ring and the surface of the compression tube. For the pressure loss of the secondary reservoir Itoh et al. [143] defined a factor ψ in,

$$\varepsilon' = \psi\varepsilon \tag{39}$$

where ε, called the driving force factor of the piston, is the ratio of the initial pressure of the secondary reservoir gas and the diaphragm rupture pressure, and $\psi = 0.9$ for their medium size reflected shock tunnel HEK. The value of ψ depends on the dimensions of the secondary reservoir and the piston launcher mechanisms [143], as well as the fill pressure and velocity of the reservoir gas [144]. For the piston friction loss, Itoh et al. [143] found a friction factor of 0.15 for the HEK. Lastly, Itoh et al. [143] mentioned that the leakage of the driver gas through the piston is negligible when the piston speed is very high, which was the case in their HEK facility.

Limitations not only exist concerning wind tunnel performances, but also concerning applicable measuring techniques. As for the simulation performances, the applicable measuring techniques can be assigned to the different types of wind tunnels or the different flow regimes characterized in this paper by low, high and very high enthalpy regimes.

For the continuous running and blowdown facilities nearly all measuring techniques known from subsonic and supersonic flows are applicable. For low stagnation temperatures up to 1000 K even hot wire anemometry is possible. For higher stagnation temperatures focusing laser differential interferometry has been successfully applied. For these facilities this also allows the measurement of freestream turbulence levels which is an important parameter for characterizing the boundary layer transition behaviour in hypersonic flows. These facilities also allow accurate aerodynamic force and moment measurements due to their long running times. Heat transfer measurements are performed on a more or less routine basis but here the long running time is of

disadvantage because lateral heat conduction effects influence the measured heat transfer normal to the wall. Other measuring techniques are also applied which are listed in Table 6.

Several attempts have been made to measure freestream turbulence levels in shock tunnels. But till today no reliable measurement has been performed. Also force and moment measurements are difficult to perform. Fast force balances have been developed which in conjunction with acceleration compensation techniques allow force and moment measurements for measuring times down to two milliseconds. A few years ago a free-flight force measurement technique has been proposed and tested in the HIEST facility which might be promising for short-time force and moment measurements, and also for complicated model geometries [145].

The measuring time in the range of milliseconds make shock tunnels well suited for heat flux measurements because it is long enough to ensure a full flow establishment and short enough to reduce the effect of lateral heat conduction to a very low level. In expansion tunnels attempts have been made for measuring aerodynamic forces by stress bars. However, this is an even more complex technique which is far from regular use, and there is still the question of flow establishment and remaining testing time. A further problem of high enthalpy testing which amongst others pose a severe limitation for laser based measuring techniques is the dust produced in the shock tube which results from bursting diaphragms, sealing of pistons etc. and the erosion of the tube and inner nozzle surface at highly loaded locations. The dust forms a layer at the inner tube surface and part of it is transported by the test gas flow to the test section and model surface during the experiment. This facility dependent pollution increases with increasing total enthalpy. To the author's knowledge there is no facility avoiding this problem of dust and particle pollution. There are several attempts for performing non-intrusive laser based measurements e.g. of the species concentration at the nozzle exit flow for reflected shock tunnels. But the problem mentioned above and others still lead to a high uncertainty for these measurements.

Table 6: Standard measuring techniques of different types of test facilities

Facility	Continuous and blowdown facilities	Shock tunnels	Expansion tunnels
Type of measurements	Total temperature	-	-
	Total pressure	Total pressure	-
	Freestream temperature	(Laser methods)	-
	Freestream pressure	Freestream pressure	-
	Freestream velocity	(Laser methods)	-
	Freestream turbulence level	-	-
	Model surface pressures, local and surface mapping	Model surface pressures, local	Model surface pressures, local
	Model surface temperature and heat fluxes, local and surface mapping	Model surface heat fluxes, local, line scan, infrared thermography	Model surface heat fluxes, local
	Surface shear stresses	-	-
	Flow velocities, local and 2d	-	-
	Overall forces and moments	Overall forces and moments	(Stress bars)
	Forces and moments of flaps, rudders etc.	-	-
	Oil flow visualization	-	-
	Flow visualization	Flow visualization	Flow visualization

5.0 CONCLUSION

In this paper, the methodologies of hypersonic ground testing were reviewed. Then the characteristics and capabilities of the different hypersonic wind tunnels were discussed. The capabilities and limitations of these

facilities were quantitatively assessed in regards to the simulation of relevant flight vehicles. In addition, other limitations of the ground test facilities, such as test time, test model size and applicable measuring techniques were assessed for the most important facility types for modern hypersonics research. Additionally, the often unavoidable problem of producing thermochemically excited test flows in reflected shock tunnels and, to a lesser extent, expansion tunnels were reviewed.

The facilities were grouped into three categories according to three typical flow regimes characterized by low, high and very high total enthalpies or flow velocities. Each category of facility has its own advantages and disadvantages concerning performances, flow quality, measuring time etc. Low enthalpy facilities like continuous running and blowdown facilities allow the longest running times, detailed measurements, best knowledge of freestream properties, highly accurate data etc. but are limited to low stagnation enthalpies and therefore exclude the regime of reacting hypersonic flows. However, from the listed facilities only the AEDC Tunnel 9 is capable of a full Mach - Reynolds number simulation of most of the flight trajectory of a Mach 6 hypersonic vehicle with typically 30 m length. Problems become more severe for the high enthalpy flow regime. Conventional, detonation driven and free-piston driven shock tunnels are the most popular facilities operated at these conditions. The short running times pose a challenge for force and moment measurements and other measuring techniques. Yet unsolved is the development of a reliable, simple method for characterizing the freestream properties including its chemical composition. Especially for high enthalpy conditions the uncertainty of the freestream conditions directly influences the uncertainty of any experimentally determined aerodynamic coefficient. A full Mach - Reynolds number simulation is not possible for these flow conditions because of the required huge stagnation pressures. These also limit the facility performance because of the direct dependence of facility integrity and nozzle throat melting issues on the stagnation conditions. Expansion tunnels allow much higher stagnation pressures and temperatures than reflected shock tunnels and therefore they enlarge the simulation range especially the ρL-U scaling capability. However, limitations are given by limited driver performances and especially by the short testing time which significantly limits the maximum tolerable model size. Hence, increasing the test section size of expansion tunnels by increasing the nozzle area ratio is rather pointless. The only way to test larger models in an expansion tunnel is by scaling the entire facility. This therefore results in huge costs because the expansion tunnel would have to be at least about twice as long and have approximately at least twice the inner tube diameter compared to the smallest reflected shock tunnel which can test the given model size. Nonetheless, depending on the application, expansion tunnels are sometimes selected over reflected shock tunnels even for low and medium enthalpy conditions because expansion tunnels produce test flows with less thermochemical excitation. This is the result of the total enthalpy and total pressure multiplication feature of the unsteady expansion and the fact that the test gas is only shock processed once in the expansion tunnel. For example, the LENS XX facility allows the testing of models of feasible size at moderate total enthalpies resulting in sufficiently long testing times. In this way the advantage of less thermochemical excitation of the freestream can be utilized for high quality testing.

While reflected shock tunnels are the most prominent sufferers of excess thermochemical excitation in the test flow, expansion tunnels and even blowdown tunnels suffer this to a lesser extent as rapid expansion occur inside all these facilities. A review of literature on thermochemical nonequilibrium in expanding flows revealed the current lack of understanding in this field, which is not helped by the fact that conflicting results from independent investigations were often reported. So, experimental research in modern hypersonics involves the use of a various of different test facilities, each with its own unique capabilities and limitations.

ACKNOWLEDGEMENTS

The author would like to acknowledge Steven Lewis and Chris James of the Centre for Hypersonics at The University of Queensland for providing the performance envelope of the X2 expansion tunnel, Sam Stennett and Andreas Andrianatos of the Centre for Hypersonics at The University of Queensland for providing information on the X3 facility, Chen Xing of the China Academy of Aerospace Aerodynamics for providing

information on the FD-21 facility and Qiu Wang from the Chinese Academy of Sciences for information about JF12.

REFERENCES

[1] Stalker, R. J., "Modern developments in hypersonic wind tunnels," The Aeronautical Journal, vol. 110, no. 1103, pp. 21-39, 2006.

[2] Hornung, H. G., "28th Lanchester memorial lecture - experimental real-gas hypersonics," The Aeronautical Journal, vol. 92, no. 920, pp. 379-389, 1988.

[3] Esser, B., "Die Zustandsgrößen im Stoßwellenkanal als Ergebnisse eines exakten Riemannlösers," PhD thesis, RWTH Aachen University, Aachen, 1991.

[4] Ginoux, J. J., "Laminar boundary layers," von Karman Institute, CN 104, 1978.

[5] Hornung, H. G., "Hypersonic real-gas effects on transition," In: IUTAM Symposium on One Hundred Years of Boundary Layer Research, Springer, Berlin, Heidelberg, 2006.

[6] Bleilebens, M., & Olivier, H., "On the influence of elevated surface temperatures on hypersonic shock wave/boundary layer interaction at a heated ramp model," Shock Waves, vol. 15, no. 5, pp. 301-312, 2006.

[7] Zander, F., Morgan, R. G., Sheikh, U., Buttsworth, D. R., & Teakle, P. R., "Hot-wall reentry testing in hypersonic impulse facilities," AIAA Journal, vol. 51, no. 2, pp. 476-484, 2012.

[8] Anderson, J. D., Hypersonic and high temperature gas dynamics., Reston, Virginia, USA: AIAA Education Series, 2006.

[9] Birkhoff, G., Hydrodynamics: A study in logic, fact, and similitude, modeling and dimensional analysis, Dover Publications, Inc., 1955.

[10] de Crombrugghe, G., Morgan, R., & Chazot, O., "Theoretical approach and experimental verification of the role of diffusive transport under binary scaling conditions," International Journal of Heat and Mass Transfer, vol. 97, pp. 675-682, 2016.

[11] Clarke, J. F., "Chemical reactions in high-speed flows," Phil. Trans. R. Soc. Lond. A, vol. 335, no. 1637, pp. 161-199, 1991.

[12] Stalker, R. J., "Hypervelocity aerodynamics with chemical nonequilibrium," Annual Review of Fluid Mechanics, vol. 21, no. 1, pp. 37-60, 1989.

[13] de Crombrugghe de Looringhe, G. A., "On binary scaling and ground-to-flight extrapolation in high-enthalpy facilities," PhD Thesis, School of Mechanical and Mining Engineering, The University of Queensland, 2017.

[14] de Crombrugghe, G., Chazot, O., McIntyre, T. J., & Morgan, R, "Experimental evidence of the impact of radiation coupling on binary scaling applied to shock layer flows," International Journal of Heat and Mass Transfer, vol. 120, pp. 568-574, 2018.

[15] Belouaggadia, N., Olivier, H., & Brun, R., "Numerical and theoretical study of the shock stand-off distance in non-equilibrium flows," Journal of Fluid Mechanics, vol. 607, pp. 167-197, 2008.

[16] Lawson, J. M., & Austin, J. M., "Design of conventional and detonation-driven hypervelocity expansion tubes," In: Aerodynamic Measurement Technology and Ground Testing Conference, Atlanta, AIAA 2018-3566, 2018.

[17] Stewart, D. G., "Similarity and scale effects in combustion chambers," National Gas Turbine Establishment, Memorandum M, 129, 1951.

[18] Pulsonetti, M., & Stalker, R., "A study of scramjet scaling," In: Space Plane and Hypersonic Systems and Technology Conference, AIAA-96-4533, 1996.

[19] Karl, S., Hannemann, K., & Steelant, J., "CFD investigation of scaling laws for hydrogen fuelled scramjet combustors," In: 6th European Symposium on Aerothermodynamics for Space Vehicles, 2009.

[20] Pulsonetti, M. V., "Scaling laws for scramjets: an experimental and theoretical investigation to determine the scaling laws for scramjet engine performance at hypersonic flight conditions," Doctoral dissertation, University of Queensland, Brisbane, 1997.

[21] Stalker, R. J., Paull, A., Mee, D. J., Morgan, R. G., & Jacobs, P. A., "Scramjets and shock tunnels - the Queensland experience," Progress in Aerospace Sciences, vol. 41, no. 6, pp. 471-513, 2005.

[22] Gildfind, D. E., Morgan, R. G., Jacobs, P. A., & McGilvray, M., "Production of high-Mach-number scramjet flow conditions in an expansion tube," AIAA journal, vol. 52, no. 1, pp. 162-177, 2013.

[23] Jiang, Z., & Yu, H., "Experiments and development of long-test-duration hypervelocity detonation-driven shock tunnel (LHDst)," In: 52nd Aerospace sciences meeting, Maryland, AIAA-2014-1012, 2014.

[24] Dufrene, A., MacLean, M., Parker, R., Wadhams, T., & Holden, M., "Characterization of the new LENS expansion tunnel facility," In: 48th AIAA Aerospace Sciences Meeting Including the New Horizons Forum and Aerospace Exposition, Orlando AIAA 2010-1564, 2010.

[25] Mills, M., "Hypersonic test capabilities in tunnels B and C at AEDC's von Karman Facility," In: 53rd AIAA Aerospace Sciences Meeting, AIAA paper 2015-1336, 2015.

[26] Marren, D., & Lafferty, J., "The AEDC hypervelocity wind tunnel 9," In: Advanced Hypersonic Test Facilities, Reston, VA, vol. 198, Progress in Aeronautics and Astronautics, AIAA, 2002, pp. 467-477.

[27] Gruhn, P., & Gülhan, A., "Aerodynamic measurements of an air-breathing hypersonic vehicle at Mach 3.5 to 8," AIAA Journal, pp. 1-15, 2018.

[28] Mohamed, A. K., Henry, D., Faléni, J. P., Sagnier, P., Soutadé, J., Beck, W. H., & Schramm, J. M., "Infrared diode laser absorption spectroscopy measurements in the S4MA, F4 and HEG hypersonic flows," In: International Symposium on Atmospheric Reentry Vehicles and Systems, Arcachon, France, 1999.

[29] Grossir, G., Ilich, Z., Paris, S., & Chazot, O., "Theoretical considerations to extend the operational map of the VKI Longshot hypersonic wind tunnel," In: 32nd AIAA Aerodynamic Measurement Technology and Ground Testing Conference, Washington, D.C., AIAA 2016-3818, 2016.

[30] Buttsworth, D., "Gun tunnels," In: Experimental Methods of Shock Wave Research, Springer, Cham., 2016, pp. 381-396.

[31] Buttsworth, D. R., & Jones, T. V., "High bandwidth stagnation temperature measurements in a Mach 6 gun tunnel flow," Experimental thermal and fluid science, vol. 27, no. 2, pp. 177-186, 2003.

[32] Masson, A., Sagnier, P., & Mohamed, A. K., "The ONERA F4 high-enthalpy wind tunnel," In: Advanced Hypersonic Test Facilities, Reston, Virginia, AIAA, 2002, pp. 441-466.

[33] National Security and International Affairs Division, "World directory of aerospace vehicle research and development," Report GAO/NSLAD-90-71FS Foreign Test Facilities, United States General Accounting Office, Washington, D.C., 1990.

[34] Olivier, H., "The Aachen shock tunnel TH2 with dual driver mode operation," In: Experimental Methods of Shock Wave Research, Springer, Cham, 2016, pp. 111-129.

[35] Hannemann, K., Itoh, K., Mee, D. J., & Hornung, H. G., "Free piston shock tunnels HEG, HIEST, T4 and T5," In: Experimental Methods of Shock Wave Research, Springer, Cham, 2016, pp. 181-264.

[36] Mee, D. J., "Uncertainty analysis of conditions in the test section of the T4 shock tunnel," University of Queensland, Brisbane, Report No. 4/93, 1993.

[37] Boyce, R. R., Takahashi, M., & Stalker, R. J., "Mass spectrometric measurements of driver gas arrival in the T4 free-piston shock-tunnel," Shock Waves, vol. 14, no. 5-6, pp. 371-378, 2005.

[38] Leibowitz, M. G., & Austin, J. M., "Assessment of reflected shock runnels for Mars entry vehicle ground testing," In: 2018 AIAA Aerospace Sciences Meeting, Kissimmee, Florida, AIAA 2018-1721, 2018.

[39] Itoh, K., "Characteristics of the HIEST and its applicability for hypersonic aerothermodynamic and scramjet research," In: Advanced Hypersonic Test Facilities, Vol. 198, Progress in Astronautics and Aeronautics, Reston, VA, AIAA, 2002, pp. 239-254.

[40] Li, C., Sun, R., Wang, Y., Chen, X., & Bi, Z., "Reliability improvement of the piston compressor in FD-21 free-piston shock tunnel," In: 5th International Conference on Experimental Fluid Mechanics, Munich, 2018.

[41] Zhixian, B., Bingbing, Z., Hao, Z., Xing, C., Junmou, S., Chen, L., & Riming, S., "Experiments and computations on the compression process in the free piston shock tunnel FD21," In: 5th International Conference on Experimental Fluid Mechanics, Munich, Germany, 2018.

[42] Holden, M. S., & Parker, R. A., "LENS hypervelocity tunnels and application to vehicle testing at duplicated flight conditions," In: Advanced Hypersonic Test Facilities , edited by F. K. Lu, and D. E. Marren, Vol. 198, Reston, VA, , AIAA Progress in Astronautics and Aeronautics Series, 2002, pp. 73-110.

[43] Holden, M. S., Wadhams, T. P., & Candler, G. V. , "Experimental studies in the LENS shock tunnel and expansion tunnel to examine real-gas effects in hypervelocity flows," In: 42nd AIAA Aerospace Sciences Meeting and Exhibit, Reno, NV, AIAA-2004-0916, 2004.

[44] Holden, M., Kolly, J., & Chadwick, K., "Calibration, validation and evaluation studies in the LENS facility," In: 33rd Aerospace Sciences Meeting and Exhibit, AIAA 95-0291, Reno, NV, 1995.

[45] Abul-Huda, Y. M., & Gamba, M., "Flow characterization of a hypersonic expansion tube facility for supersonic combustion studies," Journal of Propulsion and Power, vol. 33, no. 6, pp. 1504-1519, 2017.

[46] Ben-Yakar, A., & Hanson, R. K., "Characterization of expansion tube flows for hypervelocity combustion studies," Journal of Propulsion and Power, vol. 18, no. 4, pp. 943-952, 2002.

[47] Dufrene, A., Sharma, M., & Austin, J. M., "Design and characterization of a hypervelocity expansion tube facility," Journal of Propulsion and Power, vol. 23, no. 6, pp. 1185-1193, 2007.

[48] Gildfind, D. E., James, C. M., Toniato, P., & Morgan, R. G., "Performance considerations for expansion tube operation with a shock-heated secondary driver," Journal of Fluid Mechanics, vol. 777, pp. 364-407, 2015.

[49] Toniato, P., Gildfind, D. E., Andrianatos, A., & Morgan, R. G., "Full free-stream Mach 12 scramjet testing in expansion tubes," In: 2018 Applied Aerodynamics Conference, Atlanta, AIAA 2018-3818, 2018.

[50] Andrianatos, A., Gildfind, D., & Morgan, R. G., "Driver condition development for high enthalpy operation of the X3 expansion tube," In: 31st International Symposium on Shock Waves, Japan, 2017.

[51] Lu, F. K., & Marren, D. E., "Principles of hypersonic test facility development," In: Advanced hypersonic test facilities, Reston, Virginia, AIAA, 2002, pp. 17-27.

[52] Radespiel, R., Estorf, M., Heitmann, D., Muñoz, F., & Wolf, T. , "Hypersonic Ludwieg tube," In: Experimental Methods of Shock Wave Research, Springer, Cham., 2016, pp. 433-458.

[53] Grossir, G., Ilich, Z., & Chazot, O., "Modeling of the VKI Longshot gun tunnel compression process using a quasi-1D approach," In: 33rd AIAA Aerodynamic Measurement Technology and Ground Testing Conference, Denver, AIAA 2017-3985, 2017.

[54] James, C. M., Gildfind, D. E., Lewis, S. W., Morgan, R. G., & Zander, F., "Implementation of a state-to-state analytical framework for the calculation of expansion tube flow properties," Shock Waves, vol. 28, no. 2, pp. 349-377, 2018.

[55] Resler, E. L., Lin, S. C., & Kantrowitz, A., "The production of high temperature gases in shock tubes," Journal of Applied Physics, vol. 23, no. 12, pp. 1390-1399, 1952.

[56] Lukasiewicz, J., Experimental methods of hypersonics, New York: Marcel Dekker, 1973.

[57] Hannemann, K., & Martinez Schramm, J., "Short-duration testing of high enthalpy, high pressure, hypersonic flows," In: Springer Handbook of Experimental Fluid Mechanics, Springer, Berlin, 2007, pp. 1081-1125.

[58] Sharma, S. P., & Park, C., "Operating characteristics of a 60-and 10-cm electric arc-driven shock tube - part I: The driver," Journal of Thermophysics and Heat Transfer, vol. 4, no. 3, pp. 259-265, 1990.

[59] Sharma, S. P., & Park, C., "Operating characteristics of a 60-and 10-cm electric arc-driven shock tube - part II: The driven section," Journal of Thermophysics and Heat Transfer, vol. 4, no. 3, pp. 266-272, 1990.

[60] Gai, S. L., "Free piston shock tunnels: developments and capabilities," Progress in Aerospace Sciences, vol. 29, no. 1, pp. 1-41, 1992.

[61] Morgan, R. G., "Chapter 4.2 Shock Tubes and Tunnels: Facilities, instrumentation and techniques free piston-driven reflected shock tunnels," In: Handbook of Shock Waves, Vol. 1, Academic Press, Waltham, MA, 2001, pp. 587-601.

[62] Stalker, R. J., & Besant, R. W., "A method for production of strong shocks in a gas driven shock tube," National Research Council Report GD-81, 1959.

[63] Gildfind, D. E., Morgan, R. G., McGilvray, M., Jacobs, P. A., Stalker, R. J., & Eichmann, T. N., "Free-piston driver optimisation for simulation of high Mach number scramjet flow conditions," Shock Waves, vol. 21, no. 6, pp. 559-572, 2011.

[64] Hornung, H. G., "The piston motion in a free-piston driver for shock tubes and tunnels," GALCIT Report FM, 88-1, 1988.

[65] Hornung, H. G., "Ground testing for hypervelocity flow, capabilities and limitations," California Inst. of Technology RTO-EN-AVT-186, 2010.

[66] Bakos, R., & Erdos, J., "Options for enhancement of the performance of shock-expansion tubes and tunnels," In: 33rd Aerospace Sciences Meeting and Exhibit, Reno, 1995.

[67] Olivier, H., Jiang, Z., Yu, H. R., & Lu, F., "Detonation-driven shock tubes and tunnels," In: Advanced Hypersonic Test Facilities, Reston, VA, Vol. 198, Progress in Astronautics and Aeronautics, AIAA, 2002, pp. 135-203.

[68] Grönig, H., Olivier, H., & Habermann, M., "Development of a detonation driver for a shock tunnel," In: The Review of High Pressure Science and Technology, Kyoto, 1998.

[69] Nishida, M., "Shock tubes," In: Handbook of Shock Waves, New York, Academic Press, 2001, pp. 553-585.

[70] Marineau, E., MacLean, M., Mundy, E., & Holden, M., "Force measurements in hypervelocity flows with an acceleration compensated strain gage balance," Journal of Spacecraft and Rockets, vol. 49, no. 3, pp. 474-482, 2012.

[71] Sudani, N., Valiferdowsi, B., & Hornung, H. G., "Test time increase by delaying driver gas contamination for reflected shock tunnels," AIAA Journal, vol. 38, no. 9, pp. 1497-1503, 2000.

[72] Goozée, R. J., Jacobs, P. A., & Buttsworth, D. R., "Simulation of a complete reflected shock tunnel showing a vortex mechanism for flow contamination," Shock Waves, vol. 15, no. 3-4, pp. 165-176, 2006.

[73] Stalker, R. J. & Hornung, H. G., "Two developments with free piston drivers," In: Proc. 7th Int. Symp. on Shock Tubes and Waves, Toronto, 1969.

[74] Gordon, S., & McBride, B. J., "Computer program for calculation of complex chemical equilibrium compositions and applications. Part 1: Analysis," NASA reference publication 1311, NASA Lewis Research Center, Cleveland, OH, 1994.

[75] Logan, P. F., Stalker, R. J., & McIntosh, M. K., "A shock tube study of radiative energy loss from an argon plasma," Journal of Physics D: Applied Physics, vol. 10, no. 3, pp. 323-337, 1977.

[76] Vieille, P., "Sur les discontinuités produites par la détente brusque de gaz comprimés," C. R. Acad. Sci., vol. 129, pp. 1228-1230, 1899.

[77] Reynier, P., "Survey of high-enthalpy shock facilities in the perspective of radiation and chemical kinetics investigations," Progress in Aerospace Sciences, vol. 85, pp. 1-32, 2016.

[78] Brandis, A., "Overview of recent EAST testing, modelling & analysis," ARC-E-DAA-TN54621, NASA Ames Research Center; Moffett Field, CA, United States, 2018.

[79] Resler, E. L., & Bloxsom, D. E., "Very high Mach number flows by unsteady flow principles," Cornell University Graduate School of Aeronautical Engineering, 1952.

[80] Morgan., R.G., "Chapter 4.3 Free-piston driven expansion tubes," In: Handbook of Shock Waves, vol. 1, Academic Press, 2001, pp. 603-622.

[81] Miller, C. G., "Operational experience in the Langley expansion tube with various test gases," AIAA Journal, vol. 16, no. 3, pp. 195-196, 1978.

[82] Paull, A., & Stalker, R. J., "Test flow disturbances in an expansion tube," Journal of Fluid Mechanics, vol. 245, pp. 493-521, 1992.

[83] Gu, S., Morgan, R. G., & McIntyre, T. J., "Study of the afterbody radiation during Mars entry in an expansion tube," In: 55th AIAA Aerospace Sciences Meeting, Grapevine, AIAA 2017-0212, 2017.

[84] Neely, A. J., & Morgan, R. G., "The superorbital expansion tube concept, experiment and analysis," The Aeronautical Journal, vol. 98, no. 973, pp. 97-105, 1994.

[85] Rivell, T., "Notes on earth atmospheric entry for Mars sample return missions," NASA Ames Research Center, Moffett Field, California, Tech. Rep. TP-2006-213486, 2006.

[86] Crowder, R. S., & Moote, J. D., "Apollo entry aerodynamics," Journal of Spacecraft and Rockets, vol. 6, no. 3, pp. 302-307, 1969.

[87] Weber, R. J., "Propulsion for hypersonic transport aircraft," NASA, Lewis Research Center, Cleveland, Ohio, NASA TMX51638, 1964.

[88] Gildfind, D. E., Morgan, R. G., & Jacobs, P. A., "Expansion tubes in Australia," In: Experimental Methods of Shock Wave research, Springer, Cham, 2016, pp. 399-431.

[89] Hornung, H., Sturtevant, B., Belanger, J., Sanderson, S., Brouillette, M., & Jenkins, M. , "Performance data of the new free-piston shock tunnel T5 at GALCIT," In: Shock Waves, Springer, Berlin, Heidelberg, 1992.

[90] Jiang, Z., & Yu, H., "Development and calibration of detonation-driven high-enthalpy and hypersonic test facilities," In: Experimental Methods of Shock Wave Research, Springer, Cham, 2016, pp. 285-313.

[91] Takayanagi, H., Lemal, A., Nomura, S., & Fujita, K., "Measurements of carbon dioxide nonequilibrium infrared radiation in shocked and expanded flows," Journal of Thermophysics and Heat Transfer, vol. 32, no. 2, pp. 483-494, 2017.

[92] West IV, T. K., Theisinger, J. E., Brune, A. J., & Johnston, C. O., "Backshell radiative heating on human-scale Mars entry vehicles," In: 47th AIAA Thermophysics Conference, AIAA paper 2017-4532, Denver, Colorado, 2017.

[93] Stewart, B. S., Morgan, R. G., & Jacobs, P. A., "Rocketdyne hypersonic flow laboratory as high-performance expansion tube for scramjet testing," Journal of Propulsion and Power, vol. 19, no. 1, pp. 98-103, 2003.

[94] Chinitz, W., Erdos, J. I., Rizkalla, O., & Anderson, G. Y., "Facility opportunities and associated stream chemistry considerations for hypersonic air-breathing propulsion," Journal of Propulsion and Power, vol. 10, no. 1, pp. 6-17, 1994.

[95] Gildfind, D. E., James, C. M., & Morgan, R. G., "Free-piston driver performance characterisation using experimental shock speeds through helium," Shock Waves, vol. 25, no. 2, pp. 169-176, 2015.

[96] James, C. M., Gildfind, D., Morgan, R. G., Lewis, S. W., & Fahy, E. J., "On the current limits of simulating gas giant entry flows in an expansion tube," In: 20th AIAA International Space Planes and Hypersonic Systems and Technologies Conference, Glasgow, AIAA 2015-3501, 2015.

[97] McGilvray, M., Doherty, L. J., Morgan, R. G., Gildfind, D., Jacobs, P., & Ireland, P. , "T6: The Oxford University Stalker Tunnel," In: 20th AIAA International Space Planes and Hypersonic Systems and Technologies Conference, Glasgow, AIAA 2015-3545, 2015.

[98] Silber, E. A., Boslough, M., Hocking, W. K., Gritsevich, M., & Whitaker, R. W., "Physics of meteor generated shock waves in the Earth's atmosphere – A review," Advances in Space Research, vol. 62, no. 3, pp. 489-532, 2018.

[99] Johnston, C. O., Stern, E. C., & Wheeler, L. F., "Radiative heating of large meteoroids during atmospheric entry," Icarus, vol. 309, pp. 25-44, 2018.

[100] Paull, A., "A simple shock tunnel driver gas detector," Shock Waves, vol. 6, no. 5, pp. 309-312, 1996.

[101] Skinner, K. A., "Mass spectrometry in shock tunnel experiments of hypersonic combustion," PhD Thesis, The University of Queensland, Brisbane, 1994.

[102] Stalker, R. J., & Crane, K. C. A., "Driver gas contamination in a high-enthalpy reflected shock tunnel," AIAA Journal, vol. 16, no. 3, pp. 277-279, 1978.

[103] Crane, K. C. A., & Stalker, R. J., "Mass-spectrometric analysis of hypersonic flows," Journal of Physics D: Applied Physics, vol. 10, no. 5, pp. 679-695, 1977.

[104] Stalker, R. J., & Morgan, R. G., "The University of Queensland free piston shock tunnel T-4: Initial operation and preliminary calibration," In: Fourth National Space Engineering Symposium, Institution of Engineers, Australia, 1988.

[105] Kindl, H., Olivier, H., Zhao, H., Muylaert, J., Wong, H., & Walpot, L., "Conventional flow diagnostics in shock tunnels," In: Proceedings 21st International Symposium on Shock Waves, Australia, 1997.

[106] Burtschell, Y., Cardoso, M., & Zeitoun, D. E., "Numerical analysis of reducing driver gas contamination in impulse shock tunnels," AIAA Journal, vol. 39, no. 12, pp. 2357-2365, 2001.

[107] Hannemann, K., Reimann, B., Martine, J., & Schnieder, M., "The influence and the delay of driver gas contamination in HEG," In: 21st Aerodynamic Measurement Technology and Ground Testing Conference, Denver, AIAA 2000-2593, 2000.

[108] Chue, R. S. M., Tsai, C. Y., & Bakos, R. J., "Driver gas contamination in a detonation-driven reflected-shock tunnel," Shock Waves, vol. 13, no. 5, pp. 367-380, 2003.

[109] Chue, R. S. M., Tsai, C. Y., Bakos, R. J., Erdos, J. I., & Rogers, R. C., "NASA's HYPULSE facility at GASL–a dual mode, dual driver reflected-shock/expansion tunnel," In: Advanced Hypersonic Test Facilities, Reston, Virginia, AIAA, 2002, pp. 29-71.

[110] Paull, A., Stalker, R., & Stringer, I., "Experiments on an expansion tube with a free piston driver," In: 15th Aerodynamic Testing Conference, AIAA paper 88-2018, 1988.

[111] James, C. M., Cullen, T. G., Wei, H., Lewis, S. W., Gu, S., Morgan, R. G., & McIntyre, T. J., "Improved test time evaluation in an expansion tube," Experiments in Fluids, vol. 59, no. 5, pp. 87-108, 2018.

[112] Hollis, B. R., & Perkins, J. N., "High-enthalpy aerothermodynamics of a Mars entry vehicle part 1: Experimental results," Journal of Spacecraft and Rockets, vol. 34, no. 4, pp. 449-456, 1997.

[113] Park, G., Gai, S. L., & Neely, A. J., "Aerothermodynamics behind a blunt body at superorbital speeds," AIAA Journal, vol. 48, no. 8, pp. 1804-1816, 2010.

[114] Bartz, D. R., "A simple equation for rapid estimation of rocket nozzle convective heat transfer coefficients," J. Jet Propulsion, vol. 27, pp. 49-51, 1957.

[115] Candler, G., & McConaughey, K., "Effect of water vapor on the AEDC Tunnel 9 Mach 14 nozzle flow," In: 47th AIAA Aerospace Sciences Meeting including The New Horizons Forum and Aerospace Exposition, Orlando, AIAA 2009-195, 2009.

[116] Blankson, I. M., Murthy, S. N. B., & Bruno, C., "Scramjet combustor and flow path scaling," NATO technical rept. RTO-TR-AVT-007-V2, Brussels, Belgium, 2012, Chap. 9.

[117] Rapuc, M., "Hermes measurement needs in hot facilities," In: New Trends in Instrumentation for Hypersonic Research, Springer, Dordrecht, 1993, pp. 11-23.

[118] Hurle, I. R., Russo, A. L., & Hall, J. G., "Spectroscopic studies of vibrational nonequilibrium in supersonic nozzle flows," The Journal of Chemical Physics, vol. 40, no. 8, pp. 2076-2089, 1964.

[119] Sebacher, D. I., & Guy, R. W., "Vibrational relaxation in expanding N2 and air," NASA TM X- 71988, NASA Langley Research Center, Hampton, 1974.

[120] McLaren, T. I., & Appleton, J. P., "Vibrational relaxation measurements of carbon monoxide in a shock-tube expansion wave," The Journal of Chemical Physics, vol. 53, no. 7, pp. 2850-2857, 1970.

[121] Ibraguimova, L., & Shatalov, O., "Non-equilibrium kinetics behind shock waves: experimental aspects," In: High Temperature Phenomena in Shock Waves, Berlin, Springer Berlin Heidelberg, 2012, pp. 99-147.

[122] Ruffin, S. M., "Prediction of vibrational relaxation in hypersonic expanding flows Part 1: model development," Journal of Thermophysics and Heat Transfer, vol. 9, no. 3, pp. 432-437, 1995.

[123] Kewley, D. J., "Numerical study of anharmonic diatomic relaxation rates in shock waves and nozzles," Journal of Physics B: Atomic and Molecular Physics, vol. 8, no. 15, pp. 2565-2579, 1975.

[124] Hsu, C. T., & McMillen, L. D., "Time-dependent solutions for de-excitation rates of anharmonic oscillators," The Journal of Chemical Physics, vol. 56, no. 11, pp. 5327-5334, 1972.

[125] Sharma, S. P., Ruffin, S. M., Gillespie, W. D., & Meyer, S. A., "Vibrational relaxation measurements in an expanding flow using spontaneous Raman scattering," Journal of Thermophysics and Heat Transfer, vol. 7, no. 4, pp. 697-703, 1993.

[126] Boudreau, A. H., "Characterization of flow fields in hypersonic ground test facilities," Methodology of Hypersonic Testing, Lecture Series, 3, 1993.

[127] Meador, W., Townsend, L., & Miner, G., "Effects of H2O vapor on vibrational relaxation in expanding and contracting flows," In: 34th Aerospace Sciences Meeting and Exhibit, AIAA Paper 96-0105, 1996.

[128] Gu, S., "Mars entry afterbody radiative heating: an experimental study of nonequilibrium CO2 expanding flow," PhD Thesis, School of Mechanical and Mining Engineering, The University of Queensland, Brisbane, 2018.

[129] MacLean, M., & Holden, M., "Numerical assessment of data in catalytic and transitional flows for Martian entry," In: 9TH AIAA/ASME Joint Thermophysics and Heat Transfer Conference, AIAA paper 2006-2946, San Francisco, 2006.

[130] MacLean, M., Dufrene, A., & Holden, M., "Spherical capsule heating in high enthalpy carbon dioxide in LENS-XX expansion tunnel," In: 51st AIAA Aerospace Sciences Meeting and Exhibit, AIAA Paper 2013-906, Grapevine (Dallas/Ft. Worth Region), Texas, 2013.

[131] Doraiswamy, S., Kelley, J. D., & Candler, G. V., "Vibrational modeling of CO_2 in high-enthalpy nozzle flows," Journal of Thermophysics and Heat Transfer, vol. 24, no. 1, pp. 9-17, 2010.

[132] Marineau, E., & Hornung, H., "High-enthalpy nonequilibrium nozzle flow of air: experiments and computations," In: 39th AIAA Fluid Dynamics Conference, San Antonio, Texas, AIAA 2009-4216, 2009.

[133] Olivier, H., Walpot, L., Merrifield, J., & Molina, R., "On the phenomenon of the shock stand-off distance in hypersonic, high enthalpy facilities," In: Proceedings of the First International Conference on High Temperature Gas Dynamics, Beijing, 2012.

[134] Hannemann, K., Karl, S., Schramm, J. M., & Steelant, J., "Methodology of a combined ground based testing and numerical modelling analysis of supersonic combustion flow paths," Shock Waves, vol. 20, no. 5, pp. 353-366, 2010.

[135] Trimpi, R. L., "Preliminary theoretical study of the expansion tube: new device for producing high enthalpy short-duration hypersonic gas flows," NASA TR R-133, 1962.

[136] Morgan, R. G., Neely, A. J., & Scott, M. L., "Hypervelocity carbon dioxide flow simulation," In: Shock Waves@ Marseille II, Springer, Berlin, Heidelberg, 1995.

[137] Olivier, H., "An improved method to determine free stream conditions in hypersonic facilities," Shock Waves, vol. 3, no. 2, pp. 129-139, 1993.

[138] Fay, J. A. & Riddell, F. R., "Theory of stagnation point heat transfer in dissociated air," Journal of the Aerospace Sciences, vol. 25, no. 2, pp. 73-85, 1958.

[139] Page, N. W., & Stalker, R. J., "Pressure losses in free piston driven shock tubes," In: Proc. 14th International Symposium on Shock Tubes and Waves, Sydney, 1983.

[140] Hornung, H. & Belanger, J., "Role and techniques of ground testing for simulation of flows up to orbital speed," In: 16th Aerodynamic Ground Testing Conference, 1990.

[141] Eitelberg, G., McIntyre, T., Beck, W., & Lacey, J., "The high enthalpy shock tunnel in Göttingen," In: 28th Joint Propulsion Conference and Exhibit, Nashville, TN, 1992.

[142] Tani, K., Itoh, K., Takahashi, M., Tanno, H., Komuro, T., & Miyajima, H., "Numerical study of free-piston shock tunnel performance," Shock Waves, vol. 3, no. 4, pp. 313-319, 1994.

[143] Itoh, K., S. Ueda, T. Komuro, K. Sato, M. Takahashi, H. Miyajima, H. Tanno, & H. Muramoto, "Improvement of a free piston driver for a high-enthalpy shock tunnel," Shock Waves, vol. 8, no. 4, pp. 215-233, 1998.

[144] Gildfind, D. E., "Development of high total pressure scramjet flow conditions using the X2 expansion tube," PhD Thesis, The University of Queensland, Brisbane, 2012.

[145] Tanno, H., Komuro, T., Sato, K., Itoh, K., Takahashi, M., Fujita, K., Laurence, S. & Hannemann, K., "Free-flight force measurement technique in shock tunnel," In: 50th AIAA Aerospace Sciences Meeting including the New Horizons Forum and Aerospace Exposition, Nashville, Tennessee, 2012.

[146] ONERA, "S4A," [Online]. Available: https://www.onera.fr/sites/default/files/windtunnel/pdf/S4A.pdf. [Accessed 26 October 2018].

[147] Belanger, J., & Hornung, H. G., "Transverse jet mixing and combustion experiments in hypervelocity flows," Journal of Propulsion and Power, vol. 12, no. 1, pp. 186-192, 1996.

[148] Stennett, S. J., Gildfind, D. E., Jacobs, P. A., & Morgan, R. G., "Performance optimization of X3R: a new reflected shock tunnel mode for the X3 expansion tube," In: Aerodynamic Measurement Technology and Ground Testing Conference, Atlanta, 2018.

[149] Wang, Q., Li, J. P., Zhao, W., & Jiang, Z. L., "Influence of thermal sensor installation on measuring accuracy at stagnation points," Journal of Thermophysics and Heat Transfer, vol. 31, no. 2, pp. 318-323, 2016.

[150] MacLean, M., Wadhams, T., Holden, M., & Johnson, H., "Ground test studies of the HIFiRE-1 transition experiment part 2: computational analysis," Journal of Spacecraft and Rockets, vol. 45, no. 6, pp. 1149-1164, 2008.

[151] Tanno, H., Komuro, T., Lillard, R. P., & Olejniczak, J., "Experimental study of high-enthalpy heat flux augmentation in shock tunnels," Journal of Thermophysics and Heat Transfer, vol. 29, no. 4, pp. 858-862, 2015.

[152] Tanno, H., Itoh, K., Ueda, S., Komuro, T., Sato, K., & Kodera, M., "Scramjet testing in high-enthalpy shock tunnel (HIEST)," In: Proceedings of Symposium on Shock Waves, Japan, 2002.

[153] Knisely, A. M., & Austin, J. M., "Geometry and test-time effects on hypervelocity shock-boundary layer interaction," In: 54th AIAA Aerospace Sciences Meeting, San Diego, 2016.

[154] Sharma, M., "Post-shock thermochemistry in hypervelocity CO2 and air flow," Doctoral dissertation, University of Illinois at Urbana-Champaign, Champaign, 2010.

[155] Bowersox, R. D., White, E. B., North, S. W., Marcotte, E. K., & Aguilar, G. J., "Hypervelocity expansion facility for fundamental high-enthalpy research," Final Technical Report of Contract ONR N00014-15-1-2260, Texas A and M University, College Station, 2017.